

Accuracy analysis of multi-axis machines

Citation for published version (APA):

Soons, J. A. (1993). *Accuracy analysis of multi-axis machines*. [Phd Thesis 1 (Research TU/e / Graduation TU/e), Mechanical Engineering]. Technische Universiteit Eindhoven. <https://doi.org/10.6100/IR400139>

DOI:

[10.6100/IR400139](https://doi.org/10.6100/IR400139)

Document status and date:

Published: 01/01/1993

Document Version:

Publisher's PDF, also known as Version of Record (includes final page, issue and volume numbers)

Please check the document version of this publication:

- A submitted manuscript is the version of the article upon submission and before peer-review. There can be important differences between the submitted version and the official published version of record. People interested in the research are advised to contact the author for the final version of the publication, or visit the DOI to the publisher's website.
- The final author version and the galley proof are versions of the publication after peer review.
- The final published version features the final layout of the paper including the volume, issue and page numbers.

[Link to publication](#)

General rights

Copyright and moral rights for the publications made accessible in the public portal are retained by the authors and/or other copyright owners and it is a condition of accessing publications that users recognise and abide by the legal requirements associated with these rights.

- Users may download and print one copy of any publication from the public portal for the purpose of private study or research.
- You may not further distribute the material or use it for any profit-making activity or commercial gain
- You may freely distribute the URL identifying the publication in the public portal.

If the publication is distributed under the terms of Article 25fa of the Dutch Copyright Act, indicated by the "Taverne" license above, please follow below link for the End User Agreement:

www.tue.nl/taverne

Take down policy

If you believe that this document breaches copyright please contact us at:

openaccess@tue.nl

providing details and we will investigate your claim.

**Accuracy Analysis
of
Multi-Axis Machines**

Hans Soons

Accuracy Analysis
of
Multi-Axis Machines

Proefschrift

ter verkrijging van de graad van doctor
aan de Technische Universiteit Eindhoven,
op gezag van de Rector Magnificus, prof. dr. J.H. van Lint,
voor een commissie aangewezen door het College
van Dekanen in het openbaar te verdedigen op
woensdag 16 juni 1993 om 16.00 uur

door

Johannes Augustinus Soons

geboren te Oss

Dit proefschrift is goedgekeurd door de promotoren

prof. dr. ir. P.H.J. Schellekens

en

prof. dr. ir. A.C.H. van der Wolf

Aan mijn ouders

Summary

This thesis presents a general strategy to estimate and describe the quasi-static errors of multi-axis machines. The goal is a model for the errors in the position and orientation of the end-effector relative to the workpiece during an arbitrary task.

The core of the proposed strategy is the so-called kinematic model. This model relates errors in the relative location of the end-effector to errors in the geometry of successive structural loop segments. The latter so-called parametric errors describe the combined effect of all error sources on the relevant geometry of machine components that constitute such a segment. The presented kinematic model can be applied to multi-axis machines consisting of an arbitrary serial configuration of revolute and prismatic joints.

The studied errors are those due to the limited accuracy of structural loop segments in a certain reference state, those due to static and slowly varying forces introduced by the dead weight of machine components and workpiece, and those due to thermally introduced strains in the structural loop. The respective error sources are analysed separately and their combined effect on the parametric errors is obtained by superposition. The adopted modelling strategy is founded on the empirical estimation and description of the various errors. Only for the thermal errors an analytical approach is presented based on an assumed stress-free deformation of the structural loop. The presented empirical models for the thermal deformations are based on a state-space presentation. Due to the dynamic nature of these models, they only require a relatively small number of temperature sensors to predict the thermal errors.

A general method is presented to estimate the parametric errors of multi-axis machines using artifact measurements. The use of standard regression techniques yields a uniform approach regarding the nature of the tested machine (e.g. the presence of revolute joints or finite stiffness effects), and the choice and location of the artifacts. Using statistical experimental design techniques, it is shown that the efficiency of the respective calibration can be unambiguously assessed and optimized.

The modelling strategy is applied to a five-axis milling machine and a three-axis CMM. For the milling machine, the models for the geometric and finite-stiffness errors are validated by predicting the errors of hole plate measurements executed by the machine. The models for the thermal errors are validated by predicting the observed zero-point drift of the tool during characteristic duty cycles of the spindle. The accuracy of the machine is improved by software error compensation of the geometric errors. The geometric errors of the CMM are estimated by three different methods, all using length measurements. The respective models are validated by predicting the observed errors of a large number of length measurements executed by the machine.

Samenvatting

Dit proefschrift presenteert een algemene strategie voor de schatting en beschrijving van de quasi-statische afwijkingen van meer-assige machines. Het doel is een model dat, voor een willekeurige taak, de afwijkingen beschrijft in de positie en oriëntatie van het gereedschap ten opzichte van het werkstuk.

De kern van de voorgestelde strategie is het zogenaamde kinematisch model. Dit model relateert de afwijkingen in de relatieve lokatie van het gereedschap aan afwijkingen in de geometrie van opeenvolgende machineonderdelen. Laatstgenoemde zogenaamde parametrische afwijkingen beschrijven het effect van alle afwijkingenbronnen op de relevante geometrie van een dergelijk onderdeel. Het gepresenteerde kinematisch model kan worden toegepast op meer-assige machines die uit een willekeurige seriële combinatie van rotatie- en translatie-assen bestaan.

Onderzocht zijn machineafwijkingen die worden veroorzaakt door: (1) de onnauwkeurigheid van de machineonderdelen in een bepaalde referentietoestand, (2) de elastische deformatie van de machineonderdelen als gevolg van hun gewicht en het gewicht van het werkstuk en (3) de thermische deformatie van de machineonderdelen. Deze afwijkingenbronnen zijn individueel geanalyseerd. Hun gecombineerde invloed op de parametrische afwijkingen is door superpositie verkregen. De voorgestelde modellering is gebaseerd op een empirische schatting en beschrijving van de verschillende afwijkingen. Enkel de thermische afwijkingen worden gedeeltelijk analytisch gemodelleerd. Hierbij wordt een spanningsvrije deformatie van de machineonderdelen verondersteld. De empirische modellen van de thermische afwijkingen zijn gebaseerd op een toestandsbeschrijving. In de betreffende modellen is het dynamische karakter van thermische afwijkingen geïmplementeerd. Hierdoor is slechts

een gering aantal temperatuurssensoren benodigd om de thermische afwijkingen te voorspellen.

In het proefschrift wordt een algemene methode beschreven waarmee de parametrische afwijkingen kunnen worden geschat uit de door de machine gemeten afmetingen van testobjecten. De methode is gebaseerd op standaard regressie-technieken. Hierdoor kan de methode worden toegepast op willekeurige machines, inclusief machines met rotatie-assen en machines met afwijkingen als gevolg van de eindige stijfheid van machineonderdelen. Voorts kunnen zowel de aard als de lokatie van de toegepaste testobjecten willekeurig worden gekozen. Uitgaande van de statistische theorie van proefopzetten zijn criteria ontwikkeld waarmee de efficiëntie van de betreffende kalibratie ondubbelzinnig kan worden bepaald. Tevens zijn deze criteria gebruikt om de kalibratie te optimaliseren.

De ontwikkelde strategie is toegepast op een vijf-assige freesmachine en een drie-assige coördinaten meetmachine. Voor de freesmachine zijn modellen ontwikkeld voor zowel de geometrische afwijkingen als de afwijkingen ten gevolge van gewichtsbelasting. Deze modellen zijn geverifieerd door metingen aan een gatenplaat. Hierbij zijn de modellen gebruikt om de afwijkingen in de door de machine gemeten afmetingen van dit object te voorspellen. De modellen voor de thermische afwijkingen van de machine zijn geverifieerd door vergelijking van de voorspelde en gemeten nulpuntsdrift van het gereedschap bij karakteristieke toerentalspectra van de hoofdspil. Voorts is de nauwkeurigheid van de machine verbeterd door softwarecompensatie van de geometrische afwijkingen. De geometrische afwijkingen van de coördinatenmeetmachine zijn geschat met drie verschillende methoden, die allen gebruik maken van lengtemetingen. De betreffende modellen zijn geverifieerd door vergelijking van de voorspelde en gemeten afwijkingen van een groot aantal door de machine uitgevoerde lengtemetingen.

Contents

Summary	i
Samenvatting	iii
1 Introduction	1
1.1 Multi-axis machines in modern manufacturing	1
1.2 Error classification	6
1.3 Research objectives and content thesis	12
2 The kinematic error model	15
2.1 Introduction	15
2.2 Literature overview	19
2.3 Mathematical description kinematic model	28
2.3.1 The chosen approach	28
2.3.2 Nomenclature coordinate frames	31
2.3.3 Derivation of the model	33

2.3.4	Errors of elementary measurement and positioning tasks	40
2.3.5	Calculation of compensation parameters	43
2.3.6	Higher order error terms	43
2.4	Choice location coordinate frames	45
3	Modelling parametric errors	53
3.1	Introduction	53
3.2	Geometric errors	59
3.2.1	Choice reference state	59
3.2.2	'Ordinary' geometric errors	61
3.2.3	Straightness errors	70
3.2.4	Periodic errors	72
3.2.5	Hysteresis and backlash	78
3.3	Errors due to mechanical loads	83
3.3.1	General considerations	83
3.3.2	Weight of moving machine components	85
3.3.3	Workpiece weight	91
3.4	Thermal errors	98
3.4.1	Introduction	99
3.4.2	Modelling the temperature distribution	105
3.4.3	Modelling the parametric errors	112

3.4.4	Modelling the thermal drift	115
4	Artifact based calibration	119
4.1	Introduction	119
4.2	Estimation of parametric errors	122
4.3	Calibration efficiency	126
4.4	An example	129
5	Validation	135
5.1	Error models of a five-axis milling machine	136
5.1.1	Geometric errors	136
5.1.2	Errors due to mechanical loads	145
5.1.3	Thermal errors	148
5.2	Error estimation of a three-axis CMM using artifacts	157
5.2.1	“Brute Force” calibration	159
5.2.2	Calibration using a Machine Checking Gauge	163
5.2.3	Calibration using a small number of measurements	164
6	Conclusions and recommendations	167
6.1	Conclusions	167
6.2	Recommendations	172

Bibliography	179
A Uncertainty analysis	193
A.1 Introduction	193
A.2 Uncertainty of a measured or realized position	195
B Properties of parametric errors	201
Curriculum Vitae	209
Acknowledgments	211

1

Introduction

This thesis presents a systematic approach to analyse the accuracy of multi-axis machines. The general goal is a model that describes the accuracy of a certain machine at a certain time and place. In this chapter, the need for such models is derived from general trends in modern manufacturing. An overview is presented of errors that affect the accuracy of an executed task. It is shown that multi-axis machines possess certain unique characteristics, that require the use of special modelling and calibration techniques. The adopted strategy and related content of the thesis is summarized. Due to the large variety of both multi-axis machines and their applications, a general strategy can only be considered as a first stage in the development of a full error model for a certain application. Therefore a selection is made of both multi-axis machines and error sources that are studied in more detail.

1.1 Multi-axis machines in modern manufacturing

Multi-axis machines, like Coordinate Measuring Machines (CMMs), machine tools, and industrial robots, are popular in modern manufacturing. They are used for a large variety of tasks, involving the positioning of an object or making it follow a specified trajectory in space. These objects can be tools

or parts. A multi-axis machine consists of a series of mechanical links connected together by actuated joints. The joints either provide a translation or a rotation, and usually can be controlled independently. Thus a large variety of object locations or trajectories can be realized by the same machine. The result is a multi-purpose machine able to execute complex tasks in a flexible manner. This explains the popularity of these machines, especially in piece- and batch-production. The tasks of multi-axis machines can be divided into three classes:

- **Measurement.** Here the tool is a sensor able to detect the surface of the workpiece. The sensor is moved towards a specified part of the workpiece. If a point on the workpiece surface is detected, its coordinates are calculated from the position of the joints. The measured coordinates of various points are used to estimate the dimensions and geometry of a part.
- **Machining.** Here the tool follows a specified trajectory relative to the workpiece while transforming, adding, or removing material. Typical applications are milling, turning, grinding, deburring, (spot-) welding, electrical discharge machining, and laser cutting.
- **Handling.** Here the part is moved along a specified trajectory relative to other parts or machines. Typical applications are assembly, and the loading and unloading of machines.

An illustration of the versatile nature of multi-axis machines is that none of these classes can be attributed to one group of machines only. Dea [30] reports a milling retrofit for their coordinate measuring machines to perform light machining operations. Many milling machines can exchange their cutting tool for a probe system, and thus perform measurements on the part. Industrial robots are used for both machining and handling. Recently, Keferstein [57] introduced an accurate industrial robot that can be used as a coordinate measuring machine.

The accuracy of the task performed by the multi-axis machine obviously affects the accuracy of the finished product. Traditional methods to ensure part accuracy are based on the premise that the machine performs according to

specifications or on the iterative improvement of the realized part accuracy by changing the part program and manufacturing parameters. In general, little systematic knowledge is available about the various error sources and their effect on the accuracy of the finished part. Especially for multi-axis machines, a number of trends can be identified that require a more in-depth analysis of error sources, error propagation, error estimation, and accuracy improvement techniques:

- **Part accuracy.** There is an increasing demand for higher accuracy of parts produced. Typical examples of trends that require tighter tolerances are interchangeability, automatic assembly, miniaturization, integration, design simplicity, and improved product performance and reliability (see e.g. [14, 72, 73, 74, 83, 113]). To achieve the required accuracy improvement of manufacturing equipment, various error reduction techniques are actively studied [50]. These techniques are either based on error avoidance or error compensation. Error avoidance calls for the elimination of error sources or on reducing the sensitivity of the machine structure to these sources. Error compensation attempts to cancel an error by predicting it. Here, the error is measured or estimated either before or during the manufacturing process. Using a model for the error propagation mechanism, the input or output of the machine is altered to eliminate the error. Recent developments of computer controlled machines have increased the interest in error compensation techniques. Application of these techniques, however, requires reliable error models and error estimation techniques.
- **Part geometry.** To reduce assembly efforts and the weight of products, single parts with complex geometries tend to replace assemblies. These parts require complicated manufacturing operations often executed by multi-axis machines. The complex geometry limits the possibilities of in-process gauging techniques. It also severely complicates the selection of manufacturing parameters or part program changes that might improve the realized part accuracy.
- **Quality control.** Historically, quality control and dimensional inspection activities have been focused on post-process appraisal, i.e. finding

defective material after it has been produced [11]. Obviously this approach is costly due to the large amount of scrap, rework and inspection activities that result. Furthermore, the related inspection costs become excessive when, due to increased product liability requirements, it is necessary to certify that each part produced is functionally adequate. Therefore the focus is shifting towards an improved control of the manufacturing process using deterministic manufacturing principles. Deterministic manufacturing [34] is based on the premise that, in an automated environment, the introduction and propagation of errors is highly systematic. Thus quality assurance can be practised by process monitoring rather than part monitoring. This reduces scrap, rework and conventional inspection activities. The approach requires models and sensors to monitor the accuracy of the manufacturing process, and parameters that can be adjusted to improve this accuracy.

- **Automation.** Due to the increased level of automation, machines are separated from human operators. This reduces the level of direct human intervention in the manufacturing process with associated increased reliability requirements. As stated by McClure [71], the effect of automation goes beyond a 'mere' change in controlling intelligence. First, there is a difference in the structural loop that controls the size, and thus accuracy, of the manufactured part. A typical example is the substitution of the hand-held micrometer for machine frame and scales. Second, automation enables complex operations that often prohibit a one-to-one translation of accuracy improving operator habits into automatic machine instructions. McClure [71] mentions the continuous variation of spindle speed to maintain nearly optimum cutting conditions when turning complicated shapes under numerical control. Allowing a 'warm-up' period of the machine has little effect under these conditions, since the machine is in a constant state of thermal transition. An advantage of the increased level of automation is that manufacturing processes become more deterministic. Such processes have, as discussed, better properties for quality control and quality improvement.
- **Batch production and flexibility.** In modern manufacturing there is an increasing emphasis on smaller and more varied batch-production runs. This results in the use of multipurpose multi-axis machines that

are required to make a large variety of parts. In such an environment, the practice of trial runs and iterative accuracy improvement is obviously difficult to apply. A situation that is aggravated by the increasing speed at which new products are introduced, and the related decrease in delivery times. It is therefore necessary to be able to predict the accuracy of a certain manufacturing task before the part is produced. This information can be used to determine the correct manufacturing parameters and to select a suitable machine. Also traditional statistical quality control techniques need to be expanded, so that deviations observed in a certain product family can be used to improve the accuracy of other products. This requires an approach where trends in the error sources of a machine are estimated from data on the realized accuracy of miscellaneous products. Furthermore, the large variety of products limits the possibilities of active error compensation using in-process gauging techniques. Therefore, error compensation techniques have to address error sources and error propagation. Finally, the large variety of parts produced in an arbitrary sequence severely affects the nature of the error model. This model has to be able to predict the accuracy of an arbitrary task. This is a major complication, since the introduction and propagation of errors in multi-axis machines are highly dependent on the executed task. Furthermore, some (thermal) errors are affected by previous manufacturing tasks.

- **Traceability.** Various guidelines and standards address the inspection and evaluation of the accuracy of multi-axis machines. These procedures do not provide the respective user with the tools and data necessary to calculate the (traceable) accuracy of an arbitrary task. Therefore they cannot be regarded as calibrations. Being inspection devices, the availability of (standardized) procedures to calculate the accuracy of a certain task is especially important for coordinate measuring machines. Such procedures have to ensure that traceability for coordinate metrology is just as sound as for any other aspect of dimensional metrology. Due to the versatile and multi-dimensional nature of multi-axis machines, there currently does not exist a ready-to-use reference with which they can be directly calibrated for every possible task. Therefore, it is generally accepted that a complete calibration should result in a separate

description of the errors introduced in the components of the machine [136]. These errors are then combined to calculate the accuracy of a specific task, using a suitable model of the machine.

In reaction to these trends, extensive research programs have been initiated to estimate, describe and improve the accuracy of multi-axis machines (see e.g. [8, 20, 34, 51, 50, 60, 82, 92, 96, 101, 114, 122, 144]). Despite the large effort, progress has been slow due to certain 'unique' characteristics of multi-axis machines:

- The large number of error sources that affect the accuracy of these machines in a complex manner.
- The large variety of tasks typically executed by one machine, combined with the complex dependency of error introduction and error propagation on current and, regarding error introduction, previous tasks.
- The multi-dimensional nature of the executed tasks, and the large number of variables that define these tasks.

1.2 Error classification

The accuracy of a task executed by a multi-axis machine is primarily determined by errors in the trajectory of the end-effector relative to a certain reference. This reference is generally part of the object on which the task is performed, i.e. the workpiece. Especially in case of handling operations, different references are often used during various stages of the executed task. For example, during the first stage of an assembly task, the reference might be connected to a part or the pallet holding it. After picking up the part, the reference is usually changed to the assembly in which the part is to be integrated.

For most tasks, only certain aspects of the trajectory accuracy are relevant:

- **Repeatability.** Some applications only require repeatability, i.e. the capability to reproduce an executed trajectory. A typical example is a robot programmed by teach-in techniques. Here only repeatability is required to ensure that the executed task resembles the taught task. Off-line programming, on the other hand, requires absolute accuracy of the robot and knowledge about the relative location of the robot peripherals. Therefore, link lengths and joint angles need to be accurately known.
- **Quasi-static accuracy.** For certain applications, the accuracy requirements are limited to discrete points of the trajectory reached at relatively low speeds. A typical example is the quasi-static measurement of points on the workpiece surface. Here the accuracy of the trajectory between the measurement points is of minor importance. Most machining operations, on the other hand, require good contour tracking capability or kinematic accuracy, since the tool is in contact with the workpiece during continuous parts of the trajectory.
- **Sensitive direction.** Most applications do not require accuracy of all six position and orientation components that determine the relative location of the end-effector. For example, the diameter of a cylinder during turning is mainly determined by the radial distance of the tool to the centerline of the part. Error components that only affect this distance act in the so-called sensitive direction. Relative movements of the tool in the feed and cutting speed directions do not influence the accuracy of the realized diameter (to the first order). Hence, these errors act in nonsensitive directions [18].

The accuracy of the relative end-effector trajectory is determined by the sensitivity of the so-called structural loop to various error sources. The structural loop comprises the mechanical components that realize the relative position and orientation (location) between the end-effector and the reference. It consists of the workpiece, the fixtures and peripherals holding the workpiece relative to the multi-axis machine, the multi-axis machine, and the end-effector (see Figure 1.1). The structural loop is closed by, and usually affected by, the workpiece - end-effector interaction.

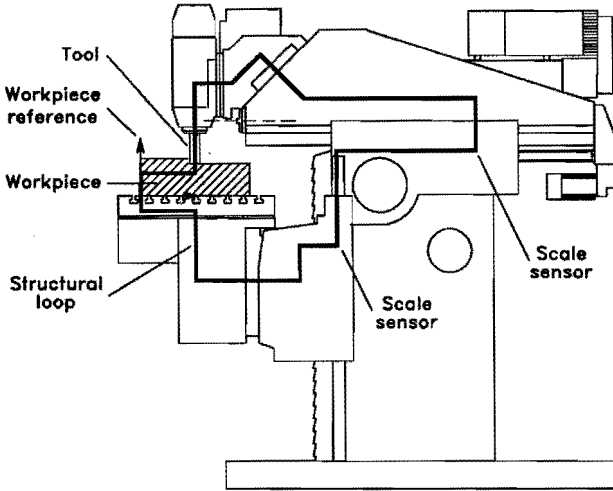


Figure 1.1: Example of the structural loop during a milling operation.

As stated in Section 1.1, a multi-axis machine consists of a series of mechanical links connected together by actuated joints. The nominal position and orientation of the end-effector is based on a model that assumes pure linear or angular motion of the joints, and an ideal geometry of the links and other components of the structural loop. The nominal trajectory of the end-effector is furthermore based on perfectly coordinated joint movements. In reality, several error sources affect the geometry of the structural loop components and the coordinated action of the joints. The result is an actual trajectory of the end-effector that differs from the nominal trajectory.

In this thesis, the accuracy analysis is limited to so-called quasi-static errors. These errors are defined as those errors of relative position and orientation between end-effector and workpiece that are slowly varying in time and are related to the structure of the structural loop itself [50]. Besides these quasi-static errors, the realized trajectory has errors related to the dynamic behaviour of the structural loop. Typical examples of the latter errors are dynamic spindle error motions, imperfections of the controller that coordinates the joint movements, servo tracking errors, acceleration dependent joint and link deflections, and vibrations, both self-induced and forced. These errors can be superimposed on the quasi-static errors and primarily affect the repeatability and kinematic accuracy of the machine.

The quasi-static errors can be divided into three general classes: those due to the geometric accuracy of components, those due to static and slowly varying forces such as the dead weight of machine components and workpiece, and those due to thermally induced strains in the structural loop.

Geometric errors are due to the limited accuracy of the structural loop components in a certain reference state. Errors due to mechanical and thermal loads are defined relative to this state. Typical examples of geometric errors are the limited flatness of the guideways, incorrect link lengths, misalignment between the guides, and the limited accuracy of the used measurement systems. A special class of geometric errors is due to incorrectly specified end-effector dimensions and workpiece location.

The term geometric errors is somewhat ambiguous, because most other error sources affect the accuracy of the trajectory by changing the geometry of the structural loop. The distinctive property of geometric error sources is that the error source remains constant during a manufacturing task. Over longer time intervals, however, they are subject to change due to wear and limited long-term dimensional stability.

Although the geometric error source remains constant, its effect is dependent on the position of the joints. Three mechanisms are responsible. First, the geometry of the guideway and the accuracy of the used measurement system introduce rotational and translational errors that are dependent on the position of the respective joint. Second, the introduced angular errors affect the position accuracy of the end-effector through Abbe offsets, that often are dependent on the position of the joints and the dimensions of the used end-effector. Finally, the direction in which errors act is affected by the position of revolute joints.

The components of the structural loop are subject to a large variety of quasi-static mechanical loads that affect the accuracy of the executed task due to the limited finite stiffness of these components. These loads can be classified as:

- **Weight effects.** Quasi-static load variations are introduced by the weight of moving machine parts, the end-effector, and the workpiece. The resulting deformation of elements in the structural loop causes quasi-static errors in the relative trajectory of the end-effector. Errors due to the weight of moving components can be dependent on the position of one joint only, in which case their effect equals those of certain geometric errors. This property is used by many manufacturers to compensate these weight effects by convex or concave machining of guides and guideways (for example the longitudinal guideway of a lathe). Here the shape of these elements is corrected, using empirical or analytical models for their deflection. This technique is not possible in case the load acting on a guideway is dependent on the position of more than one joint or on the workpiece load. For example, in horizontal arm CMMs, errors due to bending of the column are usually dependent on both the position along the column and the extension of the ram. The workpiece generally causes deformations dependent on its position and weight as well as the position of kinematic elements that support the workpiece. Similar independent variables can be identified for deformations introduced by the weight of the end-effector.
- **Clamping deformations.** In some multi-axis machines, joints are clamped during parts of the trajectory where they have to remain stationary. These clamping forces can cause deformations and displacements of the guided elements, thereby changing the accuracy of the machine. A second class of clamping deformations is related to the fixturing of the workpiece. Especially machining operations require high clamping forces to maintain the proper position of the workpiece under action of the process forces.
- **Process loads.** Dependent on the nature of the executed task, mechanical loads are usually generated at the interface between the end-effector and the workpiece. These loads cause distortions of components of the structural loop, including the workpiece. In the case of measuring tasks, the load consists of the measurement force. Although this force is relatively small (typically several tenths of a Newton), it can cause significant deflections of thin walled workpieces and the used probe stylus. In many cases, machining operations both generate significant thermal

and mechanical loads. The magnitude and direction of the cutting forces are related to the cutting parameters, and thus cause task dependent variations in the deformation of the structural loop. Tlustý [118] reports two additional mechanisms by which the cutting force causes variations in the relative deflection between tool and workpiece. First, form errors of the blank result in a varying depth of cut. The related cutting force variation causes the form error of the blank to be only partly reduced after the cut. Especially grinding operations require a large number of passes to achieve a sufficient reduction of the blank form error. Second, the compliance between tool and workpiece varies during the tool travel. Therefore, even if the cutting force is constant, the deflection varies; thus leaving a form error of the workpiece. During assembly operations, mechanical loads often occur when fitting a part into the assembly (e.g. when inserting a pin into a hole).

A large number of internal and external heat sources affect the temperature distribution of the structural loop. Typical examples are the heat generated by electronic and hydraulic systems, friction in joints and gearboxes, drives, the machining process, the operator, and the machine environment. The resulting thermal distortions of the various components often produce errors that dominate the accuracy of the executed task.

Major problems in the analysis of thermal errors are caused by the local action of the various heat sources, and the relative slow transfer of the generated heat through the structural loop. The result is an inhomogeneous temperature distribution with associated complex deformations. The dynamic relation between temperature distribution and heat sources is governed by relatively large time constants. Hence, the resulting deformations of the structural loop are affected by the action of heat sources during previous tasks. This requires either a dynamic approach to thermal error modelling, or 'complete' measurement of the temperature distribution.

1.3 Research objectives and content thesis

A systematic approach is presented to estimate and describe the quasi-static errors of multi-axis machines. The goal is a model that describes the relevant errors in the relative location of end-effector and workpiece for any position of the machine axes. This model can be used to predict the part accuracies that can be achieved by the machine, to realize traceability of executed tasks, or to enhance the machine accuracy by software compensation of the modelled errors. The first two applications require the estimation of the task accuracy from the errors in the relative trajectory of the end-effector. This usually requires additional modelling steps and, in some cases, the consideration of additional error sources (e.g. regarding the numerical properties of the estimation software used by a CMM). Except for relatively simple tasks, this analysis is beyond the scope of this thesis.

A basic philosophy in the presented analysis is that multi-axis machines have a highly deterministic nature, especially when they are numerically controlled. Many systematic errors are perceived as random due to limited information about the various error sources. A major task of error modelling is to explore how these errors can be described without resorting to an excessive number of sensors.

The adopted modelling strategy is founded on the empirical estimation and description of the various errors. The physics of error generation is considered only when it contributes to a better model or a more efficient estimation and compensation of the errors. Thus it is not intended to present a method to predict the accuracy of a machine in its design stage. However, many of the presented techniques can contribute to that purpose.

Although the presented analysis is intended for the general class of multi-axis machines, only the errors of Coordinate Measuring Machines (CMMs) and milling machines are analysed in detail. Whereas many of the developed concepts can be readily applied to other multi-axis machines, experience has shown that each class of machines, and often each factory type, has certain particular error characteristics that require dedicated analysis. Therefore

a general modelling strategy, such as described in this thesis, can only be considered as a first stage in the development of a full error model for a certain application.

The thesis is divided into three closely related parts. In part 1 (Chapters 2 and 3) a model of the machine errors is developed. Part 2 (Chapter 4) addresses the estimation of the unknown parameters in this model using artifact measurements. In part 3 (Chapter 5) the estimated model is verified by simulating and compensating the machine errors. Throughout the thesis, the developed techniques are applied to a three-axis CMM and a five-axis milling machine.

In the first stage of the modelling process (Chapter 2), a so-called kinematic model of the machine accuracy is derived. This model relates the errors in the location of the end-effector relative to the workpiece to errors in the relative location of coordinate frames attached to successive components of the structural loop. The latter so-called parametric errors describe the combined effect of all error sources on the geometry of the structural loop segment enclosed by two successive frames. The developed kinematic model can be applied to multi-axis machines composed of revolute and prismatic joints in an arbitrary serial configuration. It is completely defined by the nominal geometry of the structural loop.

In Chapter 3, the parametric errors are related to the status of the machine (e.g. the nominal position of the axes) and its environment. This requires models for the geometric, finite stiffness, and thermal errors. The thermal errors of multi-axis machines require a relatively large modelling effort. Especially if these models have to describe deflections under dynamic or transient conditions (e.g. during the heating cycle of the machine). This case either requires the use of many temperature sensors to assess the (non-linear) temperature field under dynamic conditions, or models that relate the shape of the temperature field to changes in the process parameters, heat sources, or temperature readings in time. Both approaches are studied. Theoretical analysis of the machine's thermodynamic behaviour and thermal deformations is included to improve the quality of the model and to reduce the experimental effort required for its estimation.

Direct measurement of the parametric errors is costly, both in terms of equipment and time. Practice has shown that especially geometric errors can change significantly due to machine usage, and that the resulting accuracy variation has to be checked periodically. Therefore, a general method is developed in Chapter 4 to estimate the parametric errors from relatively simple artifact measurements. Criteria are derived to evaluate the efficiency of such a calibration. These criteria address the accuracy of the estimated parametric errors and the accuracy of the resulting model for the machine errors. The criteria are applied to optimize the location and choice of the artifacts used.

Chapter 5 covers the evaluation and verification of the estimated error models by comparing the predicted and actual errors of characteristic tasks executed by the studied milling machine and the CMM. Here the models are applied to enhance the machine accuracy by software error compensation.

Finally, the research is summarized in Chapter 6. Conclusions are presented together with recommendations for future research.

2

The kinematic error model

In this chapter a so-called kinematic error model of the machine accuracy is derived. This model relates errors in the relative location of the end-effector to errors in the relative location of coordinate frames attached to successive elements of the structural loop. The latter, so-called parametric errors, describe the combined effect of all error sources on the geometry of the structural loop enclosed by two successive frames. The kinematic model enables the separation of the structural loop into different segments, whose errors can be measured and analysed independently. The developed kinematic model can be applied to multi-axis machines composed of revolute and prismatic joints in an arbitrary serial configuration. It is completely defined by the nominal geometry of the structural loop. The model has been published [108] and was successfully applied to model the geometric errors of a five-axis milling machine [115, 94]. In Appendix A, the kinematic model is used to evaluate the uncertainty of a measured or realized end-effector location, given the uncertainty of the parametric errors.

2.1 Introduction

The accuracy of a task executed by a multi-axis machine is determined by errors in the trajectory of the end-effector relative to a certain reference. Two alternative approaches are possible to model these errors.

In the first instance, errors in the relative position and orientation of the end-effector are measured for a suitable number of points within the working capacity. These measurements can be repeated for various loading and thermal conditions. Using these data, an empirical model is estimated that relates the machine errors to the position of the machine axes and other relevant variables that were varied during the measurements (e.g. workpiece weight). In general, simple linear models (e.g. polynomials) are used for this purpose. The obtained 'black box' model, whose parameters are basically vehicles for adjusting the fit to the data, does not reflect any physical considerations about error sources and error propagation.

A typical example of this approach is the 'error-matrix' method reported by Dufour [39]. Here, the position errors of a machine tool are measured and stored at various positions in the machine workspace for different loading (workpiece weight and cutting force) and thermal conditions. The error in the position of the tool under certain conditions is obtained by linear interpolation between the stored values and used to compensate the trajectory of the tool. The cited article does not describe experimental results nor a measurement setup.

Sata [92] describes a similar approach to model and compensate the geometric errors of a machining centre in a single plane. A calibrated master part consisting of nine well-finished blocks placed in lattice form on a base plate is used to determine the errors in the position and orientation of the tool. The spindle head is moved to the centre of each block, and errors in its realized position and orientation are calculated from the readings of seven displacement sensors attached to the spindle head. To calculate the error components at an arbitrary point in the plane, it is assumed that these components can be expressed by quadratic functions of the axis coordinates (including cross-terms). Using linear least squares regression, the unknown parameters in these functions are estimated from the experimental data. The choice of the model is not explained.

A 'black box' approach using linear regression techniques is also used by Theuws [115] to model the thermal errors of a five-axis milling machine. At several positions in the machine workspace the thermal drift in the position of

the tool is measured using eddy current displacement transducers. The spindle drive and spindle bearings were identified as the main heat source of this machine. Therefore various load patterns of spindle speed are applied during the experiments. Using these data, a model is estimated that relates the drift of the tool holder at the tested position to the values of various temperature sensors attached to the machine. The chosen model describes the tool drift as a weighted sum of various temperatures. Extensive statistical analysis is performed to identify the significant temperature sensors and to avoid overfitting of the data. The drift at an arbitrary position in the machine workspace is obtained by linear or quadratic interpolation between the modelled drift at the tested positions.

In the second modelling approach, known as parametric error modelling, the machine errors are described as an analytical synthesis of errors introduced in the structural loop components. The core of this approach is the kinematic error model. This model relates the errors in the relative location of the end-effector to errors in the geometry of consecutive structural loop segments. The latter so-called parametric errors describe the combined effect of the various error sources on the geometry of structural loop components that constitute such a segment, including the joints. The propagation of the parametric errors to the errors in the realized end-effector trajectory is a geometric problem, completely defined by the nominal geometry of the structural loop. The kinematic model is therefore a known mathematical entity. In general, the errors of multi-axis machines are small to such an extent that the parametric errors of different structural loop segments do not affect each other. Thus, the kinematic model enables the separation of the structural loop into different segments whose errors can be individually measured and analysed.

As shown in the next section, parametric models are successfully applied to describe the geometric errors of a large variety of multi-axis machines. The main reason for this success is that the kinematic model enables a significant reduction of the measurements required to estimate the machine errors. As explained in Section 1.2, the effect of a geometric error on the geometry of a structural loop segment is either constant or dependent on the position of the joint(s) in that segment. Dividing the machine into segments that contain only one joint, yields a model where the respective geometric parametric errors are

related to the position of one joint only. This greatly reduces the required calibration effort. For example, a machine consisting of three prismatic joints requires a calibration where the geometric errors are only measured along three lines in the workspace. In contrast, the 'black box' approach requires the errors in the location of the end-effector to be measured at many different positions in its workspace (e.g. according to a three dimensional lattice).

In this thesis we have chosen for the parametric modelling approach. The use of the known error propagation mechanism, as described by the kinematic model, results in an error model that is more reliable, requires less calibration effort, and yields more insight. Since the errors of the machine are explicitly related to the errors introduced in the components of the machine, the approach facilitates the integration of analytical and empirical considerations concerning the effect of various error sources on these components. Furthermore, the errors of the machine can be directly related to the properties and quality of the hardware components used and vice versa.

The usefulness of a kinematic error model is determined by a number of properties, that can be summarized as:

- **Completeness.** The model must contain a sufficient number of parametric errors to express any possible variation in the geometry of the structural loop that results in a relative error in the location of the end-effector in its sensitive direction.
- **Proportionality.** Small changes in the geometry of the structural loop should be reflected by small variations of the parametric errors [42]. This property is especially important to assure numerical stability of algorithms used for identification of the unknown parameters.
- **Equivalence.** The first kind of equivalence reflects the ability to establish a relationship between the functional form of the model and that of any other acceptable model [42]. For error compensation purposes, it is desirable if this equivalence can be extended to the model used in the controller or programming unit of the machine. For example, in the case of industrial robots it is advantageous if the various error parameters can be translated to an appropriate variation of the popular

Denavit-Hartenberg parameters [32] often used to describe the nominal kinematics of the robot. The second kind of equivalence refers to the ability that the identified parametric errors can be easily translated to the geometry of the components that constitute the structural loop. This capability is obviously important if the accuracy of the machine is to be related to the quality of the hardware components used. It further facilitates the integration of models that describe the response of the machine components to various error sources. Finally the parametric errors should have an easy geometric interpretation and should be easy to measure.

- **Independency.** The parametric errors used to describe errors in the geometry of structural loop segments should be mutually independent. Especially the parametric errors of a segment should not be affected by those of another segment.
- **Modularity.** In view of the large variety of multi-axis machines, the model should be modular and structured, so that it can be easily modified to be applicable to different machine structures.

2.2 Literature overview

The fundamentals of parametric error modelling can be attributed to Ernst Abbe [1]. Abbe realized that the accuracy of measured or generated displacements is affected by unwanted angular motions of the machine's moving elements. In single axis distance measuring problems, Abbe showed that first order measurement errors are introduced that approximately equal the product of the angular motion with the distance between the line of motion and the effective axis of the displacement measurement system. This distance is usually referred to as the 'Abbe offset' (see Figure 2.1).

In his paper, Abbe briefly notes that the displacement errors introduced by unwanted angular motions are not related to the position of the centre of rotation (to the first order). This for parametric error modelling fundamental observation can be explained using rigid body kinematics. In general the in-

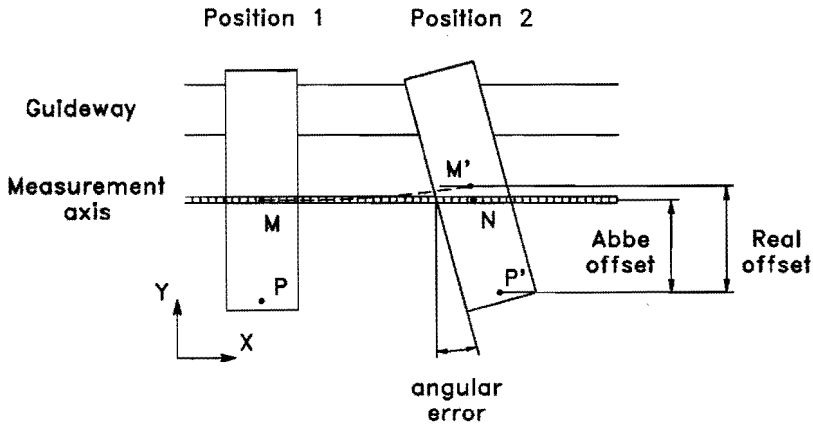


Figure 2.1: Unwanted angular motion introduces an error in the X-position of point P that approximately equals the relative angular error times the Abbe offset.

stantaneous axis of rotation of an angular error is unknown and its position is constantly changing. However, any rigid body displacement of the moving element can be described by the translation of an arbitrary reference point followed by the rotation around the translated point. In Abbe's analysis, the reference point (point M in Figure 2.1) is originally located on the effective axis of the displacement measurement system. The translation of the reference point during movement can be decomposed into a translation orthogonal to the axis of movement (straightness error) and a translation in the direction of the displacement measurement system. The latter translation is measured by the measurement system and its error is thus reduced to the measurement error of that system. The change of the Abbe offset due to the straightness error of the guideway results in a second order effect on the evaluated displacement that usually can be neglected. In fact, the exact change of the Abbe offset is usually unknown, since the effective axis of the measurement system is not necessarily straight nor aligned. Thus, the error in a generated displacement parallel to the axis of the measurement system approximately equals the sum of the relative error introduced by the displacement measurement system with the effect of the relative angular error as defined by the Abbe offset.

From Abbe's analysis it is evident that the errors in the displacement of a rigid body can be described by the errors in the position of an *arbitrary* reference point rigidly connected with that body, as well as angular errors whose centre of rotation is coincidental with the actual position of the reference point. Thus, the errors in the actual location of a carriage moved by either a prismatic or a revolute joint are described by three rotational and three translational errors, corresponding to the degrees of freedom of that body. From these six parametric errors, the translation of an arbitrary point on the carriage can be calculated, if its nominal position relative to the reference point is known. For most multi-axis machines the parametric errors are very small. It is sufficient to define them as translations and rotations along/about mutually perpendicular axes, usually the machine axes (See Figure 2.2).

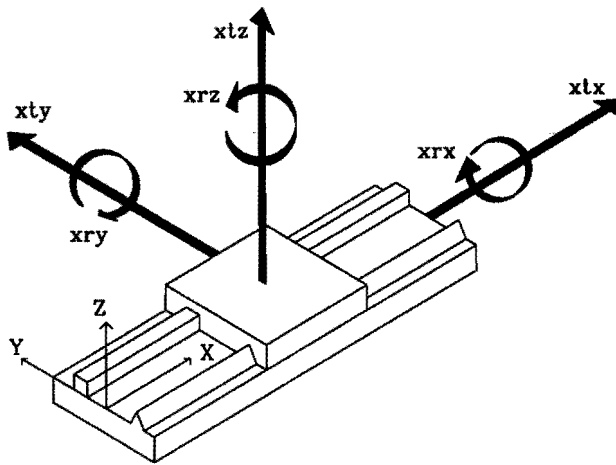


Figure 2.2: The three rotational and three translational errors in the location of a carriage. The used notation is according to the VDI-2617 guideline on the performance evaluation of CMMs [124]. Here the first character of each error denotes the axis of movement.

As stated in the introduction of this chapter, the accuracy of a task executed by a multi-axis machine is determined by errors in the trajectory of the end-effector relative to a reference. In general, the location of this reference relative to the machine is determined by an alignment procedure using the machine. This implies that for a machine consisting of one joint, only variations of the various rotational and translational errors during a task are impor-

tant, not their absolute values. In case of a prismatic joint, the workpiece is usually aligned to the average line of motion of the carriage. Therefore translational errors orthogonal to the nominal movement (straightness errors) are measured and defined relative to the average line of movement (usually specified in a least squares sense). Similarly, the errors of a revolute joint are usually defined relative to the average axis of rotation. This implies that translational and rotational errors along/about axes orthogonal to the joint axis have no once-per-revolution sinusoidal component. In case of a revolute joint, however, constant errors in the geometry of the moving element are important. This is due to the change in the effect of these errors dependent on the position of the joint. The information that parametric errors must contain to describe the relative errors in the end-effector location is more extensively discussed in Appendix B.

When two or more axes are combined, other parametric errors must be included to specify the relative location of the axes. Two of the most common are orthogonality (also called squareness or perpendicularity) and parallelism [50]. Usually the average axis of motion of one joint is defined as reference, and the other axes are defined from it. For a machine consisting of two nominally orthogonal prismatic joints, one squareness parameter is needed to describe the actual angle between the two average axes of motion. This parameter can be added as an offset value to the respective angular error of the first carriage. Similarly, a third joint would require two additional squareness parameters to describe its orientation relative to the plane spanned by the first two axes.

A number of the above concepts were collected by Schlesinger, who in 1932 established a systematic framework of measurements for acceptance testing of machine tools [97]. Formulated from the viewpoint of machine tool building, these tests were focused on the straightness of guideways, their mutual squareness, and their parallelism or squareness with the spindle axis [119]. Schlesinger's classic tests were intended for manually operated machines, where the skilled operator measured the workpiece during an operation and was able to eliminate functional effects, such as deformations due to weights, clamping forces, thermal influences, or dynamic displacement errors [59]. Especially with the introduction of NC machine tools, the measurement and definition of parametric errors were further refined, e.g. regarding the effect

of unwanted angular motions upon errors of positioning and straightness at various offsets, and spindle rotation accuracy (see e.g. Bryan [17, 18, 15], Ericson [41], and Tlusty [117, 121, 122, 119]).

For analysis, prediction, and compensation purposes, kinematic models were introduced describing the combined effect of the parametric errors on the machine accuracy. As in Abbe's analysis, the models are based on the fundamental assumption that the various errors are small compared to the characteristic dimensions of a machine task. This enables the use of first order approximations in the analysis of the effect of angular errors. Thus models are obtained where the errors in the relative location of the end-effector are expressed as a known linear combination of the various parametric errors. With the exception of misalignment errors (e.g. in the location of the workpiece relative to the machine), we found no cases in the existing literature where errors have to be described with such a high relative accuracy that second or higher order effects have to be considered. In Section 2.3 it is shown that this would lead to nonlinear kinematic models and complex error definitions.

Early approaches to kinematic modelling presented by for example Leete [64], Wong [138], French [47], and Love [65] rely on trigonometric techniques to individually analyse the effect of each parametric error. Later work is either implicitly or explicitly based on the use of coordinate frames. These frames are rigidly attached to various components of the structural loop. The parametric errors are defined as the three angular and three translational errors in the relative location of two successive frames. The mathematics of rigid body kinematics is used to model the propagation of these parametric errors to the errors in the relative location of the end-effector. This systematic approach allows a complete analysis of any machine structure without resorting to complicated and error prone geometric arguments [51].

Examples of models based on the coordinate frame approach can be found in the work of Belforte [8], Busch [20], Donmez [33, 35], Duffie [38, 37], Ferreira [45, 44, 46], Hocken [51], Kruth [60], Portman [86], Schultschik [98, 99, 100], and Zhang [144]. Only subtle differences between the various presentations can be identified, e.g. regarding the mathematical apparatus used to derive the models, the place where the errors are defined, and the treatment of machines

with moving tables. In many cases, the models are intended for the analysis of geometric errors only.

In most reports the errors between two coordinate frames are mathematically described by a 3×1 translation vector followed by a 3×3 rotation matrix. The use of a homogenous coordinate representation enables Donmez and Ferreira to model the errors between two frames by a single 4×4 transformation matrix.

The parametric errors of a certain axis are generally defined in the tip of a reference end-effector, when all axes higher in the kinematic chain from work-piece to end-effector are at home position. They are defined along/about the axes of the machine coordinate system. Thus the various coordinate frames nominally coincide when all joints are at home position. The advantage of this error definition is that Abbe offsets are only determined by the position of the machine axes and the dimensions of the used end-effector. Thus a relatively simple kinematic model is obtained that contains a minimum number of Abbe offsets and is largely independent of machine construction parameters (e.g. the position of the scales relative to the machine workspace). A disadvantage of this approach is that the parametric translation errors cannot be directly related to the straightness of the used guideways, the quality of the position measurement systems, and vice versa. This probably motivated Ferreira [45, 44, 46] to define the parametric errors in the centroid of the joints. He furthermore separates these errors into those introduced by the shape of the joint guideway and those introduced in the link connecting two joints. In early work by Schultschik [99], the parametric errors are defined on the effective line of the position measurement system of an axis, and thus can be directly related to the quality of that system. Various definitions of the parametric errors are discussed in Section 2.4.

Squareness errors are usually defined in the tip of a reference end-effector when all axes are at zero position. In some cases their definition equals that of related angular parametric errors and is implemented as an offset value 2.3. Some researchers (e.g. Kunzmann [62]) define and implement squareness as the average angular error between two axes.

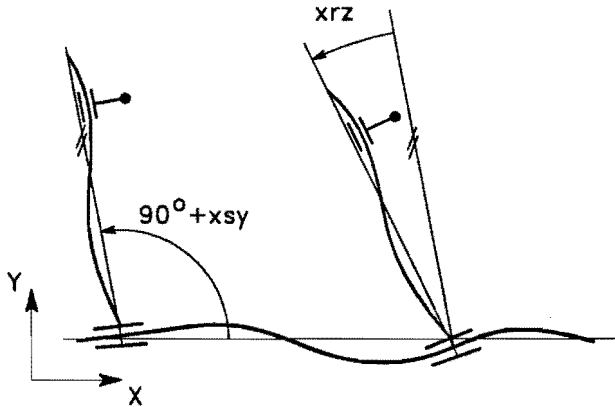


Figure 2.3: Implementation of the squareness error x_{sy} between the X- and Y- axis as an offset value for the x_{rz} error. The squareness error between both axes at a certain position equals the sum of x_{sz} and x_{rz} .

In the few cases where revolute joints have been considered (spindle errors), its parametric errors are defined in a point on the (average) axis of rotation. Neumann [79] characterizes the accuracy of a CMM rotary table by four error parameters (two translations and two rotations). These parameters are also used in the VDI-guideline on the performance evaluation of CMMs [125]. In our opinion this approach does not satisfy the completeness requirement.

Researchers who have analysed machines with moving tables (e.g. [51, 86, 33, 45, 99]) usually evaluate the kinematics of the machine from table to end-effector. Relative to the table, the definition of the parametric errors equals that of a machine with a fixed table. Hocken [51] and Schultschik [99] take a different approach. Here the structural loop is separated into two kinematic chains, one from machine base to end-effector (the tool chain [99]) and one from machine base to workpiece (the workpiece chain [99]). Both chains are evaluated from machine base to respectively end-effector and workpiece. This implies that the parametric errors of the workpiece chain will have an opposite sign to similar errors in models where the kinematic chain is evaluated from table to end-effector.

The above kinematic models were generally developed for, and applied to, measuring machines and machine tools. Although, at least in principle, these models can also be applied to industrial robots, this has to our knowledge not

been tried in the existing literature. Instead, the area of industrial robots is characterized by a different approach to kinematic modelling. Here much research is focused on describing the effect of constant errors in the nominal robot parameters used to calculate the trajectory of the end-effector as a function of the joint positions. Typical examples are errors in the geometry of links and encoder offsets. Due to the abundance of revolute joints, industrial robots are very sensitive to this class of errors. With the exception of finite stiffness effects and encoder errors, parametric errors that change with the position of the joints have received relatively little attention.

This different approach has resulted in kinematic models that usually contain fewer parametric errors than the models used to describe machine tools and measuring machines. This can be explained by considering a robot consisting of R revolute joints and P prismatic joints. In accordance with the above paragraph, we only consider the effect of constant errors in the links and joints. If all joints are at home position, 6 error variables are required to describe the errors in the location of the end-effector relative to a reference. The trajectory of the end-effector due to the movement of a prismatic joint requires two error variables that describe errors in the orientation of the joint axis. Note that all other constant errors introduced by the joint are already included in the initial location of the end effector. Similarly, a revolute joint needs only 4 error variables. These errors describe the position and orientation of the axis of rotation. Again, the constant translation and rotation errors along/about the joint axis are already included in the initial location of the end-effector. Thus the robot requires a kinematic model with $6 + 4R + 2P$ parametric errors, if its links and joints have constant errors. A formal proof of this conclusion has been presented by Everett [42, 43]. If the reference frame of the task is determined by the machine (without errors), the number of (constant) parametric errors can be reduced to $4R + 2P$.

The joints of an industrial robot are controlled by a computer which uses a kinematic model of the robot to compute the relationship between the values of the joint coordinates and the relative location of the end effector. The number and character of the parameters used in these models equals that of the above mentioned constant parametric errors. Thus the effect of constant errors can be described by (constant) errors in these parameters. Researchers who

attempted to use this approach encountered serious problems due to the lack of proportionality and independence of these parametric errors.

Since less than six parameters are used to describe the relative location of two bodies, robot models have a set of rules regarding the assignment of coordinate frames to these bodies. For example, the popular Denavit-Hartenberg convention [32, 81] requires the origin of a frame describing the location of a link to be at the intersection of a revolute joint axis and the common normal with a consecutive revolute joint (see Figure 2.4). One of the model parameters describes the distance of this origin to a similar intersection defined by the common normal with a preceding revolute joint. This distance is influenced by the relative orientation of both the preceding and consecutive revolute joints. Thus the respective error is dependent on orientation errors and is influenced by the geometry of two links. Furthermore, if consecutive axes are nearly parallel, small changes in their relative orientation can cause large changes in this error.

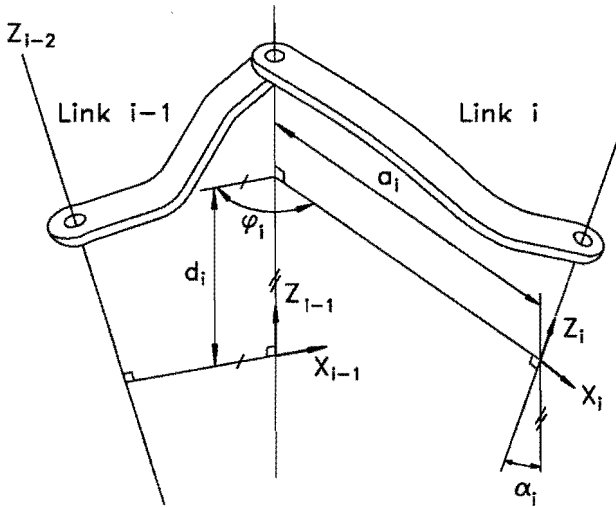


Figure 2.4: Coordinate frame placement according to the Denavit-Hartenberg convention. The relative location of two successive coordinate frames is described by the parameters d , φ , a , and α .

To overcome these undesirable characteristics, a large number of alternative kinematic models have been proposed (for a comprehensive review see e.g. [42, 146]). These models use alternative frame placement rules (e.g. for near

parallel axes) or require extra parametric errors. However, only when six parametric errors are used to describe the relative location of two frames, i.e. when there are no rules that restrict the relative location of frames attached to the actual machine structure, proportionality can be guaranteed for any machine configuration [146]. In that case the same error model can be used if variable errors have to be described. However, the various parametric errors will be mutually dependent if the analysis is limited to machines with constant errors. Since a six-errors-per-joint error model is complete, it can describe any variation in the parameters of the kinematic model used in a robot controller. If the errors are constant, both models are complete and the respective parametric errors can be extracted from each other (see e.g. Stone [112]).

2.3 Mathematical description kinematic model

2.3.1 The chosen approach

In this section, a kinematic model is derived using an explicit coordinate frame approach. The obtained model relates errors in the relative location of coordinate frames attached to end-effector and workpiece to errors in the relative location of coordinate frames attached to successive components of the structural loop. The latter (parametric) errors describe the difference between the nominal and actual geometry of structural loop components enclosed by two successive frames. The modelling method can be applied to multi-axis machines composed of revolute and prismatic joints in an arbitrary serial configuration. The explicit use of coordinate frames provides a highly systematic framework to assess the errors of multi-axis machines. Although the modelling technique is more complicated than a trigonometric or error vector approach in case of machines consisting of prismatic joints in a cartesian configuration, it especially facilitates error modelling if the machine contains revolute joints.

The derived model has a number of characteristics that can be summarized as:

- **Linear.** The errors in the relative location of the end-effector are expressed as a known linear combination of the various parametric errors. This requires two approximations. First, a first order approximation is used for the effect of angular errors (i.e. $\cos \varepsilon \approx 1$, $\sin \varepsilon \approx \varepsilon$). Second, it is assumed that the difference between the nominal and actual structural loop geometry does not significantly change the active arm of angular errors and the direction in which the various errors act. These approximations are valid for most multi-axis machines, even if they have significant finite stiffness related errors. Only if the model has to predict the errors with an extremely high relative accuracy, a nonlinear approach may be necessary. At the end of this section the merits and problems of a nonlinear approach will be discussed.
- **Two kinematic chains.** The multi-axis machine is divided into two kinematic chains. The so-called *A* chain or tool chain contains the components that support the end-effector relative to the base frame of the machine. Similarly the *B* chain or workpiece chain contains the components that support the workpiece. Both *A* and *B* chain are evaluated from machine base to respectively end-effector and workpiece. Compared to one kinematic chain from workpiece to end-effector, the use of two chains facilitates the integration of parametric error measurements into the model. It is common practice to measure these errors as [50]:
 - if the carriage function is to carry the tool (i.e. the carriage is part of the *A* chain), measurements are made relative to a nominal workpiece position.
 - if the carriage function is to carry the workpiece (i.e. the carriage is part of the *B* chain), measurements are made relative to a nominal tool position.

Furthermore, the interpretation of the resulting parametric errors is intuitively more appealing. For both *A* and *B* chain they describe the errors in the location of a moving carriage relative to a guideway.

- **Actual minus nominal.** The parametric errors in the derived kinematic model describe the difference between the actual and nominal geometry of parts enclosed by two successive coordinate frames. Here a

sign convention is used corresponding to actual geometry minus nominal geometry. Similarly, the errors in the relative location of the end-effector are defined as actual location minus nominal location. For measuring machines, however, the errors in the measured position of a point equal the reversed error in the realized position of a point (see Figure 2.5). Therefore it is common practice to define the parametric errors of CMMs according to a nominal minus actual convention (See e.g. the VDI 2617 guideline on the performance evaluation of CMMs [124]). Since many machines are used both for measuring and positioning purposes, we decided to avoid confusion and treat all devices as positioning equipment. Dependent on the function of the machine, the errors in the relative location of the tool are translated into the errors of the executed task with the appropriate signs.

- **Complete structural loop.** The derived model describes the effect of errors introduced in the complete structural loop, including errors related to the location and deformation of the workpiece.
- **Squareness as offset.** Squareness errors are implicitly contained in the model as an offset value for certain angular errors. This offset is adjusted such that the respective angular error describes the measured squareness error at a certain axis position.

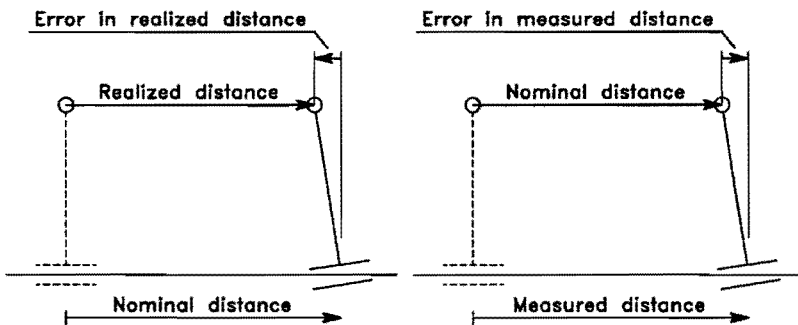


Figure 2.5: The direction of the error in a realized distance is opposite to that in the measured distance.

2.3.2 Nomenclature coordinate frames

The basic function of the kinematic model is to describe how errors in the geometry of structural loop components affect the relative location of the tool. Variations in the error propagation are only due to the position of the machine joints and the dimensions of the used end-effector (to the first order). Therefore, the number and position of the coordinate frames is chosen such that there is one kinematic element between every two frames. It should be noted that the analysis presented below can be applied to any choice of the number and orientation of the coordinate frames.

Starting with the global coordinate frame 0 attached to the base of the multi-axis machine, the orthogonal frames are successively numbered. As depicted in Figure 2.6, a prefix is added to this number in order to identify the corresponding frame as being part of chain *A* from machine base to end-effector or chain *B* from base to workpiece. Three additional frames *tl*, *wr*, and *wf* are used in the analysis. The tool frame *tl* is attached to the end-effector and describes the location of its interaction with the workpiece. The workpiece reference frame *wr* is usually attached to the workpiece and represents the reference relative to which the manufacturing task is defined. In other words, only errors relative to this frame are important. Finally, the workpiece feature frame *wf* describes the location of the workpiece area where interaction with the end-effector is desired.

The nominal location of the tool frame *tl* coincides with the nominal workpiece feature frame *wf* during those parts of the manufacturing task where there is an interaction between end-effector and workpiece. In reality, errors can be identified in the location of both frames relative to the workpiece reference frame *wr* that degrade the accuracy of the executed task. The errors in the location of frame *tl* relative to frame *wr* can be attributed to the multi-axis machine, the end-effector, and the location of the workpiece relative to the machine (i.e. alignment errors). Errors in the relative location of frames *wf* and *wr* are caused by the deformation of the workpiece, e.g. due to thermal expansion.

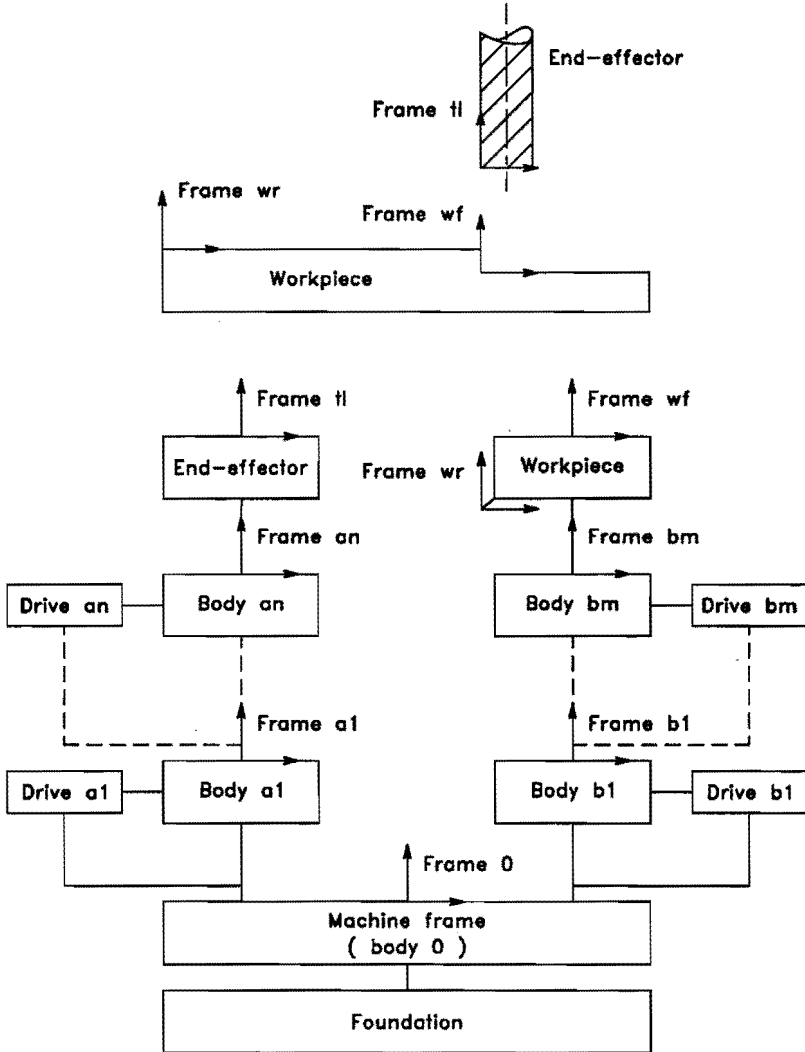


Figure 2.6: Nomenclature of the coordinate frames attached to a multi-axis machine with $n + m$ kinematic elements.

2.3.3 Derivation of the model

In this subsection, the errors in the relative location of frames tl and wr are related to the errors in the relative location of successive coordinate frames that constitute the structural loop between these frames. Dependent on the task of the machine, these errors are combined with the workpiece deformation, i.e. the errors between frames wf and wr , to describe the errors of either a realized or measured feature frame location on the undeformed workpiece.

The spatial relationship between coordinate frames can be effectively described using homogeneous transformations (see e.g. [81]). A homogeneous transformation relates the homogeneous coordinate representation of an object in two different coordinate frames by a single 4×4 matrix. The homogeneous coordinate representation of an object can be viewed as the addition of an extra coordinate to each vector, a scale factor, such that the vector has the same meaning if each component, including the scale factor, is multiplied by a constant.

The nominal relation between the homogeneous coordinates ${}_k\mathbf{p}$ and ${}_l\mathbf{p}$ of a point p in frames k and l , respectively, is described by the 4×4 transformation matrix ${}_kT_l$ [81]:

$${}_k\mathbf{p} = {}_kT_l {}_l\mathbf{p} \quad (2.1)$$

where:

$${}_kT_l = \begin{bmatrix} {}_kR_l & {}_k\mathbf{t}_l \\ 0 & 0 & 0 & 1 \end{bmatrix} \quad (2.2)$$

$${}_k\mathbf{p} = \begin{bmatrix} {}_k p_x & {}_k p_y & {}_k p_z & 1 \end{bmatrix}^T \quad (2.3)$$

In this transformation the 3×3 matrix ${}_kR_l$ describes the orientation of frame l relative to frame k . Its columns contain the unit direction vector components of the X , Y , and Z axes of coordinate frame l in terms of coordinate frame k . The 3×1 vector ${}_k\mathbf{t}_l$ specifies the position of the origin of coordinate frame l relative to frame k . Since matrix ${}_kR_l$ is orthogonal, the inverse transformation can be expressed as:

$${}_l\mathbf{p} = {}_lT_k {}_k\mathbf{p} \quad (2.4)$$

where:

$${}^i T_k = \begin{bmatrix} {}^k R_i^T & -{}^k R_i^T \mathbf{k} \mathbf{l}_i \\ \mathbf{0} & 1 \end{bmatrix} \quad (2.5)$$

For a multi-axis machine with n kinematic elements in chain A and m elements in chain B , successive application of these transformations yields the following expression for the nominal location ${}_{wr} T_{tl}$ of the tool coordinate frame tl in the workpiece reference coordinate frame wr :

$${}_{wr} T_{tl} = {}_{wr} T_0 {}_0 T_{tl} \quad (2.6)$$

$$= {}_{wr} T_{bm} \prod_{k=m}^1 ({}_{bk} T_{bk-1}) \prod_{k=1}^n ({}_{ak-1} T_{ak}) {}_{an} T_{tl} \quad (2.7)$$

In the actual multi-axis machine, errors in the geometry of structural loop components cause errors in the relative location of successive coordinate frames. Because none of the contemporary multi-axis machines shows an absence of Abbe offsets, the relevant errors in the relative location of successive frames are not limited to those in the moving direction of an enclosed kinematic element. Consequently, the following errors are to be considered in the relative location of two successive frames $k-1$ and k :

- rotational errors ${}_{k-1} \epsilon_{k_x}$, ${}_{k-1} \epsilon_{k_y}$, and ${}_{k-1} \epsilon_{k_z}$ about the X , Y , and Z axes of frame k respectively.
- translational errors ${}_{k-1} e_{k_x}$, ${}_{k-1} e_{k_y}$, and ${}_{k-1} e_{k_z}$ along the X , Y , and Z axes of frame k respectively.

In the analysis of the effect of angular errors on the machine accuracy, a first-order approximation is used (i.e. $\cos(\epsilon) \approx 1$ and $\sin(\epsilon) \approx \epsilon$). Application of this approximation yields additive and commutative properties for the various errors. Thus, the angular errors can be defined as rotations about mutually perpendicular axes. Due to these properties, the various angular and translational errors between two frames can be combined into a single vector ${}_{k-1} \underline{E}_k$, because they possess all the properties that vectors in a vector field must satisfy. Geometrically, the direction of the rotation subvector ${}_{k-1} \underline{\epsilon}_k$ represents the axis of rotation, and its length represents the magnitude of the rotation.

The first order approximation, yields the following relationship between the actual transformation ${}_{k-1}\mathbf{Ta}_k$ and its nominal ${}_{k-1}\mathbf{T}_k$:

$$\begin{aligned} {}_{k-1}\mathbf{Ta}_k &= {}_{k-1}\mathbf{T}_k \cdot \\ &\quad \text{Trans} [x, {}_{k-1}e_{k_x}] \cdot \text{Trans} [y, {}_{k-1}e_{k_y}] \cdot \text{Trans} [z, {}_{k-1}e_{k_z}] \cdot \\ &\quad \text{Rot} [x, {}_{k-1}\varepsilon_{k_x}] \cdot \text{Rot} [y, {}_{k-1}\varepsilon_{k_y}] \cdot \text{Rot} [z, {}_{k-1}\varepsilon_{k_z}] \quad (2.8) \\ &= {}_{k-1}\mathbf{T}_k (I + {}_{k-1}\delta\mathbf{T}_k) \quad (2.9) \end{aligned}$$

where:

- Trans $[x, {}_{k-1}e_{k_x}]$: translation along the local X axis by a distance ${}_{k-1}e_{k_x}$
- Rot $[x, {}_{k-1}\varepsilon_{k_x}]$: rotation about the local X axis by an angle ${}_{k-1}\varepsilon_{k_x}$
- I : 4×4 identity matrix

$${}_{k-1}\delta\mathbf{T}_k = \begin{bmatrix} 0 & -{}_{k-1}\varepsilon_{k_z} & {}_{k-1}\varepsilon_{k_y} & {}_{k-1}e_{k_x} \\ {}_{k-1}\varepsilon_{k_x} & 0 & -{}_{k-1}\varepsilon_{k_x} & {}_{k-1}e_{k_y} \\ -{}_{k-1}\varepsilon_{k_y} & {}_{k-1}\varepsilon_{k_x} & 0 & {}_{k-1}e_{k_z} \\ 0 & 0 & 0 & 0 \end{bmatrix} \quad (2.10)$$

Similarly, the actual location ${}_{wr}\mathbf{Ta}_{tl}$ of the tool coordinate frame relative to the reference can be expressed as:

$${}_{wr}\mathbf{Ta}_{tl} = {}_{wr}\mathbf{T}_{tl} (I + {}_{wr}\delta\mathbf{T}_{tl}) \quad (2.11)$$

where:

$${}_{wr}\delta\mathbf{T}_{tl} = \begin{bmatrix} 0 & -{}_{wr}\varepsilon_{tl_z} & {}_{wr}\varepsilon_{tl_y} & {}_{wr}e_{tl_x} \\ {}_{wr}\varepsilon_{tl_z} & 0 & -{}_{wr}\varepsilon_{tl_x} & {}_{wr}e_{tl_y} \\ -{}_{wr}\varepsilon_{tl_y} & {}_{wr}\varepsilon_{tl_x} & 0 & {}_{wr}e_{tl_z} \\ 0 & 0 & 0 & 0 \end{bmatrix} \quad (2.12)$$

Here transformation ${}_{wr}\delta\mathbf{T}_{tl}$ contains the errors in the location of the tool frame tl relative to the workpiece reference frame wr . It consists of angular errors ${}_{wr}\underline{\varepsilon}_{tl} = [{}_{wr}\varepsilon_{tl_x}, {}_{wr}\varepsilon_{tl_y}, {}_{wr}\varepsilon_{tl_z}]^T$ defined about the X , Y , and Z axes of the nominal tool frame tl and translation errors ${}_{wr}\underline{e}_{tl} = [{}_{wr}e_{tl_x}, {}_{wr}e_{tl_y}, {}_{wr}e_{tl_z}]^T$ along these axes. Successive application of Equation 2.9 yields the following expression for the actual location ${}_{wr}\mathbf{Ta}_{tl}$ of the tool frame relative to the workpiece reference frame:

$${}_{wr}\mathbf{Ta}_{tl} = {}_{wr}\mathbf{Ta}_{b_m} \prod_{k=m}^1 ({}_{b_k}\mathbf{Ta}_{b_{k-1}}) \prod_{k=1}^n ({}_{a_{k-1}}\mathbf{Ta}_{a_k}) {}_{a_n}\mathbf{Ta}_{tl} \quad (2.13)$$

$$\begin{aligned}
 {}_{wr}T_{tl} &= (I - {}_{wr}\delta T_{bm}) {}_{wr}T_{bm} \cdot \\
 &\quad \prod_{k=m}^1 ((I - {}_{bk}\delta T_{bk-1}) {}_{bk}T_{bk-1}) \cdot \\
 &\quad \prod_{k=1}^n ({}_{ak-1}T_{ak} (I + {}_{ak-1}\delta T_{ak})) \cdot \\
 &\quad {}_{an}T_{tl} (I + {}_{an}\delta T_{tl})
 \end{aligned} \tag{2.14}$$

Transformation ${}_{an}\delta T_{tl}$ contains the errors in the location of the tool coordinate frame tl relative to the last frame an of the tool chain. It essentially describes the errors introduced by the used end-effector. In the case of coordinate measuring machines, these errors (i.e. the position of the measured point relative to the ram) are generally related to the probe system and probe strategy used. For metal cutting machine tools, errors such as spindle-induced errors, tool misalignment, tool wear, and thermal tool expansion can be included into this transformation.

Transformation ${}_{bm}\delta T_{wr}$ contains the errors in the location of the workpiece reference relative to the last frame bm of the workpiece chain. It essentially describes the errors introduced by the peripherals used to support the workpiece relative to the machine table. The initial value of these errors is determined by the alignment procedure of the workpiece. For a fully machined or measured workpiece, the workpiece reference frame is generated by the machine. In this case, the initial errors in its relative location are determined by the errors of the machine during alignment. Thus the accuracy of the respective task is fully determined by the variation in time and place of errors in the structural loop relative to those during alignment.

In the elaboration of Equation 2.14, an approximation is made by ignoring higher order terms consisting of the product of a matrix δT with one or more similar matrices. As explained in the introduction of this section, this approximation is valid in the context of this research. The ignored terms describe the effect of the difference between the actual and nominal geometry of structural loop components on the active arm of angular errors and the direction in which the various errors act. They are discussed at the end of this section. Due to the approximation, the propagation of the errors is defined by rigid body movement, and a linear relationship between the various errors can be formulated. Combining Equation 2.11 with Equation 2.14 now yields

the following expression for the error ${}_{wr}\delta T_{il}$ in the relative location between end-effector and workpiece reference:

$$\begin{aligned}
 {}_{wr}\delta T_{il} = & - {}_{il}T_{wr} {}_{bm}\delta T_{wr} {}_{wr}T_{il} \\
 & - \sum_{k=m}^1 ({}_{il}T_{bk} {}_{bk-1}\delta T_{bk} {}_{bk}T_{il}) \\
 & + \sum_{k=1}^n ({}_{il}T_{ak} {}_{ak-1}\delta T_{ak} {}_{ak}T_{il}) \\
 & + {}_{an}\delta T_{il}
 \end{aligned} \tag{2.15}$$

In Equation 2.15 the error ${}_{wr}\delta T_{il}$ in the relative location of the end-effector are expressed as a known linear combination of the errors ${}_{k-1}\delta T_k$ in the relative location of two successive coordinate frames. For each two successive coordinate frames $k - 1$ and k the respective contribution ${}_{wr}^k\delta T_{il}$ to ${}_{wr}\delta T_{il}$ is described by:

$${}_{wr}^k\delta T_{il} = {}_{il}T_k {}_{k-1}\delta T_k {}_kT_{il} \tag{2.16}$$

The nature of this contribution can be deduced from the transform graph [81] presented in Figure 2.7. In order to obtain an explicit relationship between the various rotational and translational errors, Equation 2.16 is further expanded:

$${}_{wr}^k\delta T_{il} = \begin{bmatrix} {}_{il}R_k & {}_{il}\underline{t}_k \\ 0 & 0 & 0 & 1 \end{bmatrix} \begin{bmatrix} {}_{k-1}\delta R_k & {}_{k-1}\delta \underline{t}_k \\ 0 & 0 & 0 & 0 \end{bmatrix} \begin{bmatrix} {}_kR_{il} & {}_k\underline{t}_{il} \\ 0 & 0 & 0 & 1 \end{bmatrix} \tag{2.17}$$

$$= \begin{bmatrix} {}_{il}R_k {}_{k-1}\delta R_k {}_kR_{il} & {}_{il}R_k {}_{k-1}\delta R_k {}_{il}\underline{t}_k + {}_{il}R_k {}_{k-1}\delta \underline{t}_k \\ 0 & 0 & 0 & 0 \end{bmatrix} \tag{2.18}$$

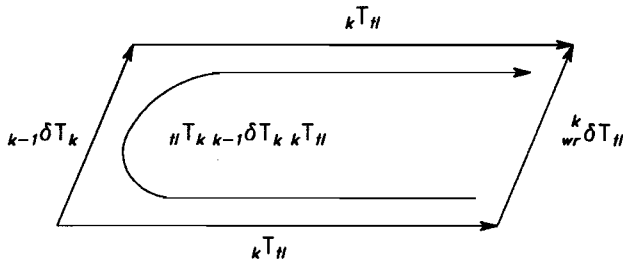


Figure 2.7: Differential transform graph for the contribution ${}_{wr}^k\delta T_{il}$ of ${}_{k-1}\delta T_k$ to the errors between frames wr and il .

Due to the first order approximation, the various errors have commutative and additive properties. Therefore the three angular errors can be combined into a single vector $\underline{\varepsilon}$. The transformation ${}_{tl}\delta R_k$ of a vector \underline{n} can be expressed as the cross product of the respective angular error vector with that vector, i.e. ${}_{tl}\underline{\varepsilon}_k \times \underline{n}$. If the column vectors of transformation ${}_k R_{tl}$ are denoted as \underline{n} , \underline{q} , and \underline{a} , Equation 2.18 can be further expanded to:

$${}^k_{wr}\delta T_{tl} = \begin{bmatrix} {}_k R_{tl}^T \begin{bmatrix} {}_{k-1}\underline{\varepsilon}_k \times \underline{n} & {}_{k-1}\underline{\varepsilon}_k \times \underline{q} & {}_{k-1}\underline{\varepsilon}_k \times \underline{a} \\ 0 & 0 & 0 \end{bmatrix} \\ {}_k R_{tl}^T \begin{bmatrix} ({}_{k-1}\underline{\varepsilon}_k \times {}_k \underline{t}_{tl}) & + {}_k R_{tl}^T {}_{k-1}\underline{e}_k \\ 0 \end{bmatrix} \end{bmatrix} \quad (2.19)$$

$$= \begin{bmatrix} \underline{n} \cdot ({}_{k-1}\underline{\varepsilon}_k \times \underline{n}) & \underline{n} \cdot ({}_{k-1}\underline{\varepsilon}_k \times \underline{q}) & \underline{n} \cdot ({}_{k-1}\underline{\varepsilon}_k \times \underline{a}) \\ \underline{q} \cdot ({}_{k-1}\underline{\varepsilon}_k \times \underline{n}) & \underline{q} \cdot ({}_{k-1}\underline{\varepsilon}_k \times \underline{q}) & \underline{q} \cdot ({}_{k-1}\underline{\varepsilon}_k \times \underline{a}) \\ \underline{a} \cdot ({}_{k-1}\underline{\varepsilon}_k \times \underline{n}) & \underline{a} \cdot ({}_{k-1}\underline{\varepsilon}_k \times \underline{q}) & \underline{a} \cdot ({}_{k-1}\underline{\varepsilon}_k \times \underline{a}) \\ 0 & 0 & 0 \end{bmatrix} \\ + \begin{bmatrix} \underline{n} \cdot ({}_{k-1}\underline{\varepsilon}_k \times {}_k \underline{t}_{tl}) \\ \underline{q} \cdot ({}_{k-1}\underline{\varepsilon}_k \times {}_k \underline{t}_{tl}) \\ \underline{a} \cdot ({}_{k-1}\underline{\varepsilon}_k \times {}_k \underline{t}_{tl}) \\ 0 \end{bmatrix} + {}_k R_{tl}^T {}_{k-1}\underline{e}_k \quad (2.20)$$

$$= \begin{bmatrix} 0 & -\underline{a} \cdot {}_{k-1}\underline{\varepsilon}_k & \underline{q} \cdot {}_{k-1}\underline{\varepsilon}_k \\ \underline{a} \cdot {}_{k-1}\underline{\varepsilon}_k & 0 & -\underline{n} \cdot {}_{k-1}\underline{\varepsilon}_k \\ -\underline{q} \cdot {}_{k-1}\underline{\varepsilon}_k & \underline{n} \cdot {}_{k-1}\underline{\varepsilon}_k & 0 \\ 0 & 0 & 0 \end{bmatrix} \\ + \begin{bmatrix} {}_k \underline{t}_{tl} \times {}_k R_{tl} \end{bmatrix}^T \begin{bmatrix} {}_{k-1}\underline{\varepsilon}_k + {}_k R_{tl}^T {}_{k-1}\underline{e}_k \\ 0 \end{bmatrix} \quad (2.21)$$

In Equation 2.21 ${}_k \underline{t}_{tl} \times {}_k R_{tl}$ denotes a 3×3 matrix whose columns contain the vector product of ${}_k \underline{t}_{tl}$ with the respective columns of ${}_k R_{tl}$. Equating the individual matrix components of Equations 2.12 and 2.21 yields the following expression for the contributions ${}^k_{wr}\underline{\varepsilon}_{tl}$ and ${}^k_{wr}\underline{e}_{tl}$ of the rotational errors ${}_{k-1}\underline{\varepsilon}_k$ and translational errors ${}_{k-1}\underline{e}_k$ to the errors in the relative location of the end-effector:

$${}^k_{wr}\underline{\varepsilon}_{tl} = {}_k R_{tl}^T {}_{k-1}\underline{\varepsilon}_k \quad (2.22)$$

$${}^k_{wr}\underline{e}_{tl} = \left[{}_k \underline{t}_{tl} \times {}_k R_{tl} \right]^T \begin{bmatrix} {}_{k-1}\underline{\varepsilon}_k + {}_k R_{tl}^T {}_{k-1}\underline{e}_k \\ 0 \end{bmatrix} \quad (2.23)$$

In Equations 2.22 and 2.23 the rotation matrix ${}_k R_{tl}^T = {}_{tl}R_k$ transforms the errors ${}_{k-1}\underline{\varepsilon}_k$ and ${}_{k-1}\underline{e}_k$ defined in frame k to the tool coordinate frame tl . The effect of the angular errors ${}_{k-1}\underline{\varepsilon}_k$ on the position error of the end-effector is

determined by their active arm ${}_{k-1}\underline{t}_{kl}$. The resulting error is again transformed to the tool frame by the rotation matrix ${}_{kl}R_{tl}^T$.

According to Equations 2.15 and 2.16, the angular and translational errors between tool and workpiece, combined in the 6×1 vector ${}_{wr}\underline{E}_{tl}$, can now be expressed as a known linear combination of similarly denoted errors in the relative location between successive coordinate frames:

$${}_{wr}\underline{E}_{tl} = - {}_{tl}F_{wr} {}_{bm}\underline{E}_{wr} - \sum_{k=1}^m ({}_{tl}F_{bk} {}_{bk-1}\underline{E}_{bk}) + \sum_{k=1}^n ({}_{tl}F_{ak} {}_{ak-1}\underline{E}_{ak}) + {}_{an}\underline{E}_{tl} \quad (2.24)$$

where:

$${}_{wr}\underline{E}_{tl} = \begin{bmatrix} {}_{wr}e_{tlx} & {}_{wr}e_{tly} & {}_{wr}e_{tlz} & {}_{wr}e_{tlx} & {}_{wr}e_{tly} & {}_{wr}e_{tlz} \end{bmatrix}^T \quad (2.25)$$

$${}_{k-1}\underline{E}_k = \begin{bmatrix} {}_{k-1}e_{kx} & {}_{k-1}e_{ky} & {}_{k-1}e_{kz} & {}_{k-1}e_{kx} & {}_{k-1}e_{ky} & {}_{k-1}e_{kz} \end{bmatrix}^T \quad (2.26)$$

$${}_{tl}F_k = \begin{bmatrix} {}_{kl}R_{tl}^T & 0 \\ \left[{}_{kl}\underline{t}_{kl} \times {}_{kl}R_{tl} \right]^T & {}_{kl}R_{tl}^T \end{bmatrix} \quad (2.27)$$

$$= \begin{bmatrix} {}_{tl}R_k & 0 \\ \left({}_{tl}\underline{t}_k \times {}_{tl}R_k \right) & {}_{tl}R_k \end{bmatrix} \quad (6 \times 6 \text{ matrix}) \quad (2.28)$$

In Equation 2.24 the 6×6 matrices ${}_{tl}F_k$ describe how the errors ${}_{k-1}\underline{E}_k$ in the relative location of two successive coordinate frames affect the errors ${}_{wr}\underline{E}_{tl}$ in the relative location of end-effector and workpiece reference. These matrices are completely defined by the nominal geometry of the structural loop. The errors ${}_{an}\underline{E}_{tl}$ in the location of the end-effector relative to the last frame an of the kinematic chain are directly added to the errors ${}_{wr}\underline{E}_{tl}$, because both are defined in the nominal tool frame tl . For some applications it is necessary to transform the errors ${}_{wr}\underline{E}_{tl}$ from the tool coordinate system to another system l , e.g. the workpiece coordinate system. This can be achieved by premultiplying the orientation and translation subvectors of ${}_{wr}\underline{E}_{tl}$ with the appropriate orientation transformation ${}_{tl}R_{tl}$. The same effect is obviously achieved by premultiplying each of the 3×3 submatrices of ${}_{tl}F_k$ with the same orientation transformation.

From a practical viewpoint, it may be worth noticing that the F-matrices follow the usual transformation rule ${}_{tl}F_{k-1} = {}_{tl}F_k {}_{kl}F_{k-1}$. The inverse F-matrix can be obtained by taking the transpose of its 3×3 submatrices. Since the nominal location of tool frame and workpiece feature frame coincide, ${}_{tl}F_{wr}$

equals ${}_{wf}F_{wr}$. The latter matrix is defined by the nominal machine task, so the explicit calculation of the nominal workpiece reference location relative to the machine (i.e. ${}_{bm}T_{wr}$) is not required.

2.3.4 Errors of elementary measurement and positioning tasks

To describe the errors of a manufacturing task, the errors ${}_{wr}E_{tl}$ between tool frame and workpiece reference frame have to be combined with the errors ${}_{wr}E_{wf}$ between workpiece feature frame and workpiece reference frame (i.e. the errors that describe the workpiece deformation). Here we have to differentiate between measurement and positioning.

Measurement

Measurement involves the estimation of the location of a workpiece feature frame wf relative to the workpiece reference frame wr . This location is calculated from the position of the machine joints when interaction is detected between workpiece and end-effector (i.e. the when the actual frames wf and tl coincide). Here a model is used based on the nominal geometry of the structural loop. Therefore, the measured relative location of the feature frame equals ${}_{wr}T_{tl}$. The real value of the measurand (quantity to be measured) equals the relative location of frame wf in the undeformed workpiece, i.e. ${}_{wr}T_{wf}$.

Using the transform graph of Figure 2.8, the error ${}^m_{wr}\delta T_{wf}$ in the measured relative location of frame wf can be expressed as:

$$(I + {}^m_{wr}\delta T_{wf}) = (I + {}_{wr}\delta T_{wf}) (I - {}_{wr}\delta T_{tl}) \Rightarrow \quad (2.29)$$

$${}^m_{wr}\delta T_{wf} \approx {}_{wr}\delta T_{wf} - {}_{wr}\delta T_{tl} \quad (2.30)$$

In the derivation of Equation 2.30, a first order approximation has been made by neglecting the second order term ${}_{wr}\delta T_{wf} {}_{wr}\delta T_{tl}$. Thus the errors ${}^m_{wr}E_{wf}$ in the measured relative location of frame wf approximately equal the errors due

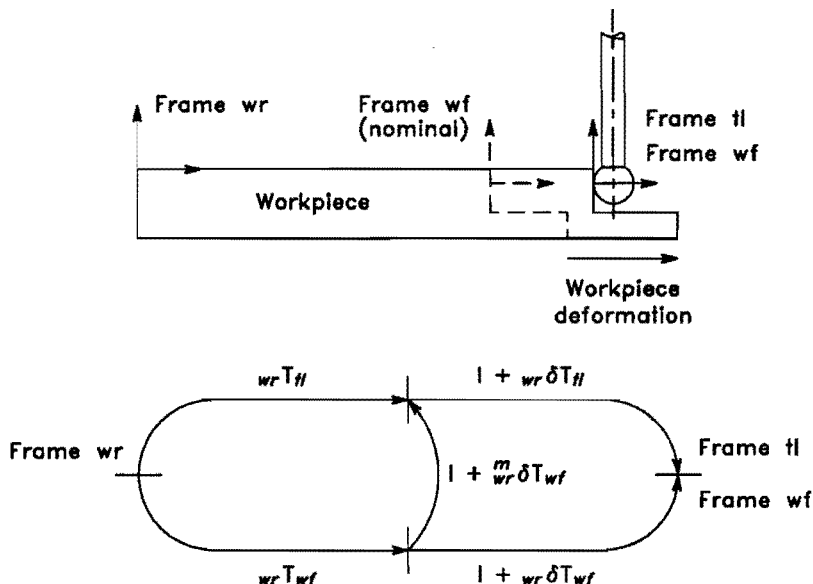


Figure 2.8: Transform graph for measurement tasks.

to the deformation of the workpiece minus the errors in the actual location of the end-effector during measurement:

$${}^m_{wr}E_{wf} = {}_{wr}E_{wf} - {}_{wr}E_{tl} \tag{2.31}$$

Note that due to the various errors, the measured feature does not equal the feature defined in the NC program of the machine. Usually this does not lead to problems, unless the characteristic dimensions of the measured object are of the same order as the errors of the structural loop.

Machining and handling

In case of machining and handling operations, the task of the machine is to realize a relative location ${}_{wr}T_{wf}$ of the workpiece feature frame wf in the undeformed workpiece. Assuming that the unwanted workpiece deformation ${}_{wr}\delta T_{wf}$ during manufacturing is reversible, the error ${}^p_{wr}\delta T_{wf}$ in the generated

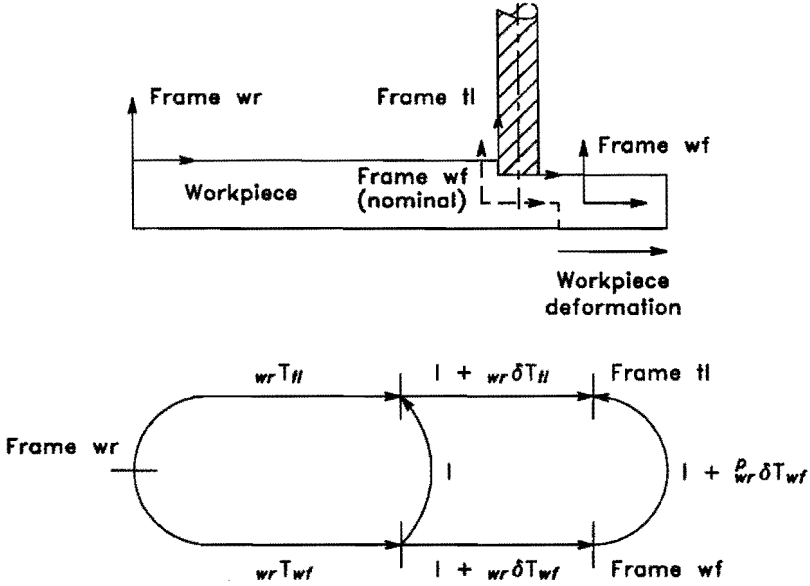


Figure 2.9: Transform graph for machining and handling tasks.

feature is determined by the actual location of the end-effector frame relative to the actual workpiece feature frame. Using the transform graph of Figure 2.9, this error can be expressed as:

$$(I + {}_{wr}^p\delta T_{wf}) = (I - {}_{wr}\delta T_{wf})(I + {}_{wr}\delta T_{tl}) \Rightarrow \tag{2.32}$$

$${}_{wr}^p\delta T_{wf} \approx -{}_{wr}\delta T_{wf} + {}_{wr}\delta T_{tl} \tag{2.33}$$

Note that in the derivation of Equation 2.33, the second order term ${}_{wr}\delta T_{wf} {}_{wr}\delta T_{tl}$ has again been neglected. Thus the errors ${}_{wr}^p\mathbf{E}_{wf}$ in the realized relative location of the feature frame wf in the undeformed workpiece approximately equal the errors in the actual location of the end-effector during manufacturing minus the errors due to the deformation of the workpiece:

$${}_{wr}^p\mathbf{E}_{wf} = -{}_{wr}\mathbf{E}_{wf} + {}_{wr}\mathbf{E}_{tl} \tag{2.34}$$

As expected, the errors during machining and handling tasks have an opposite sign to those during measurement.

2.3.5 Calculation of compensation parameters

Software compensation of measurement tasks is relatively straightforward. It can be achieved by directly subtracting the predicted errors from the measured location of the feature frame. In contrast, software compensation of positioning machines requires the calculation of correction values for the joint coordinates from the predicted errors in the relative end-effector location. The required inverse kinematics analysis is relatively complicated in case the machine contains revolute joints. However, since the errors are small, a simplified analysis is possible using the derived kinematic model.

An unknown compensation variable is added to each parametric error in the kinematic model that describes the position error of an axis. Using the kinematic model, these variables are calculated as the values that minimize some measure of the resulting (compensated) errors in the realized relative location (or trajectory) of the feature frame. Software compensation is then, in principle, achieved by adding the optimized compensation values to the set-point position of each axis. Since the (kinematic) model for the errors in the compensated feature location is linear in the correction variables, the optimization problem is usually relatively straightforward and does not require an iterative procedure. Note the implicit assumption that the (systematic) errors of the machine do not change significantly over distances of the same order as these errors. Obviously, full software compensation of all six errors in the relative location of the end-effector is only possible if the machine contains the appropriate joints. Software compensation of measurement tasks can be achieved by a similar procedure.

2.3.6 Higher order error terms

Until now, only first order effects of the various parametric errors have been considered. The result is a kinematic model that describes the errors in the relative location of the end-effector as a (known) linear combination of the various parametric errors. This section is completed with a short discussion on the merits and problems of higher order error terms.

From a mathematical viewpoint, the incorporation of higher order error terms requires the following changes in the modelling procedure presented in this section:

- Second or higher order error terms effectively destroy the additive and commutative properties of the errors between two coordinate frames (e.g. $\text{Trans} [{}_{k-1}e_{k_x}] \cdot \text{Rot} [{}_{k-1}\epsilon_{k_y}] \neq \text{Rot} [{}_{k-1}\epsilon_{k_y}] \cdot \text{Trans} [{}_{k-1}e_{k_x}]$). Thus the definition of these errors should include their order (i.e. they cannot be defined as rotations and translations along/about mutually perpendicular axes).
- In the first order model presented in this section, the effect of a parametric error on the relative location of the end-effector is completely defined by the nominal geometry of the structural loop. The incorporation of higher order effects causes the direction of a parametric error and its Abbe offset to be dependent on the parametric errors of other coordinate frames (i.e. the product ${}_{k-1}\delta T_k {}_{l-1}\delta T_l$ cannot be neglected). Note that the dependency on parametric errors belonging to the same frame combination has been discussed in the preceding item.
- In the first order model, each matrix element of the error transformation ${}_{wr}\delta T_{il}$ between end-effector and reference is related to only one of the three rotational and three translational errors between the respective frames. Thus each of the latter errors can be directly calculated from the combined error transformation of the parametric errors (which has the same structure). Due to the incorporation of higher order terms, individual matrix elements of ${}_{wr}\delta T_{il}$ will contain the effect of several rotational and translational errors between end-effector and reference. Thus a more complicated analysis is necessary to extract these errors from the combined error transformation of the parametric errors. A unique proportional solution of this procedure is not guaranteed.

The second order models presented in the literature (see e.g. [40, 103, 126, 131]) only consider the second of these items. Therefore the validity of the second order claim is suspect [105].

Second or higher order terms lead to kinematic models where errors in the relative location of the end-effector are expressed as a nonlinear combination of the various parametric errors. The second order terms typically contain the product of a nominal Abbe offset with the product of two rotational errors or the product of a rotational error with a translational error. We found no cases in the existing literature where the errors in the relative location of the end-effector have to be described with such a high relative accuracy that these terms become significant. It should also be noted that the inclusion of second or higher order terms is not only a mathematical problem. From a metrological standpoint, the estimation of these effects presents a huge challenge. A typical example is the alignment of measurement equipment to the machine axes to avoid significant 'cosine' errors. Furthermore, traditional methods to measure an individual parametric error will now be 'significantly' affected by other parametric errors. Finally, if artifacts are used to estimate the parametric errors of the machine, the measured location of the artifact cannot be directly used in the estimation since it is now 'significantly' affected by these errors (see Chapter 4).

2.4 Choice location coordinate frames

The kinematic model presented in the preceding section is valid for any choice of the number and location of the coordinate frames. In this section various placement rules for the coordinate frames are discussed. Note that the selected coordinate frame location affects the definition of the respective parametric error.

The basic function of the kinematic model is to describe how (parametric) errors in the geometry of structural loop components affect the relative location of the end-effector. Variation in the propagation of the parametric errors is related to the position of the kinematic elements, the dimensions of the used end-effector, and the nature of the executed task. A number of mechanisms are responsible:

- Movement of a kinematic element changes the structural loop. For example, movement of a carriage along a guideway increases the section of the guideway that is part of the structural loop and thus changes the propagation of errors in the geometry of that guideway.
- The Abbe offsets of angular errors are often dependent on the position of the joints and the dimensions of the used end-effector.
- The position of revolute joints can change the direction in which parametric errors act.
- The location of the task relative to the reference determines which part of the workpiece is part of the structural loop. Similarly, the location of the task relative to the end-effector determines which part of the end-effector is part of the structural loop.
- The location of the reference determines the position of the joints relative to which variation of accuracy is important.

An efficient kinematic model should describe the known variation of the error propagation, as defined by the nominal structural loop, to the fullest extent, using a minimal number of errors (i.e. coordinate frames). Thus the number and location of the coordinate frames is chosen such that there is only one kinematic element between each two frames. Since multi-axis machines typically use several end-effectors, the end-effector is also enclosed by two frames. The relevant characteristics of the task and the workpiece deformation are taken into account by the use of a workpiece reference frame and a workpiece feature frame.

The location of the workpiece reference frame is determined by the reference relative to which the task of the machine is defined. The location of the workpiece feature frame is determined by the location of the feature to be generated or measured. To facilitate the error analysis, the orientation of this frame is taken such that one or more of its axes point in the sensitive direction of the task.

Tool frame and feature frame coincide during those parts of the manufacturing task where there is interaction between end-effector and workpiece. Since the

feature frame can change during a manufacturing task, the location of the tool frame is generally not fixed relative to the end-effector. This property is required to describe the effect of a changed structural loop through the end-effector (e.g. the effect of probe sphere roundness when measuring in different directions).

The location of the other coordinate frames is arbitrary, provided that their location is fixed relative to the component whose errors they have to describe. Some possible choices are:

- **machine coordinate frame.** Here the various coordinate frames coincide with the machine coordinate frame when the joints are at home position. The resulting model is relatively simple, since the Abbe offset parameters in the model are only determined by the position of the machine axes and the dimensions of the used end-effector.
- **measurement lines.** Here the position of a coordinate frame coincides with the position where its errors are measured. The advantage of this approach is that the measured errors can be directly transferred to the model, without correcting the measurement data for the position where they have been measured. This approach also facilitates the uncertainty analysis of the estimated error model (see Appendix A).
- **machine scales.** Here the position of a coordinate frame is on the effective axis of the displacement measurement system of the respective kinematic element. Thus the parametric translation error in axis direction describes the errors of the measurement system without being 'contaminated' with the effect of angular errors.
- **centroid joints.** Here the position of a coordinate frame coincides with the centroid of the respective joint. For revolute joints this choice is usually required to obtain a workable model. For prismatic joints, it has the advantage that the respective straightness errors can be 'directly' related to the straightness of the beam.

The last two frame allocations are motivated by a desired close relation between parametric errors and errors in the geometry of machine components.

Although transformation of the latter errors to the respective parametric errors is relatively straightforward, care should be taken in the analysis of machine components using parametric error data. For example, the errors in the location of a carriage are introduced by several machine components, e.g. the carriage bearings, the guideway, and the connecting elements with a previous carriage. The parametric errors give no information on the individual contribution of each element.

A generally useful model can be obtained by placing the coordinate frames in the centroid of the various kinematic elements, with one axis aligned with the respective axis of movement. Consistent application of this rule, requires a distinction between prismatic elements whose centroid moves with the joint coordinate and those where the joint centroid remains at a fixed location (Figure 2.10). In the first case, i.e. a carriage moving on a fixed guide, the position of the joint does not affect the active arm of the respective angular errors. In the second case, i.e. a guide moving in a fixed carriage, the active arm of the angular errors is affected by the position of the joint. By considering this distinction in the allocation of the coordinate frames, a known change in Abbe offsets due to movement of the kinematic element is described by the kinematic model and not by the parametric errors. This is consistent with the purpose of the kinematic model, i.e. to describe the known error propagation mechanism as defined by the nominal geometry of the structural loop.

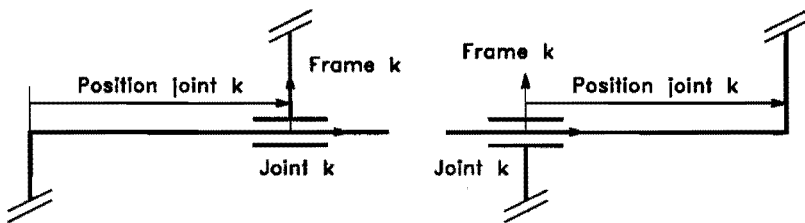


Figure 2.10: Prismatic joint with a moving and fixed coordinate frame.

In the allocation of coordinate frames to revolute joints, it is also possible to differentiate between joints where the frame rotates with the joint and those where the nominal location of the frame is unaffected by the joint position. In this case, it is not only the Abbe offset that is affected by the joint movement but also the direction in which the parametric errors act. Revolute joints

used in multi-axis machines usually have bearing surfaces distributed along the complete perimeter of the joint. Here there is no distinction between a moving and a fixed carriage and the choice between a fixed and moving frame is arbitrary. Since the error in the relative location of the coordinate frame is not only introduced in the kinematic element but also in the structural loop segment that connects the kinematic element with the preceding element, we usually prefer the use of a fixed frame. Thus the errors introduced in the respective structural loop segment do not have to be transformed in a different coordinate frame (note that the errors in the structural loop segment that rotates with the joint are described by the relation with the consecutive coordinate frame).

The choice between a moving and a fixed coordinate frame can also be motivated by the function of a kinematic element rather than the mechanism by which errors are introduced and propagated. Here the criterion is whether the location of the workpiece - end-effector interaction moves or remains stationary as a function of joint movement. Thus, a carriage used to move the end-effector calls for a moving coordinate frame, whereas a carriage used to move the workpiece is described using a fixed coordinate frame (see Figure 2.11).

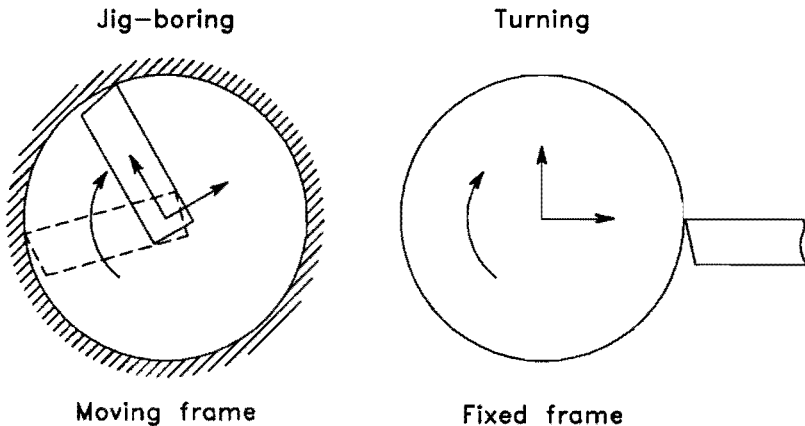


Figure 2.11: Modelling the spindle errors in jig-boring a hole (moving frame) and in turning (fixed frame).

The distinction between moving and fixed coordinate frames is incorporated into the model by introducing so-called shape and joint transformations. The shape transformation ${}_{k-1}S_k$ describes the relative nominal location between frames $k-1$ and k in case their respective kinematic elements are at home position. Joint transformation J_k describes the nominal movement of kinematic element k (see Figure 2.12). Dependent on the nature of the respective kinematic elements, the nominal relative location ${}_{k-1}T_k$ between two successive coordinate frames is expressed as:

$$\text{Moving} \rightarrow \text{moving} : {}_{k-1}T_k = {}_{k-1}S_k J_k \quad (2.35)$$

$$\text{Moving} \rightarrow \text{fixed} : {}_{k-1}T_k = {}_{k-1}S_k \quad (2.36)$$

$$\text{Fixed} \rightarrow \text{moving} : {}_{k-1}T_k = J_{k-1} {}_{k-1}S_k J_k \quad (2.37)$$

$$\text{Fixed} \rightarrow \text{fixed} : {}_{k-1}T_k = J_{k-1} {}_{k-1}S_k \quad (2.38)$$

Measurements of the parametric errors can reflect the choice of a fixed versus

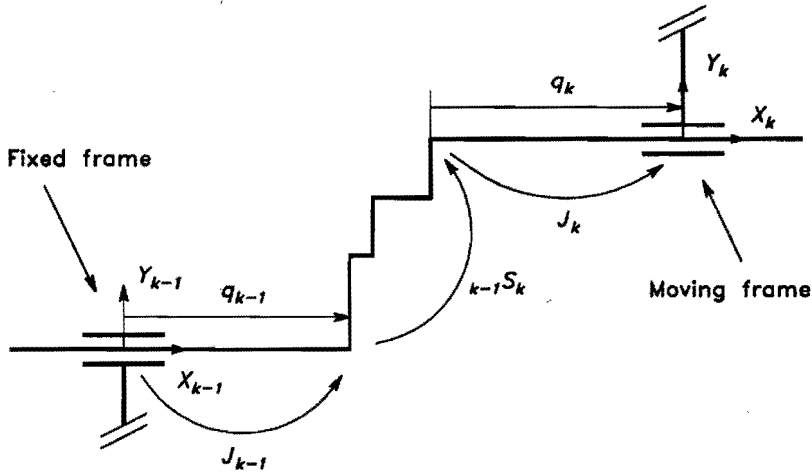


Figure 2.12: Nominal relative location of a fixed and moving coordinate frame.

a moving coordinate frame. For example, the straightness of a guideway can be measured by monitoring its displacement relative to an external fixed straightedge using an indicator mounted on the carriage. Here the respective measurements describe the parametric straightness error corresponding to moving coordinate frame. Alternatively, the parametric straightness error of a fixed frame can be measured using a stationary indicator and a straightedge mounted on the carriage (see Figure 2.13).

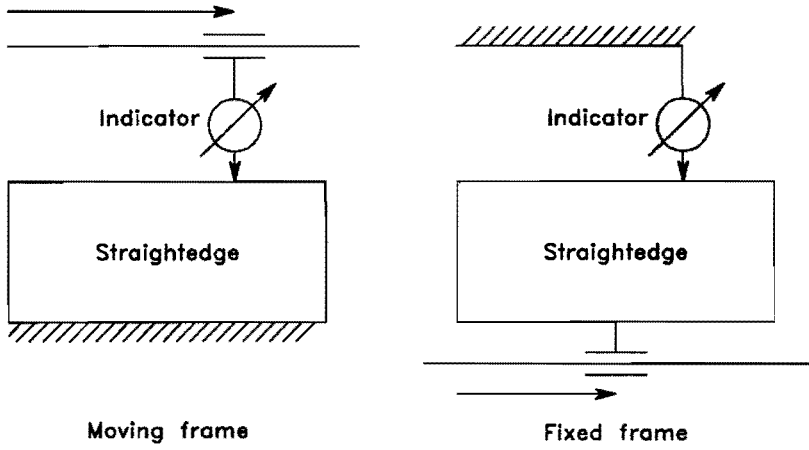


Figure 2.13: Measurement of a straightness error in case of a moving and a fixed coordinate frame.

3

Modelling parametric errors

This chapter describes modelling procedures for the quasi-static portion of the parametric errors identified in the former chapter. The analysed errors can be classified as those due to the limited geometric accuracy of machine components in an unloaded reference state, those due to the static and slowly varying forces introduced by the dead weight of machine components and workpiece, and those due to thermally induced strains in the structural loop. The errors are analysed separately and their combined effect on the parametric errors is obtained by superposition. The analysis is focused on the modelling steps and experiments required to obtain parametric error models for a certain machine. The described strategy is founded on the empirical estimation and description of the various errors.

3.1 Introduction

The kinematic model described in the former chapter relates errors in the relative location of the end-effector to errors in the relative location of successive coordinate frames attached to the structural loop. The latter, so-called parametric errors, describe the difference between the nominal and actual geometry of the structural loop segment enclosed by two successive frames. To predict the accuracy of a certain task executed by a certain machine, models are required that relate these parametric errors to the status of the machine

and its error sources. The formulation of these models is subject of this chapter.

As stated in Chapter 1, the accuracy analysis presented in this thesis is limited to errors that are slowly varying in time. These quasi-static errors can be divided into three general classes: those due to the limited geometric accuracy of components, those due to static and slowly varying forces such as the dead weight of machine components, end-effector, and workpiece, and those due to thermally induced strains in the structural loop. In this thesis, the various errors are analysed independently, and the resulting parametric errors are obtained by superposition. This implies that mutual dependencies of the various errors are neglected. This approximation is based on the following assumptions:

- Errors in the relative location of successive frames are small to such an extent that their effect on the position and orientation of mechanical loads does not affect the related deformation of the structural loop.
- The stiffness of the end-effector - workpiece interaction is low compared to the stiffness of the remaining structural loop. Errors in the relative location of the end-effector cause mechanical loads due to the stiffness of the workpiece - end-effector interface. Dependent on the stiffness ratio of this interface and the remaining structural loop (in the sensitive direction), the resulting deflection of the complete structural loop reduces the errors in the realized task. As explained in Section 1.2, the same mechanism causes the form error of the blank to be only partly reduced after a machining operation. From Tlustý's analysis of the latter effect [118], it can be deduced that during finishing cuts in milling and turning operations, the errors in the relative location of the end-effector will be typically reduced with only a few percentage points of their original values. The relatively high cutting stiffness during grinding (typically 10 to 100 times higher than during turning) can cause a relative error reduction in the order of 50%. Unfortunately, the large number of passes required to achieve a sufficient reduction of the original blank error will also reduce this error reduction in the relative location of the end-effector. Therefore, this interaction between the various errors can

be neglected for most practical applications (single pass grinding is the main exception). During measurement tasks, interaction between end-effector and workpiece is usually detected when their mutual distance or interaction force equals a certain value. In this context, the stiffness of the end-effector - workpiece interaction equals zero and hence there is no mechanism that alters the relative errors of the end-effector (to the first order). During assembly and handling operations there is no interaction zone to accommodate errors in the relative location of the end-effector. Dependent on the nature of the task and the properties of the contact surfaces (friction), these errors result in deflections of the total structural loop and relative displacements between end-effector and workpiece. Analysis of the resulting errors in the executed task is beyond the scope of this thesis.

As a first approximation, errors arising from mechanical and thermal loads are considered mutually independent. It should be noted, however, that there are several mechanisms that cause interactions in both the introduction and propagation of these error sources. First, the stiffness of (fixed) joints is affected by thermal deformations. The stiffness of a joint is determined by the effective cross-section of surface asperities of the mating surfaces. The joint changes its stiffness characteristics as thermal and mechanical contact stresses are developed at the interface, due to deformation of the contacting elements [3]. Second, the thermal contact resistance of a joint is affected by mechanical loads. Local values of the heat flux across (fixed) joints depend on the distribution of the contact resistance between the surfaces which is affected by the pressure distribution across the joint. Hence, mechanical loads affect the temperature distribution of the structural loop and thus its thermal deformation (see e.g. [3, 4]). Third, most thermal loads arise from friction between moving elements and are thus affected by the mechanical loads transferred by these elements. Finally, if components of the structural loop cannot deform freely, thermal and mechanical deformations show interactions due to the nonlinear elastic behaviour of some structural elements (typically the joints).

As stated in the introduction of this thesis, geometric errors describe the limited accuracy of the machine in a certain reference state. Part of these

errors is due to size and form tolerances of machine components. By their very nature, such errors require an empirical approach to error modelling. The other two error classes describe the change in machine accuracy due to thermal and mechanical loading. In most cases, these errors are largely determined by the nominal machine structure and not its actual realization. This enables, at least in principle, an analytical approach to error modelling. The complex mechanics of multi-axis machines, however, puts restrictions on this approach:

- The mathematical relation between structural loop deformations and thermal and mechanical loading is formulated in equations of heat transfer and elasticity. The precise analytical solution of these differential equations for this application is usually impossible, due to complex boundary conditions and the highly complex geometry of machine components. Therefore approximations have to be used. The most popular approach is based on finite difference or finite element techniques (see e.g. [2, 55, 91, 127, 130, 129]). Here the machine geometry and usually the time variable are divided into discrete parts. The result is a large system of relatively simple algebraic equations that can be solved by a computer. As the real geometry of multi-axis machines is far too complicated to be reproduced exactly at a reasonable expense, simplifications are necessary which need not to be identical for temperature and deformation calculation [130]. The complex, three dimensional nature of multi-axis machines, however, usually requires geometrically fine divisions resulting in relatively large models. These models require a large effort both in their construction and evaluation. Venugupal [127] offers a solution to the latter problem by summarizing the obtained model by relatively simple regression models estimated from the computed deformations.
- A major cause of uncertainty in analytical models for thermal deformations is the consideration of the thermal boundary conditions, that is the heat sources and heat transfer. For the heat sources, problems arise in the determination of their intensity and spatial distribution [130]. For example, heat generation due to friction in roller bearings is dependent on the lubricating system, the transferred load, the viscosity of the

lubricant, and bearing play. The latter two are affected by the temperature. Determination of the heat transfer to the environment requires proper models for both surface geometry and -properties. Also the heat transfer across cavities requires special attention. Furthermore, forced convection with increased heat transfer rates occurs in many areas (e.g. ventilation effects of spindles, belt drives and gears, coolant and lubricant circulation), and is difficult to model. The properties of both fixed and moving joints pose special problems. Although their (nonlinear) static stiffness is well understood, the nonlinear heat transfer across the joint and its dependency on both mechanical loads and temperature still requires further research (see e.g. [2]). Finally, heat dissipation and distribution by the coolant, chips, and workpiece is difficult to model, and usually dependent on the operating conditions. It should be noted that the latter problem is also present in the empirical modelling approach.

- Similar uncertainty of analytical models for the finite stiffness related deformation of the structural loop is due to the boundary conditions of machine installation and the (nonlinear) stiffness of joint assemblies. In the analysis of static deformations of large machine tools which do not have adequate inherent stiffness, it is necessary to include the physical properties of the foundation and mounting elements. Ground and soil data for this kind of computation are often not available. The static characteristics of joints (particular bearings, guideways, and flanges) have been subject to extensive experimental and analytical investigations (for a comprehensive overview see [129]). The transfer of these results to actual machines is difficult due to their dependency on manufacturing tolerances (form errors, surface roughness, hardness etc.) and assembly procedures (e.g. preload).
- A special problem in analytical models is the uncertainty of relevant material constants. For example, the thermal expansion coefficient of steel may vary from 10.5 to 13.5 ppm depending on the hardness and composition [16].
- A practical problem in the construction of analytical models is that the required detailed information on the design of the machine is often not available to organisations other than the manufacturing company.

In summary, errors due to mechanical and thermal loads depend on a large number of complex, influencing factors such as geometry, heat sources, heat transition and clamping conditions. Up to now, these values can only be accounted for in a computer model with a large factor of uncertainty. Hence the reliability of the calculation in its quantitative aspect should be judged with caution, especially regarding thermal deformations [16]. Therefore we have chosen for an empirical modelling approach. The physics of error generation is only considered when it contributes to a better model and more efficient estimation of the errors. Here it is tried to include those theoretical concepts that are independent on detailed mechanical and geometrical properties of structural loop segments.

An important step in the modelling procedure is the identification of so-called type dependent error characteristics. These comprise the common properties of errors reported for a certain class or series of machines. Especially the thermal and finite stiffness related errors of machines belonging to the same series exhibit similar characteristics. Thus it is usually not necessary to spend the large modelling effort required to describe these errors on each individual machine. Caution should be taken regarding the stiffness, heat transfer and heat generation of joints and drives. As already discussed, these properties are dependent on parameters such as preload, clearance, lubrication, form errors, and surface roughness that differ for individual machines and are subject to change due to machine usage. The geometric errors of machines belonging to the same manufacturer also exhibit type dependent characteristics. These can be often related to the nature and manufacturing of guideways and measurement systems. Although geometric errors have to be determined for each individual machine, such properties can reduce the measurement and modelling effort (e.g. regarding the required sampling density and sensitivity of error components to wear and 'accidents'). Suitable design, manufacturing, and assembly rules can significantly increase the ratio of type dependent errors and thus reduce the effort required to model the machine accuracy (e.g. for error compensation purposes).

3.2 Geometric errors

In this section, the modelling of geometric errors is discussed. Geometric errors are due to the limited accuracy of structural loop segments in a certain reference state. Errors due to thermal and mechanical loads are defined relative to this reference state. The distinctive property of geometric errors is that the error source remains constant during a manufacturing task. Hence, the geometric errors in the relative location of two successive coordinate frames are either constant or dependent on the position of the enclosed kinematic element. The latter dependency is due to variations in the guideway section, i.e. an error source, that is part of the structural loop.

3.2.1 Choice reference state

First, a definition is required regarding the reference state of a machine. It may be argued that this reference should reflect the average or characteristic state of the machine during use. Thus, relative deviations in the actual state due to thermal and mechanical loads are minimized, which reduces the accuracy requirements of models that describe their effect on the machine accuracy. On the other hand, the reference state should be stable and reproducible, in order to ensure repeatable measurements of the respective errors. Although both requirements can be met for some mechanical loads (e.g. work-piece weight), many thermal loads cause problems. For example, milling and turning machines reach a relatively stable thermal state after both spindle and joints have been active for a long time (typically 4 to 10 hours). Direct measurement procedures of geometric errors, however, often require a stationary spindle and joints. Unfortunately, the thermal distribution and related deformations of the structural loop change rapidly when these motions are halted. Furthermore, error measurement of a heated-up machine poses problems due to the thermal sensitivity of the used measurement equipment.

Alternatively, the thermal reference state may be defined as the state of the machine when all components of the structural loop have a uniform temperature distribution of 20 °C. This definition is motivated by a strict separation

of geometric and thermal errors. Unfortunately, such a reference state cannot be achieved. 'Every' multi-axis machine has heat sources that are not related to operational parameters such as spindle speed and joint movements, but that are present in relatively constant form whenever the machine is on. Typical examples are electrical circuits, servo loops that maintain constant axis positions, and lubrication systems. These heat sources cause deviations in the temperature distribution from 20 °C even if the machine environment is at exactly 20 °C.

Some researchers (e.g. [24, 45, 63]) avoid the necessity of a stable and reproducible reference state by grouping the geometric and thermal errors into one error class dependent on both temperature and position. Models for these combined errors are estimated from measurements performed at different thermal states (usually during a heating up and cooling down period of several hours). Thus, at least in principle, the thermal state during measurement needs not to be stable nor reproducible.

This approach obviously has advantages when the thermal state of the machine changes significantly in response to the joint movements required to assess the various parametric errors. Unfortunately it also has several problems. First, the position dependency of geometric errors is usually of a more irregular nature than that of thermal errors. Hence, the measurement of geometric errors requires a relatively dense sampling distribution with associated long measurement times. If during such measurements the thermal errors of the machine change significantly, the estimation of the position dependency of the various errors becomes difficult (especially when significant backlash errors are present). This situation is complicated by the relatively fast changes in the thermal errors after activating or deactivating certain heat sources (e.g. spindle rotation). Second, simultaneous estimation of geometric and thermal errors increases the dimensionality of the estimation problem with associated problems (e.g. overfitting, stability of estimation algorithms). Third, most measurement equipment used to assess the position dependency of parametric errors require a stable thermal environment. Finally, measurements of parametric errors (especially the translation errors) are generally 'contaminated' with the effect of other parametric errors. If the various errors are measured at different thermal states, these errors have to be estimated

simultaneously which again increases the dimensionality, and problems, of the estimation problem.

In our approach, the reference state corresponds to a mechanically unloaded machine (i.e. no workpiece weight nor process forces) in a thermally stable state. The latter state corresponds to a machine which has been fully warmed up by its internal constant heat sources. This is achieved by switching on the machine several hours prior to the measurements, without activating variable heat sources such as those due to spindle rotations and relatively fast joint movements. The thermal environment of the machine should be reproducible and constant during the heating up period and the measurement session. Especially regarding the effect of the environment on thermal gradients in the structural loop. The average temperature of the environment is, within limits, of minor importance, as long as it remains constant. This implies that both the temperature and thermal expansion coefficient of the machine scales need to be known, and that the temperature distribution caused by the constant internal heat sources is assumed to be independent of the environmental temperature. Care should be taken regarding changes in the temperature distribution of the structural loop due to the relatively slow axis movements required to perform the geometric measurements. In the studied machines, we encountered only slight changes in the related thermal deformations that could be compensated by relatively straightforward procedures.

It should be noted that the above reference state does not correspond to a machine whose structural loop has an uniform temperature. In our opinion such an ideal thermal state is both not practically achievable nor required. Since the thermal errors of the machine will be related to temperature changes relative to those of the reference state, the sole purpose of geometric errors is to describe the accuracy of the machine at this reference state, not a certain ideal thermal state.

3.2.2 'Ordinary' geometric errors

In this subsection, the modelling procedure of 'ordinary' geometric errors is described. Straightness, periodic and hysteresis errors are treated separately.

First a suitable choice of the respective model is discussed. Then the estimation of the unknown parameters in these models from individually measured geometric errors is described.

Despite the abundance of literature on the measurement of geometric errors (see e.g. [5, 18, 52, 53, 121, 50]), their modelling has received relatively little attention. In many studies (see e.g. [19, 144]), essentially a linear interpolation is used between the measured or estimated values of these errors at discrete positions of the respective axes.

In recent literature, this description is generalized by modelling each error as an estimated, usually linear, combination of arbitrary functions defined on the position of the joint. Thus, the dependency of an error E_i on the joint position x is expressed as:

$$E_i(x) = \sum_{l=1}^n \beta_l p_l(x) \quad (3.1)$$

Here $p_l(x)$ is an 'arbitrarily' chosen function (e.g. a polynomial term) defined on the joint position x . The unknown parameter β_l describes the contribution of this function to the parametric error. The various parameters β are estimated from the calibration data, usually by least squares regression.

This explicit use of functions in the description of the geometric errors yields major advantages. The errors can be estimated more efficiently in the presence of noisy calibration data. The location of the error measurements is not restricted to axis positions where the errors are defined. The resulting model of the machine accuracy is mathematically easier to handle (e.g. regarding the number of coefficients), has better properties for software error compensation (e.g. regarding its smoothness), and can be readily used to design efficient calibrations (see Chapter 4). Finally, besides using the functions as an approximation tool (i.e. a curve fitting tool), also statistical testing procedures can be readily applied to investigate the accuracy of the estimated error model, error trends, points of structural change, or the significance of certain errors or error components.

A fundamental modelling choice reflects whether the errors are to be described in the 'frequency' or 'time' domain. A description of geometric errors using a Fourier series is presented in [48, 67]. Such a transformation into the

frequency domain has advantages if the respective error contains periodic components. Existing techniques of approximating transformations into the frequency range, however, will supply faulty results if the error variations in relation to the range of the machine axis are of low frequency [49]. Most parametric errors belong to this class. An exception are position errors due to the displacement measurement system of the joint. These errors often show periodic components of relatively short wavelengths. Furthermore, the geometric errors of revolute joints are by their very nature periodic. Periodic errors will be discussed at a later stage. For 'ordinary' geometric errors, we have chosen for a description in the 'time' domain.

A relatively straightforward approach is the use of an ordinary n th-order polynomial to approximate the relation between the geometric error and the respective joint position. Such ordinary polynomial regression models have been used by some researchers (see e.g. [38]). They are very popular to model the relation between parametric errors or end-effector errors and the value of certain temperature sensors (see e.g. [33]). A problem of ordinary polynomial regression is that as the order of the polynomial increases the estimation problem becomes ill-conditioned due to the high correlation between some regression coefficients. Thus matrix inversion calculations, necessary to solve the estimation problem, will become inaccurate, and considerable errors may be introduced into the parameter estimates [77]. Hence the use of higher order polynomial models ($n > 3$), as reported by some researchers, is suspect, especially at the boundaries of the axis range. Nonessential ill-conditioning caused by the arbitrary choice of the origin can be removed by centring the data (that is, correcting x for its average \bar{x}), but usually this only partly solves the problem. Some of these difficulties can be eliminated by using orthogonal polynomials to fit the model [77]. This also facilitates statistical tests to assess the significance of certain parameters, and extension of the model with additional (higher order) terms (note that due to the orthogonality of the various terms the value of each model parameter does not depend on the other parameters in the model). These properties probably motivated Kruth [60] and Sartori [89] to approximate each geometric error as an estimated linear combination of (orthogonal) Legendre polynomials.

Although most mathematical functions can be used to describe the general trend of an error, their application is limited to model the frequently disjointed or disassociated nature of the remainder. That is to say that the behaviour of an error in one region of the domain may be totally unrelated to the behaviour in another region. Polynomials, along with most other mathematical functions, have just the opposite property. Namely their behaviour in a small region determines their behaviour everywhere [137]. Thus, in our opinion, the irregular nature of many geometric errors requires the use of special functions that possess this property to a lesser extent. A suitable approach to this problem is to divide the range of the joint position into segments and fit an appropriate function in each segment. This can be achieved by so-called piecewise polynomials.

Piecewise polynomials can be described as a set of polynomials defined on limited continuous parts of the domain. The various pieces join in the so-called knots, obeying continuity restrictions with respect to the function value and an arbitrary number of derivatives. The number and degrees of the polynomial pieces, the nature of the continuity restrictions, and the number and positions of the knots may vary in different situations, which gives piecewise polynomials the desired flexibility. A straightforward mathematical implementation of the continuity restrictions can be obtained by the use of truncated polynomials or '+'-functions as basic elements in the piecewise polynomial models. Their use allows the error data to be fitted by ordinary least squares, while still permitting tests regarding the significance of certain terms to be easily made [104]. A potential disadvantage of this approach is that the regression problem becomes ill-conditioned if there are a large number of knots. This problem can be overcome by using a different representation or basis of the spline called the B-spline [137]. We decided not to use this representation (or similar alternatives) due to its somewhat complicated properties in combination with the low number of knots that are generally required to sufficiently describe the errors (typically 2 to 5 knots).

In general, with m knots t_1, \dots, t_m and $m + 1$ polynomial pieces each of degree n , the truncated power representation of the error E_i with no continuity restrictions can be written as:

$$E_i(x) = \sum_{l=0}^n \beta_{0,l} x^l + \sum_{k=1}^m \sum_{l=0}^n \beta_{k,l} (x - t_k)_+^l \quad (3.2)$$

where:

$$(x - t_k)_+ = \begin{cases} (x - t_k) & \text{if } x - t_k > 0 \\ 0 & \text{if } x - t_k \leq 0 \end{cases} \quad (3.3)$$

The presence of a term $\beta_{k,l} (x - t_k)_+^l$ allows a discontinuity at knot t_k in the l th derivative of $E_i(x)$. Thus, different continuity restrictions can be imposed at different knots simply by omitting the appropriate terms. Usually it is sufficient to ensure that each model is continuous with respect to the function value and its first derivative.

An inherent problem in the construction of the functions is the unknown nature of the errors to be described. Experience with a number of similar machines or similar machine components from the same manufacturer can only partly eliminate this problem. The potential of the model to accommodate irregular errors is to an extensive degree determined by the number and degree of the polynomial pieces. If these properties are considered variable, the respective parameters enter the regression problem in a nonlinear fashion, and all the problems arising in nonlinear regression are present. The use of variable knot positions also carries the practical danger of overfitting the data, and makes testing of hypotheses concerning areas of structural change virtually impossible [104].

Unless prior information is available, we use a basic model which contains enough polynomial pieces with a fixed length and a specified maximum degree, to accommodate the most complex error expected. In the parameter estimation process, which is now restricted to the unknown parameters $\underline{\beta}$, a stepwise regression procedure is implemented to remove statistically insignificant parameters from the model. The reason for this removal is twofold:

- including insignificant parameters hardly improves the quality of the fit, but increases the variance of the estimated parameters and response.

- identification of structural parameters enhances the diagnostic properties of the model (e.g. regarding areas of structural change) and can be used in the design of the (periodic) performance evaluation (see Chapter 4).

The knots of the original model are usually spaced at equidistant intervals along the domain of the independent variable (i.e. the position of the joint). Visual inspection of the measurement data and analysis of the model residuals also guide the knot placements. For complex errors (typically errors of the measurement systems), adequate models have been obtained using quadratic piecewise polynomials with five knots, which allow a discontinuity only in the second derivative of the function (seven unknown parameters if only error variations as a function of the joint position are described ($3 - 1 + 5 \times 1 = 7$)). The smooth character of many observed errors, allows them to be accurately described by similar models having only one or two knots (three to four unknown parameters). The latter description is also used if we are only interested in the general trend of an error. The use of high-order polynomials ($n > 2$) should be avoided, unless they can be justified for reasons outside the data. It is recommended to have at least three observations at different joint positions between each two successive knots.

In assessing the validity of the estimated model, the detection and analysis of outliers (bad values in the measurement data) play an important role:

- due to the inherent flexibility of the proposed model, in combination with the nature of the least squares estimation process, outliers have a large potential influence on the estimated model.
- 'outliers' can indicate areas in which the proposed model is inadequate to describe a particular error, or in which the nature of the 'random' error in the various observations is incompatible with the use of the least squares estimation method.

The latter item is especially important when modelling scale errors. These errors often exhibit an irregular dependency on the position of the respective joint. Here clusters of outliers often indicate areas where the proposed

model is incapable to describe the observed irregularities. The problem is solved by including an extra number of suitably placed knots into the model in combination with a (locally) finer sampling distribution of the respective measurements. Although there are statistical tests available to 'automatically' identify such areas, visual inspection of various residual plots usually works best. When the sampling distribution is relatively low, we use Cook's D-statistic [77]. This statistic is a measure for the change in the residual sum of squares after removal of an observation from the dataset. It thus identifies data-points that exert a disproportional influence on the fitted model. Due to the high flexibility of the proposed model, such points do not necessarily result in high residuals. In general, the estimated model is further verified using a validation dataset (if possible measured on another day) that has not been used in the parameter estimation.

A problem when estimating the various parametric errors is that it is usually not possible to measure these errors at the location where they are defined (i.e. in the origin of the respective coordinate frame). Thus measurements of translational parametric errors are 'contaminated' with the effect of several angular parametric errors through their respective Abbe offsets. One approach to this problem calls for the sequential estimation of the various parametric errors after compensating the measurement data for the effect of parametric errors already estimated. Here the angular parametric errors are estimated before the translation parametric errors. By compensating displacement measurement data for the effect of (angular) errors already included in the model (using this model), the residual data for the respective translation parametric error 'automatically' describes this error at the location where it is defined. We use this method when the various parametric errors are individually measured. Alternatively, the various parametric errors can be simultaneously estimated such that the observed errors in the relative location of the end-effector are optimally described. This approach is used in Chapter 4 to estimate the parametric errors from errors observed in tasks executed by the machine.

Based on the above concepts, regression software is developed. The software runs on an IBM compatible personal computer and uses the MATLAB [68] software package, whose various numerical algorithms allow relatively fast

prototyping. The software was tested on several datasets using the SAS [90] statistical package as reference. Before estimating the parameters, unit length scaling [77] is applied to the response variable (i.e. the error to be modelled) and the various regressors (the values of the known functions $p_i(x)$ for each observation). Here each variable is centred for its average and scaled for its variance. This procedure reduces problems arising from round-off problems when estimating the various parameters. It is especially important when using polynomial regression models, where the range of the various regressors differs in orders of magnitude. The parameters are estimated using a QR factorisation of the regressor matrix [102]. For each interval between two knots, the estimated piecewise polynomial model is transformed to an ordinary polynomial whose domain is limited to this interval. Numerical evaluation of the resulting model is significantly faster than that of the original model based on a truncated power presentation.

As a typical example of the estimation procedure we consider the modelling procedure for the angular error around the Y-axis when moving the Z-axis of the five-axis milling machine described Chapter 5. In accordance with the VDI-2617 guideline [124] on the performance evaluation of CMMs, this error is denoted as z_{ry} . The error is measured with a laserinterferometer using the setup depicted in Figure 3.1. A total of five back and forth measurements over the total range of the Z-axis (600 mm) are automatically performed, using a sampling distance of 10 mm. At each measurement point, the axis motion is halted. After a short delay to eliminate dynamic effects induced by the axis motion, five samples of the angular error are taken. The complete measurement procedure is executed automatically using an IBM compatible personal computer that communicates with both the milling machine (through an RS232 interface) and the measurement equipment (IEEE interface). The required software was developed by Theuws [115].

Before estimating the model, the measurements are corrected for the drift of both measurement equipment and machine. Here the measurement data is divided into several cycles, each containing one back and forth run. The observed errors of each cycle are plotted as a function of the elapsed time at their measurement since the start of the cycle. A least squares best fit line is estimated through this plot. This line is an estimate for the linear drift in

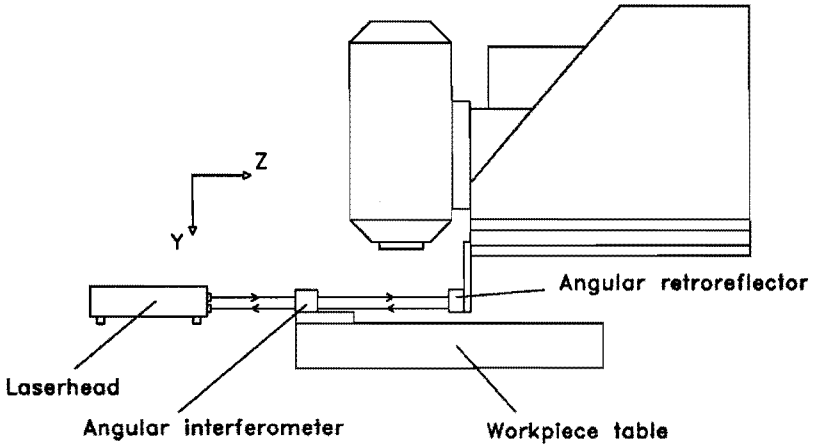


Figure 3.1: Experimental setup to measure the zry angular error.

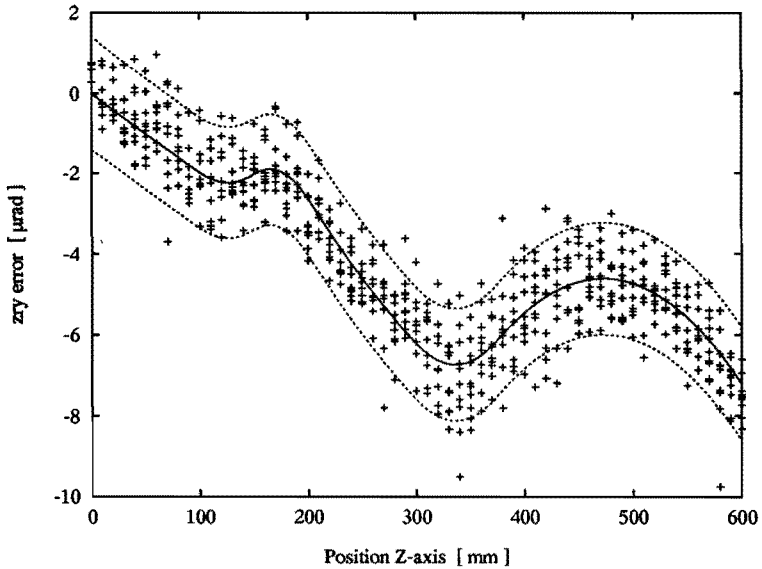


Figure 3.2: Validation measurements of the zry error and the estimated model. The dashed lines present the 95 % confidence interval of the model for individual measurements.

time. The residuals of the observed errors with respect to this line represent the drift corrected error data. This approach is only allowed, and used, when the respective error shows no (significant) backlash.

The proposed model for this error is a second order piecewise polynomial, continuous with respect to the function value and its first derivative, having 11 knots placed at 50 mm intervals. After the stepwise regression procedure, 5 knots were retained (at a significance level of 99.99 % for adding or removing a regressor). The estimated model is presented in Figure 3.2 together with a validation dataset of also five back and forth measurements executed directly after those used to estimate the model.

3.2.3 Straightness errors

Errors in the end-effector trajectory due to the linear trend of a straightness error cannot be distinguished from those due to errors in the relative orientation of the respective joint axis. As described in Appendix B, both error sources are allocated to the parametric error describing the orientation of the joint axis. Hence, a parametric straightness error has by definition no linear component (specified in a least squares sense). Similarly, the parametric errors of a revolute joint that describe rotations and translations about/along axes orthogonal to the joint axis have no once-per-revolution sinusoidal terms (also specified in a least squares sense).

When parametric errors are individually measured, these boundary conditions can be met by removing the respective trend from the measurement data. However, the unique identification of individual parametric errors from measurements of their combined effect on the relative end-effector trajectory, requires models where different parametric errors do not have the same effect on the trajectory, regardless the values of the unknown parameters $\underline{\beta}$ that describe these errors. For straightness errors this constrains the unknown parameters $\underline{\beta}$ to values where the respective linear combination of the known functions $p_i(x)$ has no linear trend in a least squares sense. Alternatively,

each known function $p_l(x)$ can be chosen such that it has no linear component, which ensures that the respective parametric error has none, regardless the values of the unknown parameters.

The latter approach is pursued in this thesis because it does not require any change to the least squares estimation procedure explained in the preceding subsection. A function $p_l(x)$ which has no linear component, can be divided into an arbitrary function $g_l(x)$, e.g. a piecewise polynomial term, and a linear term:

$$p_l(x) = g_l(x) - \alpha_1 - \alpha_2 x \quad (3.4)$$

Here the parameters α_1 and α_2 describe the least squares best fit line through the function $g_l(x)$. Given a known function $g_l(x)$, their value minimizes the integrated squared function $p_l(x)$ over the domain $[q_{i,\min}, q_{i,\max}]$ of the axis position. The respective least squares criterion is:

$$S^2(\alpha_1, \alpha_2) = \int_{q_{i,\min}}^{q_{i,\max}} (g_l(x) - \alpha_1 - \alpha_2 x)^2 dx \quad (3.5)$$

Hence their values $\hat{\alpha}_1$ and $\hat{\alpha}_2$ must satisfy:

$$\frac{\partial S^2}{\partial \alpha_1} \Big|_{\hat{\alpha}_1, \hat{\alpha}_2} = -2 \int_{q_{i,\min}}^{q_{i,\max}} (g_l(x) - \hat{\alpha}_1 - \hat{\alpha}_2 x) dx = 0 \quad (3.6)$$

$$\frac{\partial S^2}{\partial \alpha_2} \Big|_{\hat{\alpha}_1, \hat{\alpha}_2} = -2 \int_{q_{i,\min}}^{q_{i,\max}} (g_l(x) - \hat{\alpha}_1 - \hat{\alpha}_2 x) x dx = 0 \quad (3.7)$$

Which simplifies to:

$$\begin{bmatrix} \hat{\alpha}_1 \\ \hat{\alpha}_2 \end{bmatrix} = \begin{bmatrix} (q_{i,\max} - q_{i,\min}) & \frac{1}{2}(q_{i,\max}^2 - q_{i,\min}^2) \\ \frac{1}{2}(q_{i,\max}^2 - q_{i,\min}^2) & \frac{1}{3}(q_{i,\max}^3 - q_{i,\min}^3) \end{bmatrix}^{-1} \int_{q_{i,\min}}^{q_{i,\max}} \begin{bmatrix} g_l(x) \\ g_l(x)x \end{bmatrix} dx \quad (3.8)$$

Similarly, a function $p_l(x)$ which has no once-per-revolution sinusoidal component, can be decomposed into an arbitrary function $g_l(x)$ and a sinusoidal term:

$$p_l(x) = g_l(x) - \alpha_1 \cos(x) - \alpha_2 \sin(x) \quad (3.9)$$

Where x denotes the position of the joint in radians. Given a known function $g_l(x)$, the parameters α_1 and α_2 again minimize the integrated squared function $p_l(x)$ over the domain $[q_{i,\min}, q_{i,\max}]$ of the axis position. Their values can be

calculated using a similar procedure as that described for straightness errors. If the range of the joint position equals 2π rad, this yields:

$$\begin{bmatrix} \hat{\alpha}_1 \\ \hat{\alpha}_2 \end{bmatrix} = \frac{1}{\pi} \int_0^{2\pi} \begin{bmatrix} g_i(x) \cos(x) \\ g_i(x) \sin(x) \end{bmatrix} dx \quad (3.10)$$

Note that these parameters equal the first set of Fourier terms for $g_i(x)$.

3.2.4 Periodic errors

Periodic errors are often introduced by the displacement measurement system of a joint. A typical example is the leadscrew-resolver arrangement often used in machine tools to monitor and change the position of a prismatic joint. Here periodic errors are introduced due to leadscrew misalignment, errors in the bearing elements between nut and screw, encoder errors, and defective coupling between leadscrew and resolver (e.g. gear eccentricity and encoder shaft runout). By their very nature, revolute joints exhibit periodic errors. The average error motion profile of revolute joints can only involve frequencies which are equal to or are whole-number multiplies of the axis rotational frequency [18]. The systematic residual error motion however is periodic with arbitrary frequencies. Drive components, bearings, and encoders can cause periodic systematic errors that are synchronized with the axis movement, but not necessarily of the same frequency.

In the existing literature (see e.g. [33]), periodic errors are generally modelled as an estimated linear combination of trigonometric functions. The unknown parameters in these models are either estimated from the (approximated) frequency domain description of the error data, or by nonlinear least squares regression of individual trigonometric terms (note that the frequency of such a term enters the regression problem in a nonlinear fashion). In this thesis we have generalized the latter approach by modelling each periodic term as an estimated linear combination of arbitrary known functions. The argument of these functions equals the wavelength fraction of the periodic term at the current joint position. Here, the continuity restrictions at the interface between two periods can be varied in accordance with the nature of the periodic term. This approach enables the approximation of many observed periodic errors using a significantly lower number of terms (i.e. estimated parameters)

than those based on a trigonometric representation. Furthermore, it reflects the spirit of many existing commercial algorithms used for the software error compensation of periodic (leadscrew) errors.

Both periodic and non-periodic terms are estimated simultaneously. Individual estimation of both terms (e.g. by filtering the non-periodic components from the measurement data) is difficult in case the wavelength of the periodic term is of the same order as the range of the joint position. The same argument applies to the estimation of several periodic components with different wavelengths.

The used regression model of a parametric error E_i with m periodic terms is:

$$E_i(x) = \sum_{l=1}^n \beta_l p_l(x) + \sum_{k=1}^m \sum_{l=1}^{n_k} \beta_{k,l} v_{k,l}(x, \tau_l, \varphi_{k,l}) \quad (3.11)$$

Here, $v_{k,l}(x, \tau_l, \varphi_{k,l})$ represents an 'arbitrarily' chosen periodic function with a frequency equal to or whole number multiplies of τ_l^{-1} . The phase parameter $\varphi_{k,l}$ describes the location of this function in the domain of the joint position x . Since this parameter enters the regression problem in a nonlinear fashion, it is only used if the nature of the periodic terms is approximately known and changes rapidly in limited parts of its domain (a typical example is the saw-toothed wave observed in position errors of machines having an integer based software compensation algorithm). In general, the phase of a periodic term is implicitly described by the linear regression parameters $\beta_{k,l}$ belonging to functions of the same fundamental wavelength τ_l . This approach is similar to the use of a cosine and sine function of equal wavelength and phase instead of one trigonometric function with an appropriate phase shift.

The periodic functions $v(x, \tau, \varphi)$ are constructed in the following manner:

$$v(x, \tau, \varphi) = g(w(x, \tau, \varphi)) - \sum_{c=1}^{nc} w(x, \tau, \varphi)^c \alpha_c \quad (3.12)$$

where:

$$w(x, \tau, \varphi) = \begin{cases} \frac{x - \varphi}{\tau} & \text{if } \varphi \leq x < \varphi + \tau \\ w(x + \tau, \tau, \varphi) & \end{cases} \quad (3.13)$$

Here, $g(w(x, \tau, \varphi))$ represents an arbitrary function. Its argument $w(x, \tau, \varphi)$ equals the wavelength fraction of the periodic term at joint position x . The

parameter α_c and its polynomial term w^c are introduced to ensure continuity of the $(c - 1)$ th derivative of $v(w)$ at the interface between two wavelengths (i.e. at $w = 0$). These parameters are fully defined by the chosen function $g(w)$ and the respective continuity restrictions. For example, if continuity is required with respect to the function value and its first derivative, the respective parameters α_1 and α_2 are calculated as:

$$\begin{cases} g(0) = g(1) - \alpha_1 - \alpha_2 \cdot 1^2 \\ g'(0) = g'(1) - \alpha_1 - 2\alpha_2 \cdot 1 \end{cases} \Rightarrow \quad (3.14)$$

$$\begin{bmatrix} \alpha_1 \\ \alpha_2 \end{bmatrix} = \begin{bmatrix} 1 & 1 \\ 1 & 2 \end{bmatrix}^{-1} \begin{bmatrix} g(1) - g(0) \\ g'(1) - g'(0) \end{bmatrix} \quad (3.15)$$

In general, piecewise polynomial terms are used for the functions $g(w)$. The respective knots, continuity restrictions, and maximum degree are fixed parameters during the estimation. Thus, only the various wavelengths enter the regression in a nonlinear fashion. For the tested machines, visual analysis of the measurement data provided sufficient information about a suitable choice of their initial values. After convergence of the estimation procedure, a significant parameter analysis is applied to eliminate 'unnecessary' parameters. Here the various wavelengths remain at a fixed value. Adequate models for periodic terms have been obtained using quadratic piecewise polynomials having one to four knots.

As an example, we consider the X-axis linear displacement error of the milling machine described in Chapter 5. In accordance with the VDI-2617 guideline [124] this error is denoted as x_{tx} . The error is measured with a laserinterferometer using the setup depicted in Figure 3.3. Again the measurement is static, i.e. the axis position is stationary during each observation. The result of two back and forth measurements using a sampling distance of 10 mm are presented in Figure 3.4. The presented data are compensated for the effect of angular errors and the thermal expansion of the X-axis measurement scale (using the values of three Pt-100 temperature sensors attached to the scale). The linear trend in the error data is largely due to the used scale mounting, which prohibits free thermal expansion of the scale (The average temperature of the scale during measurement was 25 °C). This effect will be discussed in Chapter 5.

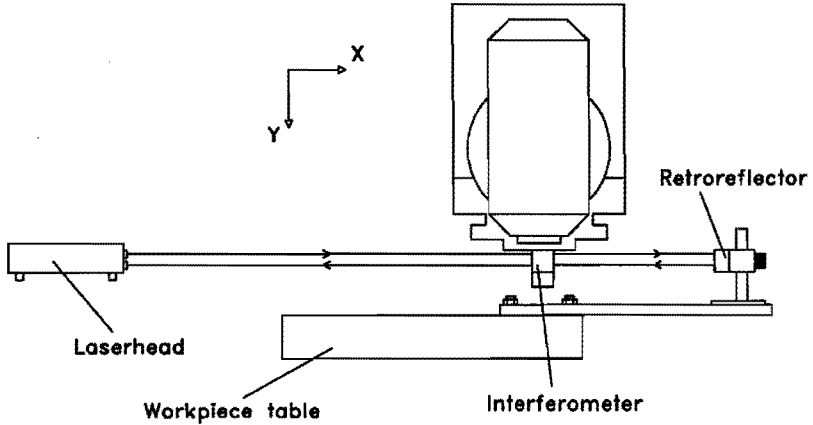


Figure 3.3: Experimental setup to measure the xtx displacement error.

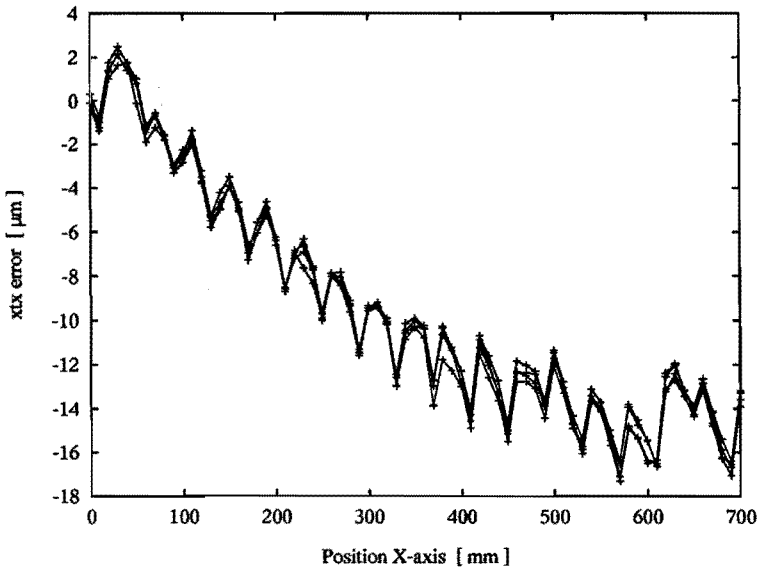


Figure 3.4: Measured xtx error (two back and forth measurements, sampling distance 10 mm). Successive observations are connected by solid lines to highlight the periodic nature of the error.

The observations suggest that this error has a periodic component with a wavelength of approximately 40 mm. However, further analysis showed that in reality the observed periodic trend is due to a periodic error with a wavelength of 635 μm . This false interpretation, caused by the chosen sampling distance, underlines the recommendation in many guidelines on the performance evaluation of multi-axis machines to use 'random' sampling distances when assessing the quality of measurement systems (or whenever periodic errors are expected).

To estimate the periodic term, the error was measured over a relatively short axis range of 50 mm using a sampling distance of 0.01 mm. The estimated autopower spectrum of the error using these measurements is depicted in Figure 3.5. Using the measurement data, a model for the periodic component is estimated. The estimated model is based on a second order piecewise polynomial which has three knots and is continuous up to and including the first derivative. The estimated wavelength equals 635.025 μm (this large number of digits is required since there are approximately 1100 wavelengths in the axis range). This wavelength corresponds to the pitch of the measurement scale and is probably caused by alignment errors between scale and the diode array sensor.

The nonperiodic trend of the error is estimated using two back and forth measurements of the error with a sampling distance of respectively 1 and 3 mm. Before estimating the respective model, the error data is compensated for the estimated periodic component. In contrast to earlier remarks, we have chosen for this sequential estimation of periodic and nonperiodic terms because of the small dimension of the wavelength and a significant drift in the 50 mm measurement. This drift is related to the long time required to execute the measurement and might be affected by local self-heating of the scale-sensor combination.

Due to the small wavelength of the periodic term, successful application of the model requires a repeatable homing procedure of the machine after powerup. In this case, the measurement system uses a reference marker to find its zero position, and the repeatability of this process is quoted in the order of its resolution (1 μm). To verify the estimated model, the error was measured

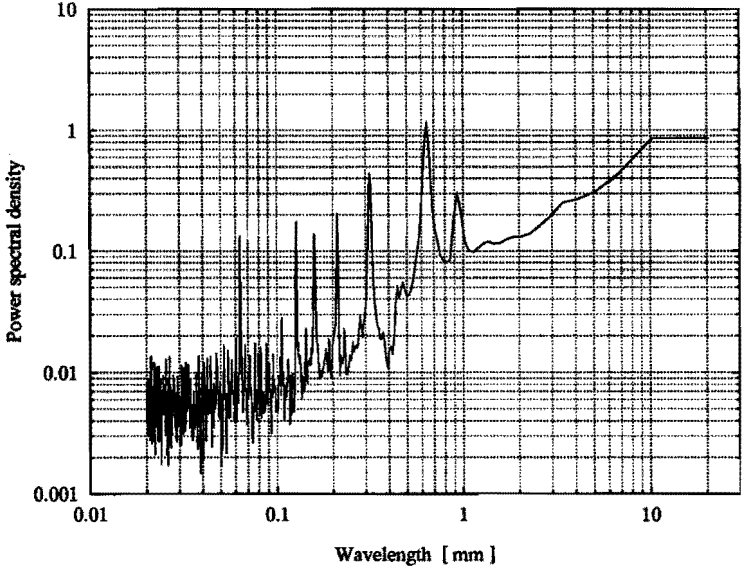


Figure 3.5: Estimated power spectral density of the xtx error. The spectrum is scaled so that a sine wave having an amplitude of 1 μm corresponds to one unit.

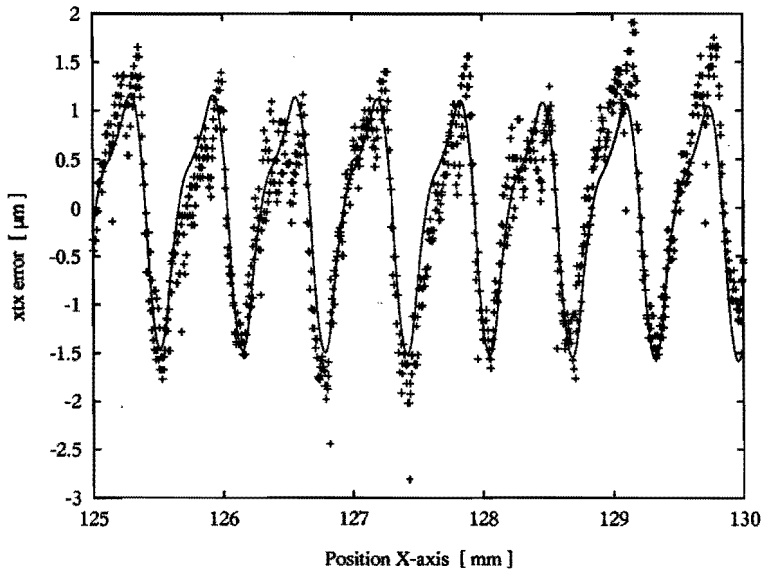


Figure 3.6: Measured xtx error (one back and forth measurement over 25 mm, sampling distance 0.01 mm). The model is presented by a solid line.

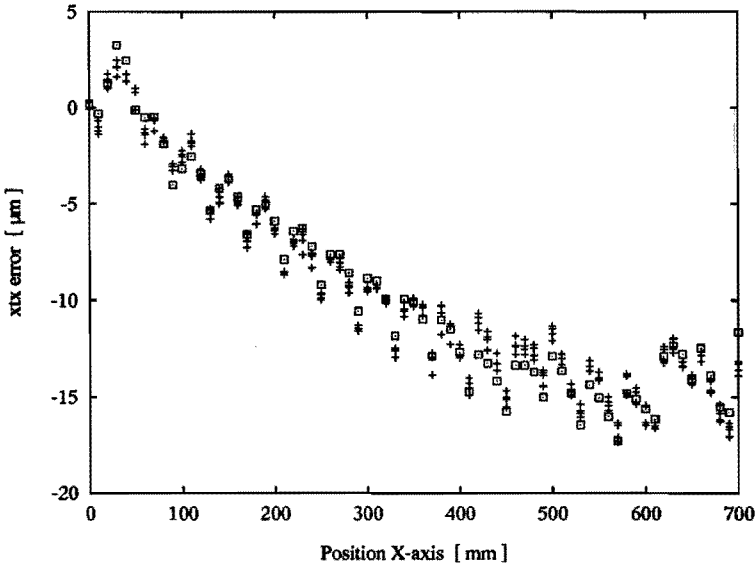


Figure 3.7: Measured x_{tx} error (two back and forth measurements, sampling distance 10 mm). The observed and predicted errors are indicated by respectively '+' and '□'.

using a sampling distance of 0.01 mm and 10 mm (both after rehoming the machine). The respective results are presented in Figure 3.6 and 3.7.

3.2.5 Hysteresis and backlash

Hysteresis errors are the residual errors that occur when a load acting on structural loop components is increased and decreased over a cyclic pattern. When such a pattern is established, these errors are usually highly reproducible [75]. The term backlash is generally used to describe the hysteresis errors that result from looseness between interacting mechanical parts [27]. For an 'unloaded' machine, load variations are due to the weight and inertia of moving machine components, and the forces exerted by the drives.

Clearance between components causes an error term whose sign changes with the sign of the applied load. For geometric errors, the sign of the respective backlash error is dependent on the direction of the axis motion. Its value may

depend on the position of the machine axes due to variations in clearance (e.g. due to straightness errors of the guideway), but is unrelated to the axis travel before motion reversal.

Due to friction, an applied load can vary within a certain range without affecting the position of a component. Due to the compliance of machine components transferring the load, errors are introduced. Hence, hysteresis errors occur whenever a component subject to friction changes its direction of motion (either wanted or unwanted motion). For geometric errors, the sign of the respective hysteresis term is again dependent on the direction of axis motion. A typical example is the hysteresis error that arises when an axis is driven by a leadscrew whose angular position is used to monitor the position of the slide. Elastic deformation of the leadscrew causes a position error whose sign changes with the direction of axis motion and whose value is dependent on the axis position (note that the leadscrew length that is part of the structural loop is dependent on the axis position).

When friction is involved, the value of the hysteresis error generally depends on the (apparent) axis travel before motion reversal. Three mechanisms are responsible. First, from the leadscrew example it is apparent that axis motion may be detected without actual movement of the slide. Thus the hysteresis error after an apparent motion reversal is dependent on the position within this 'dead-zone'. Second, generally several components subject to friction are arranged in series. Due to the compliance of the connecting elements, hysteresis errors will occur that depend on the history of the applied load. The respective memory is embodied by the mutual distance (load) between the various components. Finally, the weight of the moving components causes loads that depend on the position of the slide(s). As the axis motion is reversed, it is not the load but the load variation that changes its sign. Combined with the former mechanism, this generally results in a gradual change in hysteresis errors as the axis motion is continued. The changed contact conditions in a joint during loading and unloading cause a similar hysteresis error [128]. Further complications arise when the coefficient of friction is dependent on the speed of axis travel. Notorious are the stick-slip errors at low speeds.

Due to the highly reproducible nature of most hysteresis errors they can be predicted if the direction of axis motion is known and adequate pre-travel is made. The used approach is generally based on several back and forth measurements of a geometric error over the complete range of the respective axis. Separate models are estimated for the error observed for positive and negative axis motion. Dependent on the direction of axis motion, one of these models is used to predict the respective error. This approach is used by many researchers (see e.g. [33]) and is an option in most commercial software error compensation algorithms (especially for machine tools). Successful application, however, requires that the hysteresis error is independent of the axis travel before and after motion reversal. Although, at least in principle, the respective 'memory' can be modelled, there are some dangers. The main problem is that the effect of the axis travel history may change due to vibrations and other disturbances of the structural loop. Therefore we decided not to model the latter class of hysteresis errors. When it occurs, the average error is modelled and the respective hysteresis is treated as an uncertainty whose boundary values are estimated from the difference between the back and forth error.

A typical example of such a hysteresis error occurred in the studied five-axis milling. Due to wear, the adjustment of the Y-axis bearings changed, resulting in an angular hysteresis error around Z. The dependency of this error on the position of the X-axis carriage was measured with a laserinterferometer using the setup depicted in Figure 3.8. The results of back and forth measurements (static) over a decreasing range of the X-axis are shown in Figure 3.9. The observed hysteresis was highly reproducible.

In this case, there is a gradual increase of the hysteresis error as axis motion is continued after a reversal in axis movement. Hence, a model that changes the error curve selection as motion is reversed will be inadequate. The nature of the observed hysteresis can be explained by considering the simplified mechanism depicted in Figure 3.10. Here the Y-axis carriage C is connected with the Y-axis guideway G through a spring k and a clearance s . As force F is applied, an error e will occur between carriage and guideway. Due to the clearance s and friction W , the relation between the error e and applied force F will exhibit hysteresis as shown in figure 3.11. In this case, force F

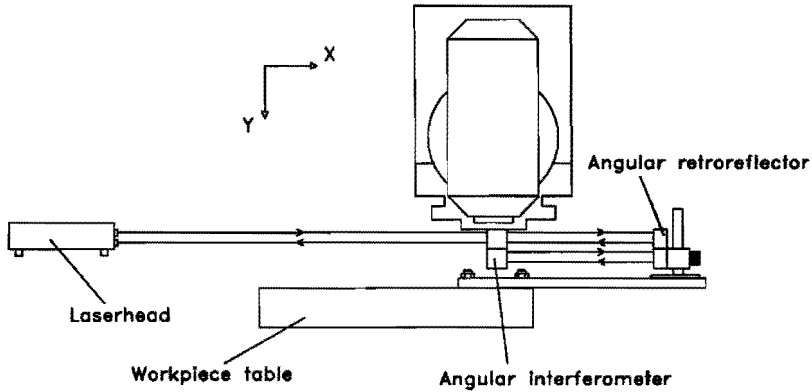


Figure 3.8: Experimental setup to measure the xrz angular error.

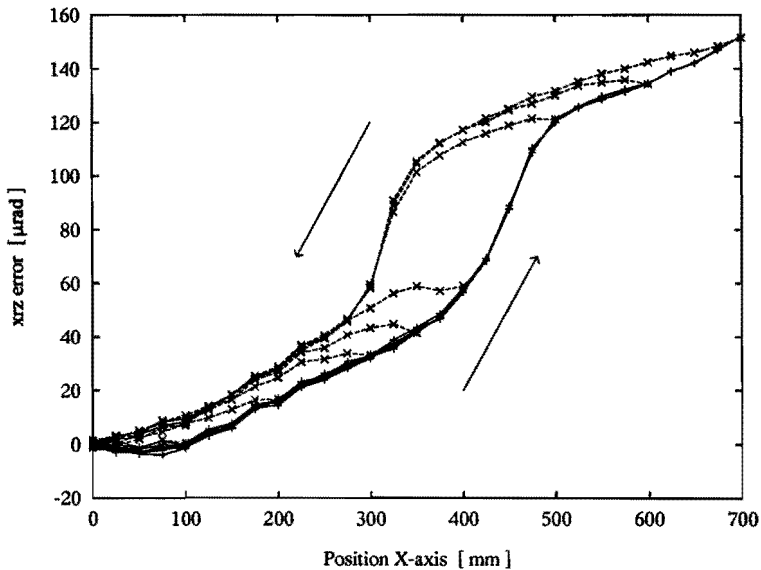


Figure 3.9: Measured xrz error (average of two measurement series, sampling distance 25 mm). Presented are several back and forth measurements, starting at $X = 0$, over a decreasing axis range. Solid and dashed lines represent, respectively, positive and negative axis motion.

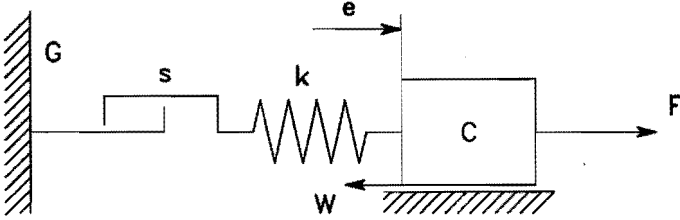


Figure 3.10: Mechanism that might be responsible for the observed hysteresis.

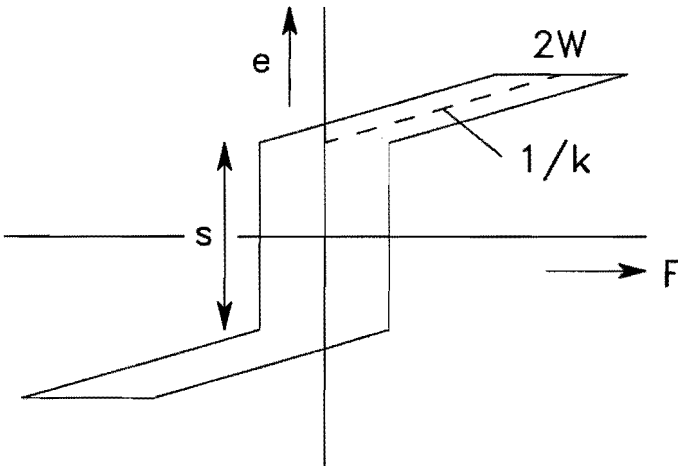


Figure 3.11: Relation between error e and force F of the described mechanism.

is introduced by the moment exerted by the X-axis carriage (approximately 500 kg). This moment is proportional with the position of the X-axis carriage relative to the Y-axis (i.e. F is a measure for the relative X-axis position). Due to this moment, the error e will differ for the various bearings resulting in an angular error. The agreement between Figures 3.11 and 3.9 indicates that the described mechanism might be largely responsible for the observed hysteresis error, especially if a spring is added parallel to the clearance. Fortunately, the observed hysteresis could be reduced to insignificant levels by adjusting the Y-axis bearings.

3.3 Errors due to mechanical loads

The structural loop is subject to a large variety of mechanical loads. These loads affect the accuracy of the executed task due to the compliance of structural loop components. In this section the modelling procedure of the respective parametric errors is discussed. The analysis is limited to the effect of load variations introduced by the weight of moving machine components and workpiece.

3.3.1 General considerations

As stated in Chapter 1, the quasi static mechanical loads acting on the structural loop are classified as weight, clamping, and process forces. These categories differ in both their effect and introduction. The deadweight of a machine component, the workpiece, or the end-effector generally 'only' affects the structural loop segment that connects the respective component with the machine foundation. In contrast, process forces are transferred through the complete structural loop, and therefore cause deformation of all its components. Furthermore, the direction of process forces is dependent on the executed task. The effect of clamping forces is generally limited to the clamped object (e.g. a carriage and the respective guideway section, or the workpiece).

Variations in deadweight loads are related to the position of the joints that connect the respective mass to the machine foundation, and the position and mass of workpiece and end-effector. Hence, the respective influence quantities are generally well defined. The main exception is the variation in workpiece load (both its position and value) due to material removal during machining. Determination of the effective workpiece load using strain gauges is a possible solution to this problem (see e.g. [109]). Regarding the deformation of the workpiece table, the distribution of the workpiece load on the table needs to be known. Unless the workpiece is supported by well defined fixtures, this load distribution is influenced by form deviations of both workpiece and table and hence difficult to predict.

As stated in Chapter 1, the process force during measurement tasks is relatively small (typically several tenths of a Newton). Significant deformations of the structural loop are generally confined to the used probe system, probe stylus, and workpiece. Regarding workpieces, significant errors have been observed for thin walled workpieces and workpiece materials of low stiffness. Deformations due to the measurement force can be predicted when both its value and direction are known. Estimation of this force, however, has proven to be difficult. First, although measurement probes are designed to detect the workpiece surface when a defined measurement force has been reached, practice has shown that this 'trigger' force varies dependent on the direction and speed of probing. Due to the generally low stiffness of the probe stylus, this force variation causes errors dependent on the direction and speed of probing and stylus properties (e.g. its length). This effect is usually referred to as probe lobing. These errors can be predicted and compensated by datuming the probe/stylus combination in various directions (e.g. using a sphere). Due to the weight of the stylus, probe lobing is generally affected by the orientation of the probe. Second, friction between stylus tip and workpiece surface causes a deviation between the direction of the measurement force and the workpiece normal when the latter does not coincide with the probe approach direction. Combined with the preferred deflection direction of the probe, this also increases the measurement force and related errors. Significant fluctuations in the friction coefficient have been reported for combinations of similar materials and surface roughness [87]. (For a comprehensive review of these effects (and other errors of probe systems) see e.g. [7, 21, 54, 84, 85])

The process forces and related structural loop deflections during machining operations have received much attention (see e.g. [119, 128]). Often, with light finishing cuts, the effect of their static component on the deflection of the structural loop is negligible due to the relative high static stiffness of modern machine tools [118, 121]. According to Tlustý [120], the strong periodically variable force components during finishing require a dynamic approach. The relation between a variable force, variable deflections and their imprints on the machined surface can be modelled but is rather complex. The force characteristics are furthermore affected by tool wear. Hence, models of these errors based on static stiffness characteristics of the structural loop together with relatively simple process force calculations are usually not adequate [120].

In this thesis, the effect of process forces on the machine accuracy is not considered. The required analysis of the probe system, machining process, and (dynamic) structural loop stiffness (in various directions) is beyond the scope of this research. The same argument applies to the dedicated analysis required to predict the process forces of an assembly task. Clamping deformations of both workpiece and structural loop elements are also not considered. In the next subsections the analysis is limited to the effect of load variations introduced by the weight of moving machine components and workpiece. Although many researchers report that the respective deflection of the structural loop may cause significant errors, their modelling has received little attention.

3.3.2 Weight of moving machine components

Variations in the deadweight load exerted by a machine component are related to the position of joints that position the respective mass relative to the machine foundation. The resulting deflection of the structural loop is generally confined to the segment that supports the mass relative to the foundation. Hence, the parametric errors that describe the actual geometry of this segment can be related to the position of more than one joint. The dependency of a parametric error on the position of joints other than that enclosed by the respective coordinate frames can usually be summarized as:

- errors in the relative location of successive frames are not affected by the position of a revolute joint with a vertical axis or a prismatic joint with an arbitrary axis, provided that they are lower in the kinematic chain that provides the connection with the machine foundation.
- The position of a prismatic joint with vertical axis of movement only affects errors in the relative location of frames directly connected to it.

The first item addresses the notion that the load transferred through a structural loop segment is only affected by the deadweight of structural loop components higher in the kinematic chain from the machine foundation. Hence the deflection of this segment is not affected by the position of joints lower in the kinematic chain. However, movement of a revolute joint with a non-vertical axis changes the orientation of the deadweight load relative to the structural loop segment, and hence should be considered even though it is lower in the kinematic chain. The load transferred by body 0, which is connected to the machine foundation, is affected by the deadweight of both tool and workpiece chain. This implies that the parametric errors that describe deviations in the actual geometry of this body (i.e. \underline{E}_{a1} and \underline{E}_{b1}) can be related to the position of all joints in the structural loop.

The second item is motivated by the notion that the deadweight load acting on a structural loop segment does not change if a mass is moved in the gravity direction. Note, however, that movement of a vertical prismatic joint changes the structural loop between the successive coordinate frames that enclose this joint. Hence the respective deflection, and thus parametric errors, will be dependent on the position of this and other joints.

It may be argued that the usefulness of the kinematic model is limited, or alternatively that the model should be changed, whenever a parametric error depends on the position of more than one joint. After all, two similar parametric errors that are related to the same joint position can be lumped together without affecting the completeness of the error model. Ultimately, a parametric error dependent on the position of all joints can be used to fully describe the respective translation or rotation error between tool and workpiece without using the error propagation mechanism of the kinematic model and

other similar parametric errors. Retaining the original kinematic model (i.e. six parametric errors per joint), however, has some advantages. The dependency of a parametric error on the position of joints other than that enclosed by the respective coordinate frames is usually of a very regular, predictable nature (often linear). This regularity is related to the notion that such joints only affect the load (often its moment) acting on the respective structural loop segment in a usually known way. Combining different parametric errors will result in a more complex dependency that requires more effort in both its measurement and modelling.

In many cases there are no interaction terms in the dependency of a parametric error on the position of two joints. Hence the respective independent terms can be allocated to different parametric errors describing the same translation or rotation, but dependent on the position of one joint only. In fact, by measuring the end-effector trajectory relative to the workpiece, it is both not possible nor required to separate such terms from geometric or other parametric errors dependent on the same joint position. Hence the geometric parametric errors discussed in the preceding section generally contain errors due to the compliance of the complete structural loop.

The combination of geometric and finite stiffness related parametric errors has an important, often overlooked, effect on error modelling. If errors in the geometry of structural loop segments are constant, there may exist an analytically defined relation between straightness and angular errors. Some researchers (see e.g. [44]) approximate straightness as an integrated angular error. For most carriage configurations, however, this relation is more complex and has to include the relative position of the bearings and their stiffness (in case of kinematically over-determined bearings). Essentially, the relation between straightness and angular errors is based on the assumption that the geometry of the guideway is constant and determines both these errors. Unfortunately, the compliance the structural loop causes changes in the geometry, position, and orientation of the guideway as the respective carriage is moved. Hence the discussed correlation between angular and straightness errors can generally not be assumed.

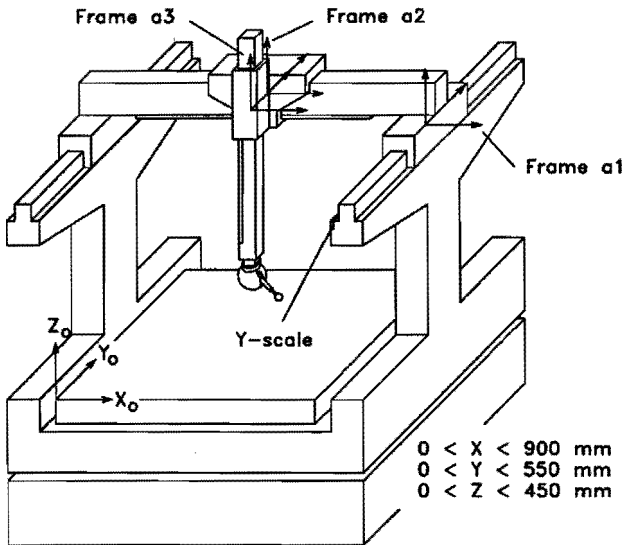


Figure 3.12: Three axis gantry style CMM.

As an example of errors due to the weight of moving components, we consider the gantry style coordinate measuring machine depicted in Figure 3.12. The tool chain of this machine comprises three prismatic joints, two with a horizontal and one with a vertical direction of movement. Using the preceding rules, the dependency of the respective parametric errors on the position x , y , and z of the joints can be summarized as:

$$\underline{E}_{a1} = \underline{E}_{a1}(x, y) \quad (3.16)$$

$$\underline{E}_{a2} = \underline{E}_{a2}(x) \quad (3.17)$$

$$\underline{E}_{a3} = \underline{E}_{a3}(z) \quad (3.18)$$

Due to the compliance of the columns that support the Y-axis guideways, the parametric errors \underline{E}_{a1} between frames 0 and a1 are dependent on both the position of the Y- and X-axis. Especially the angular error ϵ_{a1x} around the X-axis and the translation error e_{a1y} in Y-direction have significant interaction terms between both carriage positions. The latter dependency was determined by measuring the displacement of the Y-axis scale as a function of both the X and Y position. The respective measurement setup is depicted in Figure 3.13. The measured dependency of the Y-axis scale displacement on the X-axis carriage position is depicted in Figure 3.14 for several positions of the

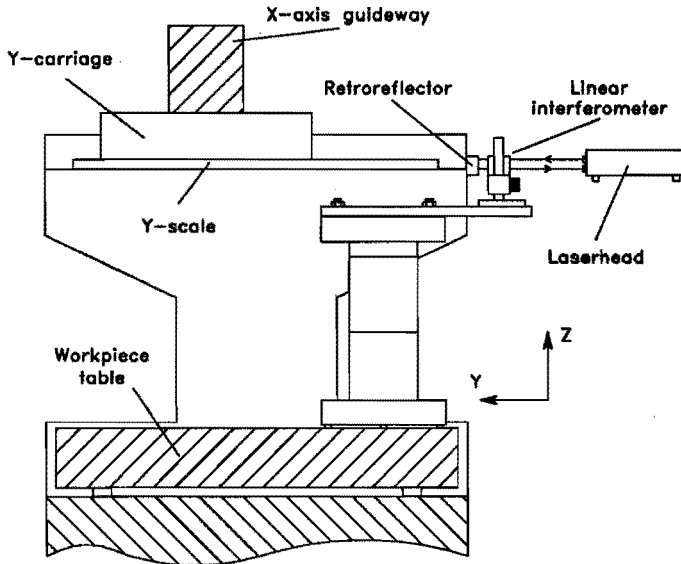


Figure 3.13: Experimental setup to measure the dependency of the Y-axis scale displacement on the position of the Y- and X-axis carriage.

Y-axis carriage. As expected, the dependency on the X-axis carriage position is linear. The model used to describe this error equals:

$$e_{a1y} = \beta_1 y + \beta_2 x + \beta_3 xy \quad (3.19)$$

The unknown parameters $\underline{\beta}$ in this model were estimated by linear least squares regression using the measurement data depicted in Figure 3.14. Obviously, this model of e_{a1y} needs to be augmented with the scale error of the Y-axis. This is achieved by measuring the displacement error in Y-direction of the probe relative to the table along an arbitrary measurement line parallel to the Y-axis. From this data, the effect of parametric errors already modelled (i.e. the displacement of the Y-scale and various angular errors) are subtracted. The estimated model of the residual error data is then combined with the model of Equation 3.19 to obtain the complete model of the e_{a1y} error.

The measured e_{a1x} angular error between frames 0 and a1 and its estimated model are depicted in Figure 3.15. This error was measured using electronic levels placed on the workpiece table and the X-axis guideway. Also in this case, the dependency of the error on the X-axis carriage position is linear. The irregular dependency of the error on the Y-axis carriage position is caused by

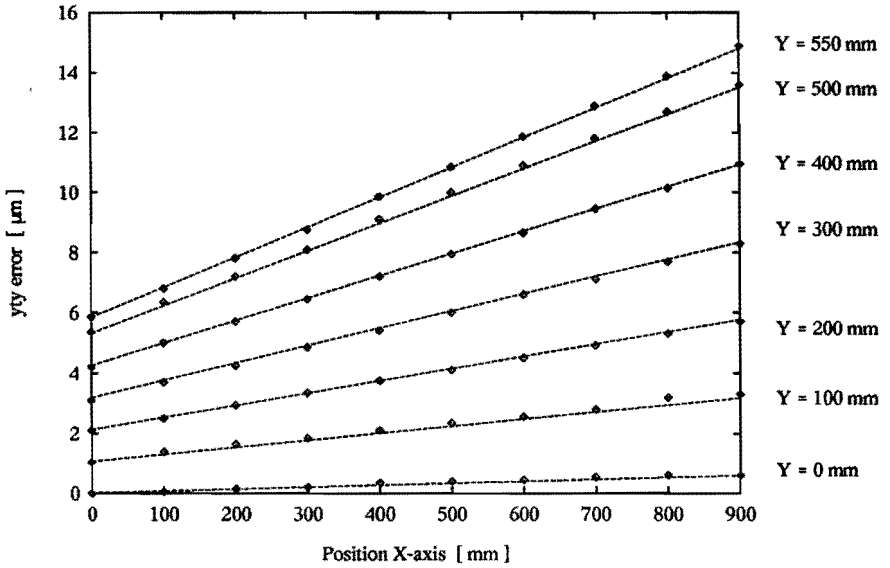


Figure 3.14: Measured translation of the Y-axis scale for various positions of the Y-axis carriage. The lines present the estimated model.

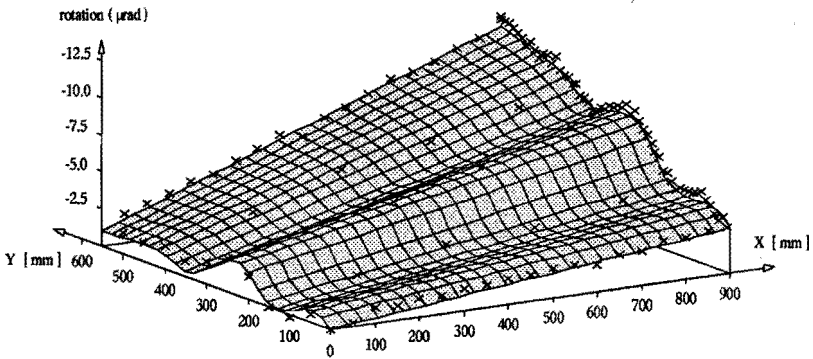


Figure 3.15: Measured ϵ_{a1x} error and the respective model (presented by a solid grid).

the geometric errors of both Y-axis guideways. The estimated error model has a similar structure as that of Equation 3.19 although, in this case, piecewise quadratic terms are used for the various Y-axis dependencies.

3.3.3 Workpiece weight

The workpiece weight has a similar effect on the deflection of the structural loop as the weight of the machine table. Only in this case, both position and value of the load can be changed. The affected segment of the structural loop is generally confined to the components that support the workpiece relative to the foundation. When this segment (i.e. the workpiece chain and body 0) contains kinematic elements, the workpiece is a moving weight. Hence, the parametric errors that describe the structural loop deflection due to the workpiece weight are not only dependent on the position and value of this weight but also on the position of kinematic elements in the workpiece chain. The latter dependency is governed by similar rules as those discussed in the preceding subsection.

To illustrate the errors introduced by the workpiece weight and the respective modelling procedure we consider the five-axis milling machine depicted in Figure 3.16 and described in Chapter 5. The workpiece chain of the machine contains two prismatic joints, one vertical and one horizontal, and one revolute joint B with a vertical axis. The presented analysis is limited to the effect of the workpiece load on the angular error around the X-axis in the orientation of the end-effector relative to the workpiece table. Only changes in this error relative to the situation with no workpiece load are analysed. It is not our intention to present a generalized modelling procedure. Rather it is shown that errors introduced by the workpiece load can be assessed and modelled using relatively simple procedures.

First an experiment is performed to assess whether the dependency between workpiece load and angular deflection is linear. Here, the orientation variation of the workpiece table relative to the end-effector is monitored at a certain fixed position of the machine axes as the workpiece load is increased and decreased. The analysed angular error is measured as the difference between

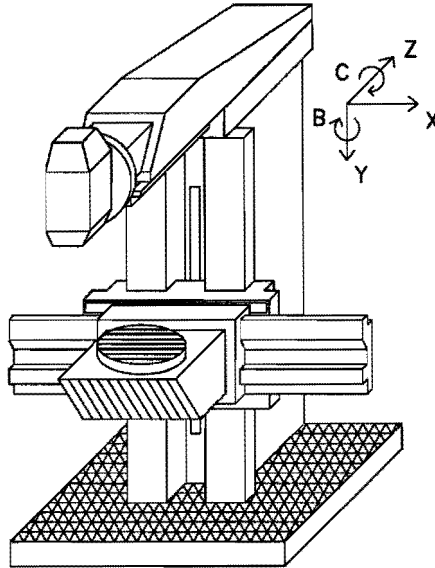


Figure 3.16: Five-axis milling machine.

the indications of two electronic levels mounted on respectively the workpiece table and the end-effector (see Figure 3.17). The error is measured relative to the end-effector since the majority of the structural loop deflection occurs in the workpiece chain. The applied workpiece loads equal 0, 1750, 3500, and 4900 N. The latter load approximately equals the maximum load recommended by the manufacturer (5000 N). The loads are applied to the centre of the workpiece table through a relatively small support of 150×100 mm ($X \times Z$). The experiment was executed at the right edge of the machine workspace ($X = 650$ mm). The respective measurements are depicted in Figure 3.18.

The results suggest a highly linear relation between workpiece load and angular error which significantly simplifies the succeeding analysis. There occurs hysteresis but this was not further analysed. The simultaneously measured angular deflection around the Y- and Z-axis (using respectively a laserinterferometer and two additional levels) also show a linear dependency on the workpiece load. These errors are, however, significantly smaller in magnitude.

The preceding experiment addressed the combined deflection of all structural loop segments in response to the workpiece weight. To assess the dependency of this deflection on the position of the machine axes, further experiments are

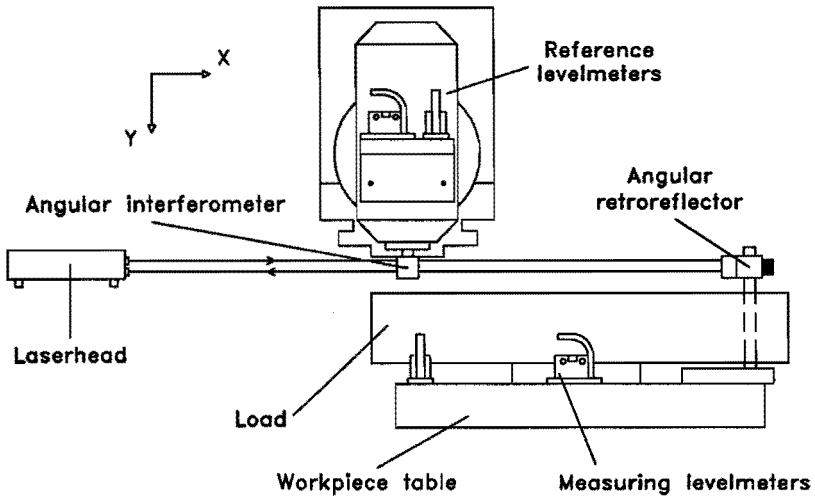


Figure 3.17: Experimental setup to measure the change in orientation of the workpiece table relative to the end-effector due to the workpiece weight.

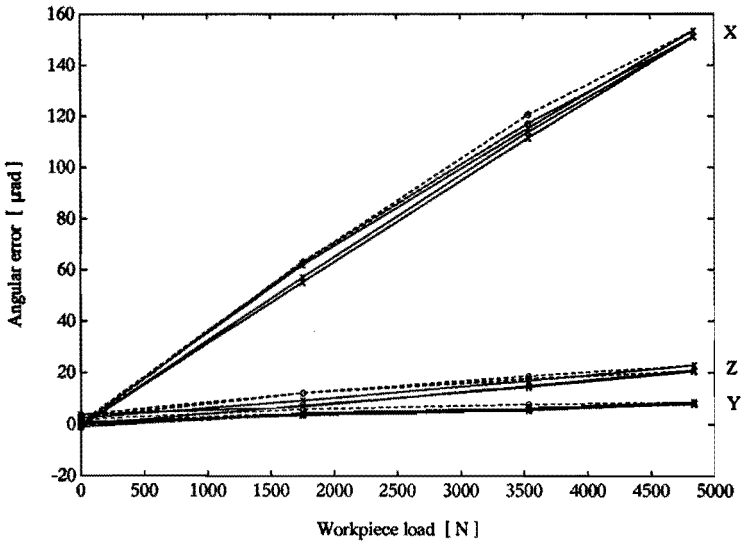


Figure 3.18: Angular error of the workpiece table relative to the end-effector as a function of workpiece weight. Solid and dashed lines represent, respectively, the increase and decrease of the applied workpiece weight. (Three runs, load at centre table, X = 650 mm, Y = 490 mm).

required that focus on structural loop segments associated with individual parametric errors. First the parametric errors that describe the deflection of the machine frame (body 0) are analysed.

The machine frame supports the workpiece relative to the foundation. The respective deadweight load is determined by the position of the workpiece relative to this frame. The position where the load is introduced in the machine frame is furthermore affected by the position of the Y-axis. Hence the relative deformation of the machine frame due to the workpiece weight is related to the positions of all axes in the workpiece chain. Movement of the B-axis, however, can also be described by an appropriate translation of the workpiece on the table. Translation of the workpiece on the table in X-direction has a similar effect as movement of the X-axis (excluding axis positions at the boundary of the workspace). Hence the major dependencies that require analysis are the position of the Y- and X-axis, and the Z-position of the workpiece on the table.

Regarding the studied angular error, deformation of the machine frame affects, in principle, the mutual squareness of the Y- and Z-axes, and the y_{rx} and z_{rx} errors (rotation around X when moving respectively the Y and Z carriage). Dependency of the z_{rx} error on the workpiece load is unlikely, since the respective guideway section is not part of the structural loop affected by the workpiece weight. Similarly, the effect of the workpiece weight on the y_{rx} error and the YZ-squareness error is expected to be relatively small, since the respective guideway segment (i.e. the machine frame between Y-axis and Z-axis carriage) is only marginally affected. Note that the machine frame between foundation and Y-axis carriage is not part of the structural loop. Bending of this frame section due to the workpiece load does not change the location of the end-effector relative to the workpiece.

To assess the validity of the above assumptions, the y_{rx} error is measured for several positions of the X-axis both without and with workpiece weight. The used measurement setup equals that of the preceding experiment (see Figure 3.17). The used workpiece weight of 4900 N is located at the centre of the workpiece table. The measurement results are depicted in Figure 3.19. In the unloaded case, the y_{rx} error is affected by the position of the X-axis carriage. This cross-coupling is probably related to the different load distribution of the

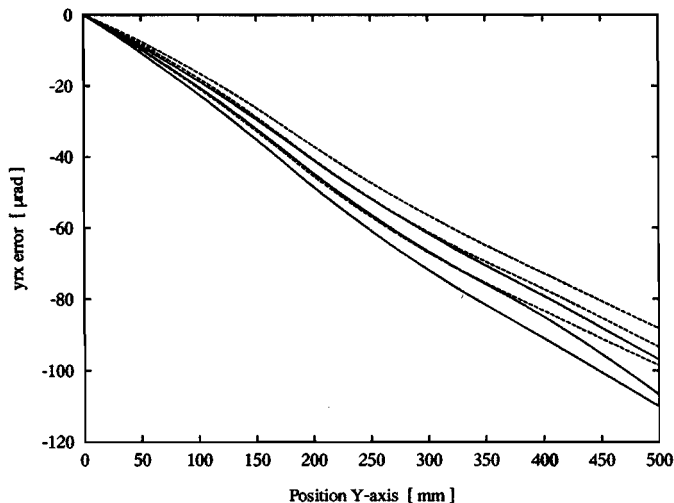


Figure 3.19: y_{rx} error at several positions of the X-axis carriage. The solid and dashed lines represent, respectively, the error without and with workpiece weight (4900 N, centre table). The upper, middle, and lower curve of each set correspond to an X-axis carriage position of respectively $X = 0$, $X = 350$, and $X = 700$ mm. The various curves are estimated from 5 back-and-forth measurements using a sampling distance of 25 mm.

Y-axis bearings due to the weight and position of the X-axis carriage. Apparently, the workpiece load does not change this dependency of the y_{rx} error on the position of the X-axis carriage. However, the dependency of the error on the Y-carriage position is changed over approximately the same amount as a change in X-carriage position from centre to left ($X = 350$ to $X = 0$). This similarity is not surprising, since the applied workpiece weight approximately equals that of the X-axis carriage (4850 N). Based on these measurements, the dependency of the y_{rx} error on the workpiece weight is modelled as an error proportional to the observed difference between the loaded and unloaded error at $X = 0$. Since the y_{rx} dependency on the workpiece weight is relatively small and apparently related to the exerted moment of the workpiece weight around the Z-axis, its dependency on the workpiece position in Z-direction is not further analysed.

Next we consider the deflection of the X-axis guideway due to the workpiece load. Regarding the studied angular error, this deflection affects the relative

change in the xrx roll error as the X-axis carriage is moved. The mechanism in this case is torsion of the X-axis guideway caused by the moment exerted by the workpiece load. The error was measured using the setup of Figure 3.17. Some results are depicted in Figures 3.20 and 3.21. Since the guideway is supported in its centre, the angular error increases as the carriage is moved from its centre position ($X = 350$ mm). A uniform guideway cross-section would result in a linear dependency. The observed, somewhat parabolic, error curve is due to the contribution of the Y-axis carriage to the guideway stiffness. The model used to describe the change in the xrx error due to a workpiece weight of F_w located at a position of $b3p$ relative to the table centre (i.e. relative to coordinate frame $b3$) equals:

$$xrx(X, F_w, b3p) = xrx(X, 4900, 0) \cdot \frac{F_w}{4900} \cdot \frac{375 - b3p_x}{375} \quad (3.20)$$

Here $xrx(X, 4900, 0)$ represents the fitted piecewise polynomial model for the observed xrx error due to a workpiece weight of 4900 N located at the table centre. The used constant of 375 mm equals the distance between the table centre and the centroid of the X-axis guideway in Z-direction. Its use is somewhat suspect in the centre of the X-axis range where the Y-axis carriage contributes to the guideway stiffness. In Figure 3.21 the predicted and observed xrx error is presented for a workpiece load of 2600 N.

We now need to determine the constant deflection of the various structural loop segments between the Y-axis and the B-axis, i.e. the components that do not depend on the X- and Y-position of the machine axes. These components determine the parallelism error between the B-axis and Y-axis due to the workpiece load. They are measured as the orientation variation of the workpiece table relative to the end-effector at a certain fixed position of the machine axes as the workpiece load is increased and decreased. The respective results are depicted in Figure 3.22. The linear dependency of the error on the position of the workpiece load in Z-direction suggests that the compliance of the X-axis and Y-axis bearings are the main contributing factors. Bending of the Y-axis or X-axis carriage would result in a nonlinear dependency. The model for this error is based on a fitted straight line though the error values corresponding to the maximum load case. Since the angular deflection is linear in the workpiece load, the deflection under an arbitrary load is calculated as an appropriate fraction. The estimated error is implemented as an offset

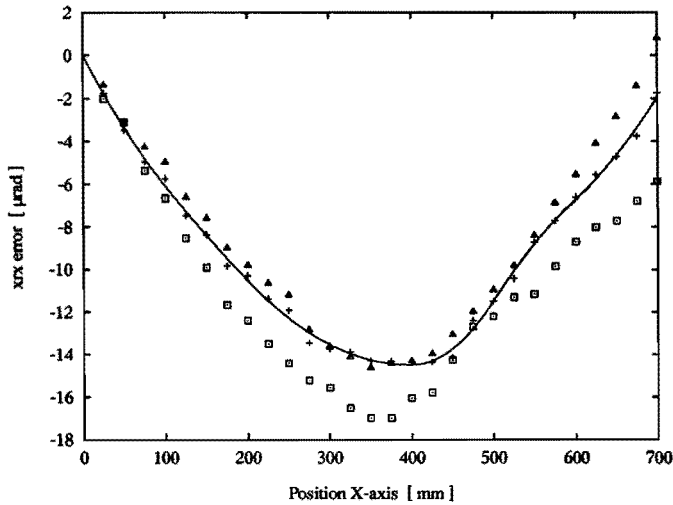


Figure 3.20: Change in the xrx error due to a workpiece load of 4900 N. The symbols Δ , +, and \square represent the average of five back-and-forth runs with the load located at a X-position of respectively -208 mm, 0 mm, and 208 mm relative to the table centre. The line represents the predicted xrx for all load positions according to Equation 3.20.

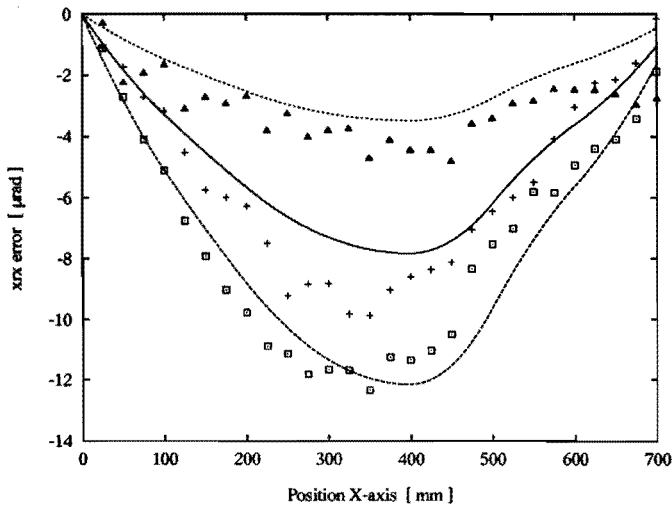


Figure 3.21: Change in the xrx error due to a workpiece load of 2600 N. The symbols Δ , +, and \square represent the average of five back-and-forth runs with the load located at a Z-position of respectively 208 mm, 0 mm, and -208 mm relative to the table centre. The lines represent the predicted errors according to Equation 3.20.

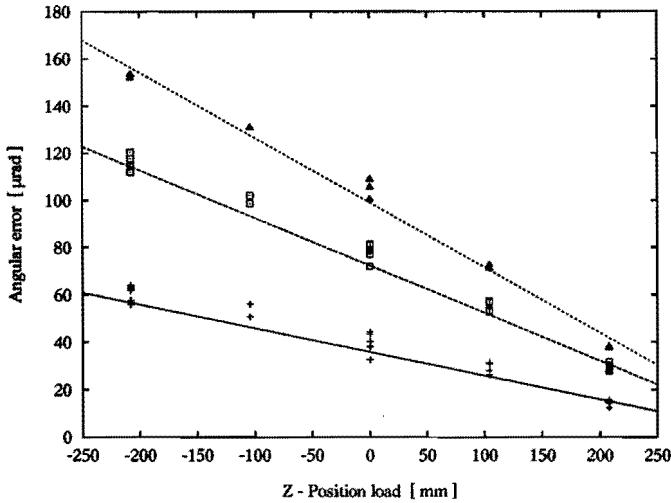


Figure 3.22: Angular error around X of the workpiece table relative to the end-effector as a function of workpiece weight and -position. The symbols +, \square , and Δ represent, respectively, a workpiece load of 1750, 3500, and 4900 N. The various lines represent the respective model. (X = 650 mm, Y = 490 mm).

value for the various x_{rx} error curves in such a way that the respective x_{rx} error equals this offset at the tested position.

To complete the model for the angular error around X, the deflection of the workpiece table relative to the B-axis has to be determined (and the table deformation). In contrast to the parallelism error between B-axis and Y-axis, the respective angular deflection has an axis of rotation that changes its orientation when the B-axis is moved. Note that the experiment described in the preceding paragraph assesses the combined value of both these errors.

3.4 Thermal errors

The structural loop is subject to a large variety of thermal loads. These loads affect the accuracy of the executed task due to the thermal deformation of structural loop components. In this section, the modelling procedure of the respective errors is discussed. Three models are derived. The first two

models are empirically estimated. They describe the dynamic response of respectively the temperature distribution and the thermal drift to various heat sources. The third model reflects an analytical approach to relate the thermal parametric errors to the temperature distribution of the structural loop. The latter is either estimated from temperatures measured by sensors distributed over the complete structural loop or described by the output of the first empirical model. The analytical model is based on the approximation of stress-free thermal deformation of the structural loop.

3.4.1 Introduction

The thermal deformation of the structural loop in response to various internal and external heat sources is a major error source affecting the accuracy of measured or machined parts [16, 71, 50]. The respective mechanism is depicted in Figure 3.23. This figure is a summary of the diagram compiled by Bryan [13, 16] and McClure [71]. The various heat sources are presented at the top of the chart. Heat dissipation from these sources by conduction, convection, and radiation results in a certain temperature distribution of the structural loop with consequent deformations.

A uniform temperature distribution different from 20 °C does not affect the accuracy of the executed task, provided that all components of the structural loop, including the workpiece, have the same coefficient of thermal expansion. In practice, the structural loop often contains components of different materials. Notorious is the respective difference in thermal expansion between measurement system and workpiece. In case the various structural loop components can expand freely, calculation of the resulting uniform deformation of each component is relatively straightforward, provided that the expansion coefficients are known. However, due to the uncertainty of these coefficients, errors will exist whenever tasks are executed at temperatures other than 20 °C. McClure [70] reports uncertainties in coefficients of expansion that vary from $\pm 5\%$ for common steels to $\pm 25\%$ or more for non-metals. A complicated situation arises when components of different materials mutually restrict their thermal expansion. The resulting non-uniform deformations often introduce both angular and displacement errors. Their modelling is dif-

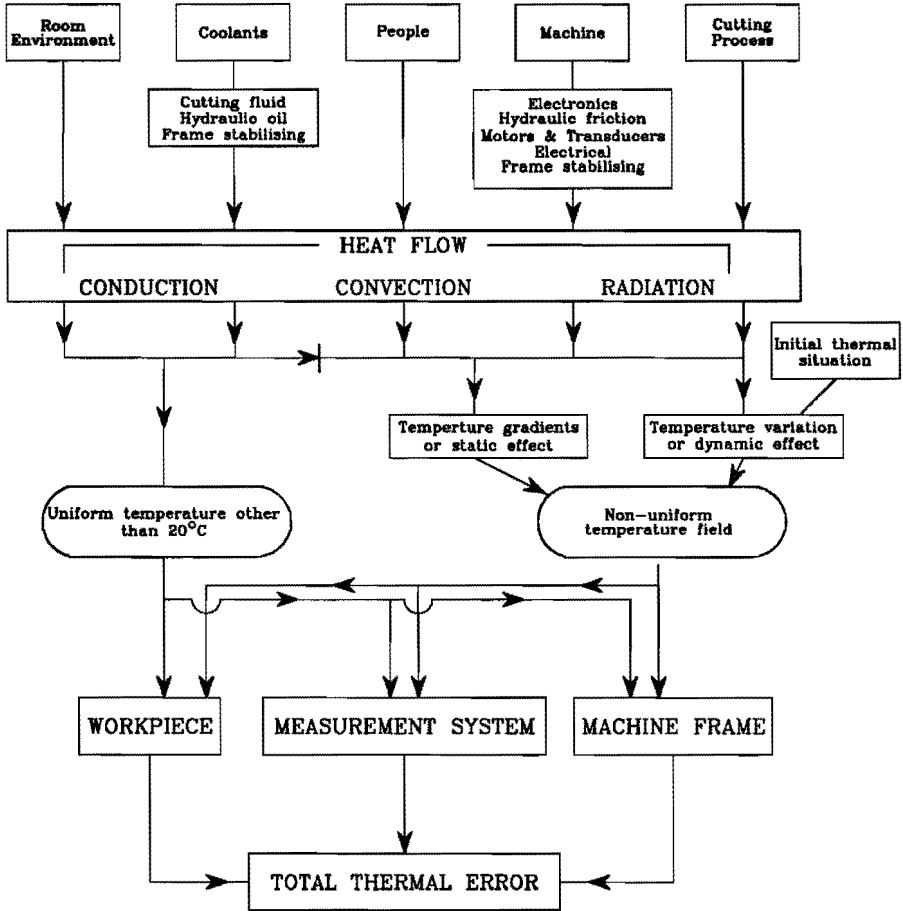


Figure 3.23: Diagram of thermal effects in manufacturing and metrology [16].

ficult, since the resulting thermal stresses require stiffness analysis of the affected components. Especially the workpiece fixturing during machining requires special attention to avoid these effects.

An uniform environmental temperature and (well distributed) coolant systems (e.g. an oil shower [13, 31, 71]) are the only heat sources that can create uniform temperature distributions. This is indicated in the diagram of Figure 3.23 by an unidirectional arrow. The local action of remaining heat sources causes thermal gradients in the structural loop resulting in a non-uniform thermal deformation. If both the heat sources and the structural loop remain constant, steady-state gradients develop. These gradients cause a non-uniform thermal deformation of the structural loop resulting in both angular and displacement errors. Modelling the steady-state distortion of the structural loop is, however, generally not a sufficient solution. Changes in the thermal environment, the structural loop, and the various (internal) heat sources will result in transient effects, that need to be considered for most manufacturing tasks.

A first cause of transient changes in the thermal distribution of the structural loop is related to the environmental temperature variation, both in its gradients and average value. Due to differences in the volume-to-surface ratio, specific heat, and density of structural loop segments, their response to such variations will differ, resulting in transient thermal gradients. The same argument applies to the response of different structural loop segments to changes in the internal heat sources. Here the effect is usually even more profound due to the local action of these sources. The common practice of pre-warming the machine cannot be considered as a satisfactory solution, mainly due to the need to shut down certain heat sources (e.g. the spindle) to load the workpiece, change tools, measure, etc. [13]. Movement of machine carriages poses an additional source of transient effects. First, the structural loop changes, resulting in different heat-flow pathways, time constants, and overall surface geometry. Second, a structural loop segment acting as a heat sink at a certain location may, after movement to a cooler area of the machine, act as a heat source for that area. In other words, the movement of carriages

represents a special mode of heat transfer. Third, the frictional heat generated during movement represents a variable heat source, whose position relative to structural loop segments changes during movement.

Dependent on the chosen input, either one, two, or three models are required to analytically describe the thermal errors. The first model relates the heat flows into the structural loop to operating conditions like spindle speed, joint movements, and ambient temperature. The second model describes how these heat flows affect the temperature distribution of the structural loop. The third model relates the errors in the location of the end-effector relative to the workpiece to this temperature distribution. Empirical models can be used to directly express the errors in the relative end-effector location as a function of either operating conditions, heat-flows, or temperature distribution (or some measure thereof).

Yoshida [141, 139, 140] uses the assumption of stress-free thermal deformation to analytically model the thermal errors of a lathe and a milling machine as a function of the temperature distribution under steady state conditions. Approximately 50 temperature sensors are used. A method to reduce the number of sensors is presented, based on an assumed exponential form for the temperature field around the heat source. Similar analytical models are presented by Balsamo [6], Cresto [28], Sartori [88], and Trapet [123] to model the thermal errors of CMMs. The first three authors use regression procedures to estimate various parameters in the analytical model (e.g. the coefficients of thermal expansion) based on the observed errors of the CMM when measuring artifacts. All authors report a large number of sensors. Trapet and Loock [95] use their analytical model to describe the thermal errors of the five-axis milling machine described in Chapter 5. Here they introduced a new description for the thermal roll error of a beam. Venugopal [127] presents analytical solutions for the thermal deformation of thin walled cubic machine structures based on the measured temperature of the corner points in time.

A number of empirical models have been reported that relate the thermal errors to the temperature distribution (see e.g. [24, 33, 45, 63, 80, 115, 127]). Here either the parametric errors or the resulting errors in the location of the end-effector are related to the readings of a number of characteristic

temperature sensors by relatively simple regression models. The presented models are static, i.e. the thermal errors at a certain time are expressed as a function of the measured temperatures at that time. Some researchers (e.g. [115]) use various statistical techniques to reduce the number of required sensors and to avoid overfitting.

Finite element and finite difference techniques are used by many researchers to model the thermal errors (see e.g. [2, 12, 22, 55, 69, 80, 93, 127, 130, 142]). In general these techniques are used to calculate both the temperature distribution and the resulting deformations. The input to these models are analytically or empirically determined heat flows. In some cases, the measured temperature distribution is taken as input. Sata [93] proposes a method to evaluate the intensity of the heat sources based on the measured values of temperatures in close proximity to these sources. As stated in the introduction of this chapter, especially the prediction of the temperature distribution is difficult due to the many uncertainties in the thermal boundary conditions.

A very interesting approach is presented by McClure [71]. He proposes a model where the thermal errors in the relative location of the end-effector at a certain position are related to the change of environmental temperature and operating conditions in time. The parameters in this dynamic model are empirically estimated using step-response tests. Many of his ideas have been incorporated in the presented analysis of this section.

Obviously the effect of model uncertainty is minimized if the temperature distribution of the structural loop is taken as input. The inherent defects of this approach is that many temperature sensors are required to assess this field, especially under transient conditions. The heat flow model looks promising, except for the requirement of heat-flux transducers. The costs of such devices and the problem of their proper location in the machine makes this approach not attractive. Taking operating conditions as input has the advantage that generally no extra sensors have to be attached to the machine. Unfortunately, the relation between operating conditions and heat flows is often dependent on the temperature (resulting in nonlinear models) and sensitive to wear.

In this thesis we have chosen for a modified version of the heat flow approach. Here temperature sensors are attached to the machine in close proximity to the various heat sources. The change in the sensor readings is taken as a measure for the respective heat flows. This approach requires two models. First, the temperature distribution of the structural loop has to be related to the values of a limited number of temperature sensors. Second, a model is required that relates the obtained temperature distribution to the various parametric errors.

The first model is empirically derived. Here a large number of additional temperature sensors are temporarily attached to the machine at various locations. Based on the measured temperature elevations during a characteristic duty cycle of the machine, a dynamic model is estimated that relates the measured temperatures of the additional sensors to the values of the sensors located near the heat sources and the ambient temperature. The additional sensors used to estimate the model can then be removed from the machine. This approach is motivated by the reluctance of manufacturers to place a large number of sensors on machines, mainly because of reliability problems and the costs of their installation.

The second model, relating the modelled temperature elevations to the various parametric errors, is analytically derived. Here we make the approximation of stress-free thermal deformation of the machine, which results in a model that is not related to detailed geometric properties of the structural loop (e.g. the beam cross-sections). This model can also be used to predict the parametric errors using a large number of temperature sensors attached to the structural loop (i.e. without using the first model).

A second approach to thermal error modelling is presented where errors in the relative location of the tool are directly expressed as a function of the observed temperature elevations of a limited number of sensors (including the ambient temperature). Essentially this involves a combined estimation of the models discussed in the previous paragraph. The model is again dynamic, which enables a significant reduction of the required temperature sensors. The model is obtained by an empirical modelling procedure. Since no parametric errors are estimated, the validity of the model is restricted to a limited part of the ma-

chine workspace. Several of such models, and a suitable interpolation scheme, are required to describe the machine errors in the complete workspace. This approach is similar to that reported by McClure [71]. However, instead of operating conditions, the observed thermal elevations near the heat sources are taken as input.

As a first approach, the various models are restricted to the following conditions:

- No cooling liquid.
- Movement of the carriages is either slow or restricted to a limited axis range. This restriction is related to the described heat transfer due to carriage motion.

3.4.2 Modelling the temperature distribution

In this subsection we consider the estimation of the temperature distribution of the structural loop in response to various heat sources. The respective model describes the departure of the temperature distribution from that during the reference state (the machine accuracy in this state is already described by the geometric model).

The heat transfer problem to be solved can be described as follows ([71]). The structural loop is an object of rather complicated geometry that occupies a three dimensional region B bounded by a surface S . The surface is divided into n patches S_i that are subject to different thermal boundary conditions, e.g. a heat flow q_i or a temperature T_i . Heat is transferred from the structural loop to the environment through the remaining portion S_n of the surface by convection and radiation.

In this analysis we make the following assumptions:

- the body B has no internal heat generation.
- the material properties are independent of temperature and isotropic.

- radiation and convection can be combined into one convective heat flow.

Under these conditions, the energy balance of a differential volume of body B leads to the Fourier heat equation as follows [23]:

$$\frac{\partial}{\partial x} \left(\lambda \frac{\partial T}{\partial x} \right) + \frac{\partial}{\partial y} \left(\lambda \frac{\partial T}{\partial y} \right) + \frac{\partial}{\partial z} \left(\lambda \frac{\partial T}{\partial z} \right) = \rho c \frac{\partial T}{\partial t} \quad (3.21)$$

Where T is temperature, t is time, ρ is density, λ the thermal conductivity, and c the specific heat of the material. The partial differential equation is linear in T and homogeneous. The various boundary conditions are summarized as:

$$S_1 : \lambda \frac{\partial T}{\partial n_1} = u_1(t) \quad (3.22)$$

$$S_2 : T = u_2(t) \quad (3.23)$$

$$S_3 : \lambda \frac{\partial T}{\partial n_3} = u_3(t) \quad (3.24)$$

⋮

$$S_n : \frac{\lambda}{h} \frac{\partial T}{\partial n_n} + T = T_{amb} = u_n(t) \quad (3.25)$$

Here n_i is the outward-directed normal vector of surface element S_i . The first boundary condition describes a prescribed heat flux $u_1(t)$. The second boundary condition describes a prescribed surface temperature $u_2(t)$. The final boundary condition corresponds to a convective heat transfer to the environment having a temperature of T_{amb} . Here h denotes the convection heat transfer coefficient. The respective surface S_n comprises the remaining portion of S where no other boundary conditions are specified. The specification of this boundary condition can be further refined in case the machine is subjected to environmental gradients, sunlight, etc. This can be achieved by dividing S_n into different surface patches with different boundary conditions. However, the analysis presented below only requires the definition of additional inputs $u_i(t)$ that characterize these effects, not an exact formulation of the respective boundary condition.

The body B has an initial temperature described by:

$$T(\vec{p}, t = 0) = v(\vec{p}) \quad (3.26)$$

Since both the boundary conditions and the heat equation are linear in T , the temperature at a certain point \vec{p} and time t can be obtained by superposition:

$$T(\vec{p}, t) = \sum_{i=1}^n T_i(\vec{p}, t) + T_v(\vec{p}, t) \quad (3.27)$$

Here $T_i(\vec{p}, t)$ represents the temperature distribution of B when the initial temperature and all functions u_j equal zero except for $j = i$. $T_v(\vec{p}, t)$ represents the temperature distribution that results from the initial temperature $v(\vec{p})$ when all functions u_j equal zero. The principle of superposition can also be applied to describe the response of the temperature distribution $T_i(\vec{p}, t)$ to a time dependent boundary condition $u_i(t)$. Using Duhamel's (convolution) theorem, this response equals:

$$T_i(\vec{p}, t) = \int_0^t h_i(\vec{p}, t - \tau) u_i(\tau) d\tau \quad (3.28)$$

Here $h_i(\vec{p}, t)$ equals the temperature distribution of body B at time t due to a unit impulse in the boundary condition u_i at $t = 0$ when all other inputs u_j and the initial temperature equal zero. If these functions can be obtained, we have all the information required to calculate the response of the temperature distribution to the various time dependent boundary conditions. Unfortunately, the complex geometry of the structural loop precludes their analytical derivation.

To get a feeling for the nature of the impulse response, we take a closer look at the problem when all inputs u_i equal zero. Observe that, due to the linearity and homogeneity of this problem, if two functions $w_1(\vec{p}, t)$ and $w_2(\vec{p}, t)$ each satisfy the heat equation and the boundary conditions, any linear combination of these solutions does the same. The method of separation of variables makes use of the above by producing a lot of special solutions $w_j(\vec{p}, t)$ that satisfy the heat equation and the boundary conditions. These solutions are then added with suitable constants c_j to produce a solution that also satisfies the initial condition $v(\vec{p})$ [78]. The special solutions $w_j(\vec{p}, t)$ have the form of a product of a function $P(\vec{p})$ times a function $\Theta(t)$:

$$w_j(\vec{p}, t) = P(\vec{p}) \Theta(t) \quad (3.29)$$

Substitution of this solution in the heat equation yields:

$$\Theta \frac{\partial}{\partial x} \left(\lambda \frac{\partial P}{\partial x} \right) + \Theta \frac{\partial}{\partial y} \left(\lambda \frac{\partial P}{\partial y} \right) + \Theta \frac{\partial}{\partial z} \left(\lambda \frac{\partial P}{\partial z} \right) = \rho c P \dot{\Theta} \quad (3.30)$$

separating the variables,

$$\frac{1}{P \rho c} \left(\frac{\partial}{\partial x} \left(\lambda \frac{\partial P}{\partial x} \right) + \frac{\partial}{\partial y} \left(\lambda \frac{\partial P}{\partial y} \right) + \frac{\partial}{\partial z} \left(\lambda \frac{\partial P}{\partial z} \right) \right) = \frac{\dot{\Theta}}{\Theta} \quad (3.31)$$

The left hand side of equation 3.31 only contains position dependent terms whereas the terms of the right hand side are only functions of time. Hence both left and right hand side can only equal a constant value $-\gamma$. It is known that γ is a positive real number to ensure that the solution will decay to zero as time increases (note that we are still considering a problem where all inputs equal zero). Equating the right hand side of Equation 3.31 to $-\gamma$ yields:

$$\dot{\Theta} = -\gamma \Theta \quad (3.32)$$

This equation has the solution:

$$\Theta = d_\gamma e^{-\gamma t} \quad (3.33)$$

Here the subscript γ on the constant d indicates that this constant can be different for different values of γ . The product solution for $w_j(\vec{p}, t)$ can now be expressed as:

$$w_j(\vec{p}, t) = P_j(\vec{p}) e^{-\gamma_j t} \quad (3.34)$$

In general there are an infinite number of values for γ that satisfy both the heat equation and the (homogeneous) boundary conditions. However, their value increases rapidly with j , so usually only a limited number m have to be taken into account. Hence the response $T_v(\vec{p}, t)$ of the temperature distribution to a certain initial temperature distribution $v(\vec{p})$, while all inputs $u_i(t)$ remain zero, equals:

$$T_v(\vec{p}, t) = \sum_{j=1}^m c_{v,j} P_j(\vec{p}) e^{-\gamma_j t} \quad (3.35)$$

Here the constants $c_{v,j}$ are estimated from the initial temperature $v(\vec{p})$. We now consider the solution for the step response $T_{S,i}(\vec{p}, t)$ of the temperature distribution to a certain input $u_i(t)$ when all other inputs and the initial temperature equal zero. This nonhomogeneous problem can often be converted into a homogeneous one by the use of a partial solution $T_{P,i}(\vec{p})$ to the nonhomogeneous problem. A suitable choice would be the steady-state solution which satisfies the (nonhomogeneous) boundary conditions but not the initial condition [78]. The total solution can be expressed as the sum of this steady-state solution and a solution $T_{v,i}(\vec{p}, t)$ of the homogeneous problem with all inputs zero and an initial temperature that equals the negated steady-state solution:

$$T_{S,i}(\vec{p}, t) = T_{P,i}(\vec{p}) + T_{v,i}(\vec{p}, t) \quad (3.36)$$

where:

$$T_{v,i}(\vec{p}, 0) = -T_{P,i}(\vec{p}) \quad (3.37)$$

The general solution to the problem with all inputs zero and a certain initial temperature is presented in Equation 3.35. Hence the solution for $T_{S,i}(\vec{p}, t)$ is of the format:

$$T_{S,i}(\vec{p}, t) = T_{P,i}(\vec{p}) + \sum_{j=1}^m c_{i,j} P_j(\vec{p}) e^{-\gamma_j t} \quad (3.38)$$

Differentiating this step response yields the desired impulse response $h_i(\vec{p}, t)$:

$$h_i(\vec{p}, t) = \sum_{j=1}^m -\gamma_j c_{i,j} P_j(\vec{p}) e^{-\gamma_j t} \quad (3.39)$$

Combining equations 3.27, 3.28, 3.35, and 3.39 yields the following expression for the temperature distribution of body B :

$$T(\vec{p}, t) = \sum_{i=1}^n \sum_{j=1}^m -\gamma_j c_{i,j} P_j(\vec{p}) \int_0^t e^{-\gamma_j(t-\tau)} u_i(\tau) d\tau + \sum_{j=1}^m c_{v,j} P_j(\vec{p}) e^{-\gamma_j t} \quad (3.40)$$

The response of this system in time is determined by a number of time constants γ_j^{-1} . The temperature distribution at a certain instance is described by the so-called eigenfunctions $P_j(\vec{p})$. The combination of a time constant γ_j^{-1} with the respective eigenfunction $P_j(\vec{p})$ can be viewed as a certain mode of the system. The various inputs u_i 'excite' these modes in a different manner resulting in a certain temperature distribution.

Equation 3.40 describes the response of a distributed multivariable system. An efficient framework to model such systems is the state-space description. Here the history of the system at a certain time is summarized in a so called state vector \underline{x} . The system is then described by two equations. First, an equation that relates the time derivative of the state vector to both the state vector and the input signals at a certain time. Second, an equation that describes the output of the system at a certain time as a function of the respective state and input signal. Equation 3.40 suggests that the history of the input signal u_i regarding the mode with time constant γ_j^{-1} can be summarized by the state $x_{i,j}$ defined as:

$$x_{i,j} = \int_0^t e^{-\gamma_j(t-\tau)} u_i(\tau) d\tau \quad (3.41)$$

For input signal u_i , we now combine the various state components $x_{i,j}$ into one state vector \underline{x}_i . The respective state-space model can be expressed as:

$$\dot{\underline{x}}_i = A_i \underline{x}_i + B_i u_i \quad (3.42)$$

$$T_i(\vec{p}, t) = C_i \underline{x}_i \quad (3.43)$$

Where:

$$A_i = \begin{bmatrix} -\gamma_1 & & \\ & \ddots & \\ & & -\gamma_m \end{bmatrix} \quad (3.44)$$

$$B_i = \begin{bmatrix} 1 \\ \vdots \\ 1 \end{bmatrix} \quad (3.45)$$

$$C_i = [C_{i,1}(\vec{p}) \ \cdots \ C_{i,m}(\vec{p})] \quad (3.46)$$

$$C_{i,j}(\vec{p}) = -\gamma_j c_{i,j} P_j(\vec{p}) \quad (3.47)$$

Combining the state vectors associated with the various inputs into one state vector \underline{x} yields:

$$\dot{\underline{x}} = A \underline{x} + B \underline{u} \quad (3.48)$$

$$T(\vec{p}, t) = C \underline{x} \quad (3.49)$$

Where:

$$A = \begin{bmatrix} A_1 & & \\ & \ddots & \\ & & A_n \end{bmatrix} \quad (3.50)$$

$$B = \begin{bmatrix} 1 & 0 & \cdots & 0 & 0 \\ \vdots & \vdots & & \vdots & \vdots \\ 1 & 0 & \cdots & 0 & 0 \\ & & \ddots & & \\ 0 & 0 & \cdots & 0 & 1 \\ \vdots & \vdots & & \vdots & \vdots \\ 0 & 0 & \cdots & 0 & 1 \end{bmatrix} \quad (3.51)$$

$$C = [C_{1,1}(\vec{p}) \ C_{1,2}(\vec{p}) \ \cdots \ C_{n,m}(\vec{p})] \quad (3.52)$$

$$\underline{x} = \begin{bmatrix} \underline{x}_1 \\ \vdots \\ \underline{x}_n \end{bmatrix} \quad (3.53)$$

It should be noted that the chosen state contains more components than required to sufficiently describe the history of the system. The effect of input signals related to the same time constant γ_j^{-1} can be lumped into one state component without affecting the completeness of the model. This can be readily deduced from the response of the temperature distribution to its initial value. We have chosen for the presented state definition because it contains no position dependent elements.

From equation 3.49, the response $T_k(t)$ of a temperature sensor located at position \vec{p}_k can be expressed as:

$$\dot{\underline{x}} = A\underline{x} + B\underline{u} \quad (3.54)$$

$$T_k = C\underline{x} \quad (3.55)$$

Here the $1 \times (nm)$ row vector C contains constant coefficients only dependent on the position of the temperature sensor. Hence the response of several temperature sensors is described by augmenting C with one row vector for each sensor.

To determine the response of these sensors to various input signals, the elements of matrix C have to be estimated as well as the m time constants γ_j^{-1} . These parameters are empirically estimated using the observed change in sensor readings during a characteristic duty cycle of the machine. Here the machine axes are not moved which restricts the estimated model to a limited part of the machine workspace. The vector of input signals \underline{u} contains the observed readings of temperature sensors located in close proximity to the machine heat sources. Since the experiments start from a machine in its reference state (i.e. that described by the geometric model), the components of the state vector at the start of each duty cycle are assumed to be zero. From the measurement data the parameters are simultaneously estimated by nonlinear least squares regression using the Levenberg-Marquardt method (the time constants γ^{-1} enter the regression in a nonlinear fashion). Here the various parameters are adjusted such that the least squares sum of the residuals between the observed and predicted temperature elevations is minimized. Since the various temperatures are measured at discrete time intervals, a discrete version of the state space model is used.

In Chapter 5, the method will be applied to estimate the temperature distribution of a five-axis milling machine in response to the heat generated by the spindle drive.

3.4.3 Modelling the parametric errors

In this subsection, models are derived that describe the changes in the parametric errors due to a temperature distribution different from that in the reference state. Here the temperature distribution is assumed to be known, for example from the model described in the preceding subsection or by a sufficient number of temperature sensors distributed over the structural loop. In the latter two cases, the temperature distribution is approximated by a piecewise linear interpolation between the various sensor locations.

In this subsection the various parametric errors are analytically derived. To facilitate the analysis, we make the basic assumption of stress-free thermal deformation of the structural loop. Stress-free thermal deformation of a structural loop component is only related to the temperature distribution of that component and relatively global geometric entities (e.g. the length of a beam but not its cross-section). Since multi-axis machines contain many components of relative complex geometry, this facilitates the analysis to a great extent.

Stress-free thermal expansion requires that structural loop components having a different coefficient of thermal expansion do not restrict each others thermal deformation. Furthermore, stress free thermal expansion of a structural loop component only occurs if its temperature distribution equals [10]:

$$T(x, y, z, t) = a(t) + b(t)x + c(t)y + d(t)z \quad (3.56)$$

In this analysis we will consider the structural loop as consisting of several beam-like structures that can expand without mutual interaction. As a first approach, we make the Bernoulli-Euler assumption that sections which are plane and perpendicular to the axis before thermal loading remain so after loading, and that the effect of lateral contraction may be neglected (i.e. Poisson's ratio may be taken equal to zero). Under these assumptions, the

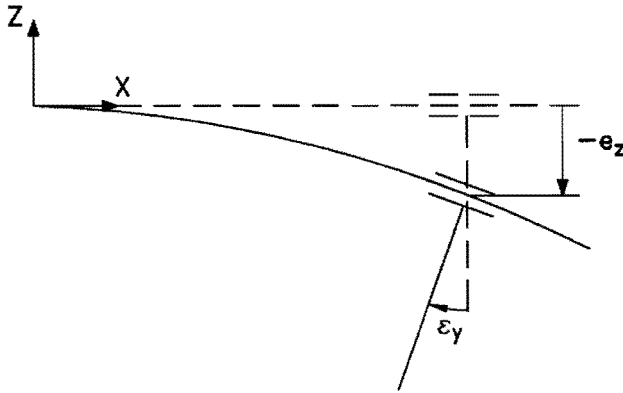


Figure 3.24: Bending of a beam due to a thermal gradient.

restrictions on the thermal distribution required for stress-free deformation can be relaxed to [10]:

$$T(x, y, z, t) = a(x, t) + c(x, t)y + d(x, t)z \quad (3.57)$$

Here the X -coordinate is taken along the main axis of the beam. The extension of the beam due to the temperature distribution can be expressed as:

$$e_x = \int_0^x \alpha T dx \quad (3.58)$$

Where T denotes the temperature relative to that of the reference state. By relatively straightforward geometric arguments, the angular deflection of the beam about the Y - and Z -coordinate can be derived as [116] (see Figure 3.24):

$$\varepsilon_y = \int_0^x \alpha \frac{\partial T}{\partial z} dx \quad (3.59)$$

$$\varepsilon_z = -\int_0^x \alpha \frac{\partial T}{\partial y} dx \quad (3.60)$$

The deflection (i.e. 'straightness') of the beam can be obtained by integration as:

$$e_y = \int_0^x \varepsilon_z dx \quad (3.61)$$

$$e_x = -\int_0^x \varepsilon_y dx \quad (3.62)$$

Thus we have obtained expressions for five of the six errors that describe the relative location of two coordinate frames located on the beam axis. The sixth error ε_x describes torsion around the beam axis. It can be shown that

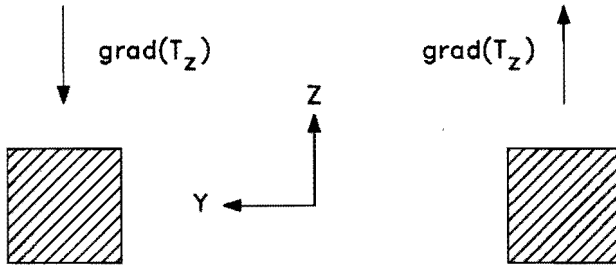


Figure 3.25: Two beams that experience a different temperature gradient.

under the above assumptions, thermoelastic torsional rotation of one end of the bar relative to the other does not exist [116]. In practice, however, thermoelastic roll errors do occur. This can be understood by visualizing two parallel beams in a horizontal plane (see Figure 3.25). If there is a vertical temperature gradient the beams will bend. If this gradient differs between the beams their deflection will be different for the same X -coordinate. Hence a carriage supported by the two beams will experience a roll error as it moves in X -direction. These considerations suggest that torsion occurs in a beam whenever there is a differential gradient (i.e. $\frac{\partial^2 T}{\partial y \partial z}$). The description of this error is still under investigation.

Using the above equations, the errors in the relative location of two coordinate frames due to stress-free thermal deformation can be modelled in a relatively straightforward manner. These parametric errors are then entered in the kinematic model of Chapter 2 to obtain the errors between end-effector and workpiece. Here it is not necessary to remove the best fit straight line through the straightness errors.

A problem in the application of this modelling procedure to multi-axis machines is the effect of scale expansion and scale displacement on the machine accuracy. As depicted in Figure 3.26, the structural loop that describes the displacement error in a certain coordinate direction should include the respective scale and its mounting. However, the structural loop that determines the displacement errors in other directions, and the various angular errors,

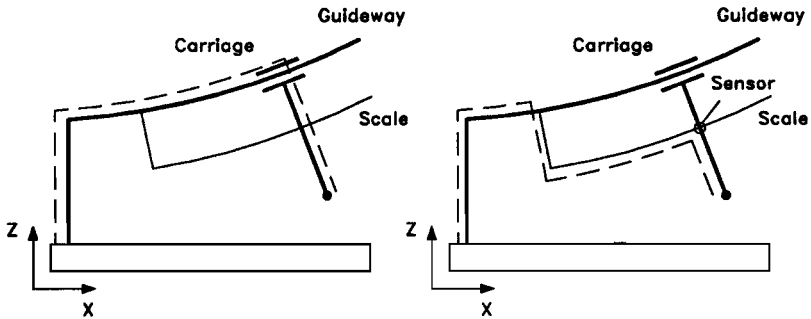


Figure 3.26: Different structural loops to describe displacement errors in X - and Z - direction.

is determined by the guideway, not the scale. Hence, whenever scales are mounted at some distance from the guideway, the model should describe the expansion of several structural loops.

The main advantage of the described method lies in its simplicity and the generation of parametric errors. Hence deviations in the complete workspace of the machine can be derived using the kinematic model. It should be noted, however, that its application is rather time-consuming and involves several uncertainties (e.g. the coefficients of thermal expansion). It also may be argued that the assumption of stress free deformation limits the usefulness of the method, especially regarding the allowed temperature distributions. On the other hand, the limited information about the temperature distribution of structural loop segments often results in a modelled temperature distribution that belongs to the stress-free class.

The method will be applied in Chapter 5 to model the thermal errors of a five-axis milling machine.

3.4.4 Modelling the thermal drift

In this subsection, errors in the relative location of the tool are directly expressed as a function of the observed temperature elevations of a limited number of sensors in time. This involves an implicit combination of both previous thermal error models and the kinematic model.

The derived state space model for the temperature distribution $T(\vec{p}, t)$ of the structural loop equals:

$$\dot{\underline{x}} = A\underline{x} + B\underline{u} \quad (3.63)$$

$$T(\vec{p}, t) = C\underline{x} \quad (3.64)$$

Here the state vector \underline{x} summarizes the history of the inputs \underline{u} and is a function of the time t . Matrix A contains the unknown time constants γ^{-1} , and matrix B is known. Each element of row vector C describes the contribution of a state variable x_i to the temperature $T(\vec{p}, t)$ at a point \vec{p} of the structural loop. The elements of C are an unknown function of \vec{p} . The model is only valid for fixed carriages.

The thermal deformation of the structural loop at a certain time is determined by its temperature distribution at that time. The resulting errors ${}_{wr}\underline{E}_{st}$ in the relative location of end-effector and workpiece are obtained by the integration of the temperature distribution or its derivatives along certain paths through the structural loop. These paths are affected by the position \underline{q} of the joints. Hence, errors in the relative location of the end-effector are a function of the temperature distribution $T(\vec{p})$ of the structural loop and the position of the joints \underline{q} . Combining these deliberations with the state-space model for the temperature distribution, yields the following state-space model for the errors ${}_{wr}\underline{E}_{st}$:

$$\dot{\underline{x}} = A\underline{x} + B\underline{u} \quad (3.65)$$

$${}_{wr}\underline{E}_{st}(\underline{q}, t) = C_E \underline{x} \quad (3.66)$$

Here matrix C_E describes how the elements of the state vector \underline{x} affect the errors ${}_{wr}\underline{E}_{st}$. It contains six rows, of which each corresponds to a rotation or translation error of ${}_{wr}\underline{E}_{st}$. For a certain machine, the matrix C_E is a highly complicated function of the position of the joints. It should be noted that the time constants that define matrix A are also related to the position of the joints.

The presented state-space model for the errors ${}_{wr}\underline{E}_{st}$ is used to predict these errors at a certain position of the joints. At this position, the elements of matrix C_E need to be estimated as well as the time constants γ^{-1} in matrix A . These parameters are again empirically estimated using the observed thermal

drift during a characteristic duty cycle of the machine. The used estimation algorithm is identical to that used to estimate the state-space model for the temperature distribution.

In practice, models are estimated at several characteristic positions of the machine axes. The drift at an arbitrary axis position is obtained by linear interpolation between the modelled drift at the tested positions. In Chapter 5, this approach is used to model the thermal errors of a five-axis milling machine.

4

Artifact based calibration

In this chapter a method is presented to determine the quasi-static errors of multi-axis machines using artifact measurements. The parametric errors of the machine are estimated by standard linear regression analysis. An uniform approach is obtained with respect to the nature of the studied machine, and the choice and location of the artifacts. Statistical experimental design analysis provides unambiguous mathematically defined criteria to evaluate and optimize the capabilities and efficiency of the calibration. At the end of this Chapter, an example of the method is presented. The method is applied in Chapter 5 to estimate the geometric errors of a three-axis CMM using a variety of artifacts and calibration strategies, all based on length measurements.

4.1 Introduction

The tremendous growth in the application of numerically controlled multi-axis machines has been accompanied by many studies on the modelling, identification, and (software) compensation of their errors. Results of these studies have been partially incorporated into various guidelines and standards which address the inspection and performance evaluation of such machines. In general, these procedures do not provide the respective user with the tools and data necessary to calculate the (traceable) accuracy of a specific task. Therefore they cannot be regarded as calibrations. Being inspection devices, the

availability of standardized calibration procedures is especially important for Coordinate Measuring Machines. Such procedures have to ensure that traceability for coordinate metrology is just as sound as for any other aspect of dimensional metrology.

Due to the versatile and multidimensional nature of multi-axis machines, there currently does not exist a ready-to-use reference with which they can be directly calibrated for every possible task. Therefore, it is generally accepted that a complete calibration should result in a separate description of the errors introduced in the components of the machine (e.g., angular, squareness, straightness, and scale errors). These so-called parametric errors are then combined to calculate the accuracy of a specific task, using a suitable model of the machine's kinematics.

In this chapter we consider the estimation of the parametric errors using artifact measurements. In recent years, a variety of such methods have been suggested and applied. They comprise the measurement of suitable reference artifacts, such as ring gauges [58], hole plates [62, 60], space frames [56, 8], and (laserinterferometric) step gauges [145], in various locations. From the observed deviations, the parametric errors are calculated (often at discrete positions of the machine axes), usually by trigonometric analysis. The large interest in these methods is due to a number of important advantages over the conventional direct measurement of the parametric errors. Direct measurement provides comprehensive information on the machine condition with a possible high sampling density, but requires much time, skill, and expensive equipment. In contrast, the artifact measurements can usually be performed by a local operator, although the subsequent estimation and analysis of the parametric errors still presents problems due to the lack of appropriate software. A fundamental advantage of artifact-based calibration methods is that the machine accuracy is estimated from observed deviations of tasks which resemble the *intended* operation of the machine. Therefore, these methods can be directly applied to software error compensated machines.

The chosen approach (see also [8, 44, 56, 60, 106, 108, 107]) to the estimation of the parametric errors from artifact measurements is essentially different from the usually applied trigonometric analysis. In the first stage of the pro-

posed method, a model is built of the machine accuracy, including a suitable description of its parametric errors. According to the nature of the measured artifact(s), an algebraic *linear* relation is next established between the respective deviations in their measurement and the unknown parameters describing the parametric errors. Finally, these parameters are estimated by standard linear regression techniques, such that the residual sum of squares between the modelled and observed errors in the measured feature(s) is minimized.

It may be thought that the above degree of formality is not always necessary. This may be so. However, in our experience, its proper use confers a number of advantages:

- **Uniformity of approach** affording meaningful comparative assessments. The same regression techniques are used regardless the nature and location(s) of the artifact(s) used, the desired detail level of the estimated errors, or the nature of the machine being studied. This includes machines with revolute joints or machines with significant finite stiffness related errors.
- **High calibration efficiency** and results unaffected by the errors associated with approximate or ad hoc approaches. For example, the often complicated separation of the simultaneous effect of various parametric errors on the artifact measurements, is ‘automatically’ realized by the regression technique. Therefore, artifact locations where many errors affect the accuracy of the measurements can be meaningfully used in the estimation.
- **Standard linear regression analysis.** Usually “off-the-shelf” software can be used to solve and analyse the complete estimation problem. An extensive amount of well known statistically based techniques can be readily applied, e.g. , in the design of the calibration setup, and the verification and analysis of the accuracy of the estimated error model.

As indicated, the proposed estimation procedure can be applied to virtually any artifact, either calibrated or uncalibrated. Regarding the nature of the feature used to estimate the machine errors, we prefer length. Length can be realized

by dimensionally stable artifacts that are easy to handle, can be accurately calibrated, and are cheap to produce. The possibility of measuring length by laserinterferometric means, implies that a high sampling density can be obtained, and that the procedure can be applied to machines of virtually any size. Many artifacts allow the automated measurement of different lengths in many locations. Finally, length can be measured or realized by almost every multi-axis machine.

4.2 Estimation of parametric errors

In the first stage of the estimation method, a model is built of the machine errors, including a suitable description of its parametric errors. As indicated in the introduction, this model is used to inter- and extrapolate the calibration data in order to be able to predict the accuracy of an arbitrary machine task. This process is based on two assumptions:

- The effect of a certain parametric error on the location of the end-effector is completely defined by the kinematic model of the machine.
- The relation between a certain parametric error and the status of the machine (e.g. the position of its axes) can be 'accurately' approximated by a finite amount of calibration data.

The kinematic model presented in Chapter 2, describes the errors in the relative location of the end-effector as a known linear combination of the various parametric errors \underline{E} . Regarding the errors \underline{e} in a realized or measured end-effector position, this model can be summarized as:

$$\underline{e} = \mathbf{F}\underline{E} \quad (4.1)$$

In equation 4.1, the vector \underline{E} contains the parametric errors at the analysed position. The matrix \mathbf{F} describes how these parametric errors affect the errors \underline{e} in the relative position of the end-effector. As described in Chapter 2, this matrix is completely defined by the nominal geometry of the machine, the

end-effector dimensions, and the position of the axes. In Chapter 3, each parametric error E_i was modelled as a linear combination of 'arbitrary' functions p_l defined on the position of the machine axes and other relevant variables (contained in vector \underline{x}):

$$E_i = \sum_{l=1}^n p_l(\underline{x}) \beta_l \quad (4.2)$$

An important consideration in the choice of the parametric functions $p_l(\underline{x})$ is that components of different parametric errors should not have the same effect on the accuracy of the machine tool. This would lead to singularities in the parameter estimation. For example, in the model for a straightness error, these functions should be constructed to ensure that the error has no linear component (already described by a squareness error), regardless the values of the unknown parameters $\underline{\beta}$ (See Section 3.2 and Appendix B). In this respect, special attention must be paid to the formulation of errors which, due to finite stiffness effects, are related to more than one axis position.

To estimate the parameters $\underline{\beta}$ from deviations observed when measuring or generating artifacts, we need a suitable model that relates these deviations to errors in the realized (relative) position of the end-effector when 'measuring' these artifacts. Using the following approximation, a *linear* relation is obtained that greatly simplifies the subsequent estimation process:

The difference between the measured and actual position and orientation of an artifact has a negligible effect on the measurement errors of its features.

This approximation enables the separation of the artifact's location estimation from the machine's error analysis. Thus the measured position and orientation can be directly used in the estimation of the machine's errors, even though this location is affected by these errors. Usually, the approximation only yields problems for machines whose errors change significantly over intervals of the same order as its errors. Also if the calibration has to predict the errors with an extremely high relative accuracy, a nonlinear approach may be necessary.

As an example, we consider an artifact whose length L is described by the distance between the points \vec{N}_1 and \vec{N}_2 (see Figure 4.1). The coordinates

of these points are measured as \vec{P}_1 and \vec{P}_2 respectively. Using the above mentioned approximation, the observed error ΔL in the measured length L_{meas} can be modelled as a *known* linear combination of the measurement errors $\Delta\vec{P}_1$ and $\Delta\vec{P}_2$:

$$\Delta L = \frac{(\vec{P}_2 - \vec{P}_1)}{L_{meas}} \cdot (\vec{P}_2 - \vec{P}_1) - \frac{(\vec{N}_2 - \vec{N}_1)}{L} \cdot (\vec{N}_2 - \vec{N}_1) \quad (4.3)$$

$$\approx \frac{(\vec{P}_2 - \vec{P}_1)}{L_{meas}} \cdot ((\vec{P}_2 - \vec{P}_1) - (\vec{N}_2 - \vec{N}_1)) \quad (4.4)$$

$$= \frac{(\vec{P}_2 - \vec{P}_1)}{L_{meas}} \cdot (\Delta\vec{P}_2 - \Delta\vec{P}_1) \quad (4.5)$$

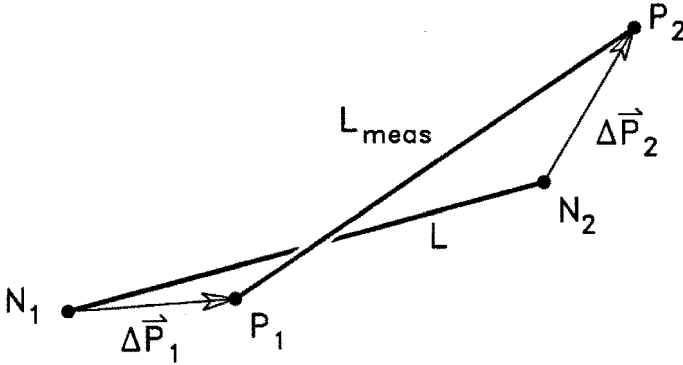


Figure 4.1: Measurement of a length.

In relation 4.5, the observed error ΔL is approximated as the projection along the estimated feature of errors in the relative position of the probe tip. Although this result (i.e., the neglect of cosine errors) may seem trivial, it is essential to note that a linear relation is obtained. Also the kinematic model of the machine (see equation 4.1) and the models for the various parametric errors (see equation 4.2) are linear in respectively the parametric errors \underline{E} and the unknown parameters $\underline{\beta}$ that describe these errors. Thus, the appropriate combination of these models yields a relation in which the measurement error Δa_i of a feature a_i is expressed as a (known) linear combination of the unknown parameters $\underline{\beta}$:

$$\Delta a_i = \sum_{k=1}^p i g_k(\underline{x}_i) \beta_k + \gamma_i \quad (4.6)$$

In equation 4.6, γ_i represents the measurement error due to non-repeatable and non-modelled machine errors. Vector \underline{x}_i contains the variables which describe the relevant status of the machine and its environment during the measurement of the artifact (e.g., the position of the machine's axes for each measured point). The known function ${}_i g_k(\underline{x}_i)$ describes the effect of parameter β_k on the feature's measurement error. The computation of this function is a straightforward but rather tedious procedure. Basically the values of the related known function $p_k(\underline{x})$ in relation 4.2, which describes the effect of parameter β_k on the respective parametric error, are calculated for the status of the machine when measuring the artifact's end points. These values are then inserted in relation 4.1 to obtain the effect of β_k on the displacement error of the probe tip for the various measured points. In case of length measurements (see equation 4.5), ${}_i g_k(\underline{x}_i)$ is computed as the dot product of the difference between both displacement errors with the direction vector along the measured length.

The proposed calibration procedure, based on the measurement of m artifact features throughout the machine's workspace, can be presented mathematically as:

$$\Delta a_i = \sum_{k=1}^p {}_i g_k(\underline{x}_i) \beta_k + \gamma_i \quad i = 1, 2, \dots, m \quad (4.7)$$

$$= {}_i \underline{g}(\underline{x}_i)^T \underline{\beta} + \gamma_i \quad i = 1, 2, \dots, m \quad (4.8)$$

Which we express in matrix notation as:

$$\Delta \underline{a} = X \underline{\beta} + \underline{\gamma} \quad (4.9)$$

Here $\underline{\gamma}$ is the vector of 'random' errors, assumed to be independent and identically distributed with mean 0 and variance σ^2 . Row i of the $m \times p$ matrix X contains the function values ${}_i g_1(\underline{x}_i), \dots, {}_i g_p(\underline{x}_i)$. Since the above model is linear in the unknown parameters $\underline{\beta}$, they can be estimated using linear least-squares analysis [77]:

$$\hat{\underline{\beta}} = (X^T X)^{-1} X^T \Delta \underline{a} \quad (4.10)$$

In the case of calibrations which use artifacts of unknown constant dimensions, the vector $\underline{\beta}$ has to be expanded to include these dimensions. Obviously, at least one measurement of a known dimension has to be made.

In general, the regression technique transfers the effects of errors or error components not present in the proposed error model to those that are. Thus, the estimated model optimally describes the observed errors in the artifact measurements. In case the calibration data is representative of the machine tasks, this yields a high predictive quality of the estimated model for the machine accuracy, even if a simplified error model is used. In the latter case, the estimated parametric errors describe 'average' properties, and will not be equal to the actual parametric errors. In this respect, special care must be taken to avoid overfitting of the calibration data.

4.3 Calibration efficiency

In this section mathematical criteria are developed to describe and optimize the efficiency of a calibration. The efficiency and potential of a calibration with respect to the choice and location(s) of the artifact(s) used, can be assessed by two criteria:

- the assembly of error parameters which can be estimated from the calibration's observations.
- the accuracy of these estimators, given a certain repeatability of an artifact measurement.

The proposed model for the systematic errors of the machine affects these criteria in a structural manner. Hence, every calibration is a compromise between its efficiency in the estimation of modelled errors and its ability to detect errors not implemented in the proposed model. As an example of this concept, consider the problem of estimating the relation between an independent variable x and a dependent variable y . Suppose the experimenter is allowed to take 10 observations of y at certain discrete values of x (assumed to be achieved without errors). If the relation between x and y is known to be exactly linear, an experimental design of 5 observations at x_{\min} and 5 observations at x_{\max} will result in the most accurate estimation of this relation, given a certain constant variance in the observations of y . Note

however that a departure of the actual relation between x and y from the proposed model cannot be detected from these observations. In case there is no a priori information available about the possible relation between x and y , an experimental setup with the 10 observations uniformly distributed over the domain of x is preferred. Such a design has however a low efficiency in the estimation of this relation, if it is indeed linear.

With respect to the calibration of multi-axis machines, there is a priori information available regarding the kinematic model. Also type dependent properties usually provide information concerning the independent variables of a parametric error and, in some cases, a class of suitable functions to be used in its model (e.g. regarding the placement and number of knots). Further specification of the proposed model for each error in the kinematic model is dependent on the goal of the performance evaluation or calibration. For example, if the value of a parametric error has to be determined at certain discrete points, as is the case with most current performance evaluations, a first order piecewise polynomial might be chosen with knots at these points. An impression of the various errors can be obtained when using low order piecewise polynomials whose complexity, i.e. the number of unknown parameters $\underline{\beta}$, is restricted by the allowed measurement effort. In order to check the estimated software error correction, the model can be chosen in accordance with the functions associated with the identified significant parameters in the various models.

From equation 4.10, the potential of the calibration to estimate the unknown parameters $\underline{\beta}$ can be assessed by the following rule [61]:

a linear combination $\underline{\lambda}^T \underline{\beta}$ of the parameters $\underline{\beta}$ can be estimated from the calibration observations, if $\underline{\lambda}^T$ is part of the vectorspace spanned by the rows of X .

In case all the parameters $\underline{\beta}$ can be estimated, the efficiency of the calibration can be further assessed by [61]:

- the variance-covariance matrix of the estimated parameters $\hat{\beta}$:

$$\text{Cov}(\hat{\beta}) = \sigma^2 (X^T X)^{-1} \quad (4.11)$$

- the variance of the predicted deviation when measuring a feature at a certain location:

$$\text{Var}(\Delta a | \underline{x} = \underline{x}_i) = \sigma^2 \underline{g}(\underline{x}_i)^T (X^T X)^{-1} \underline{g}(\underline{x}_i) \quad (4.12)$$

Both 4.11 and 4.12 depend on the design of the calibration setup only through the $p \times p$ matrix $(X^T X)^{-1}$. This suggests that a good calibration setup will be one that makes this matrix small. Since there is no unique size ordering of $p \times p$ matrices, various real-valued functions have been suggested as measures of 'smallness'. Some criteria (see e.g. [110, 111]) focus on the quality of the estimated parameters (minimization of the determinant, trace, or maximum eigenvalue of $(X^T X)^{-1}$). Others address the quality of the estimated response surface for the errors in the artifact measurements (minimization of the maximum or average variance predicted errors).

In addition to the design of an efficient calibration, the criteria serve a major role in the statistical verification of the estimated error model. For example, equation 4.12 can be used to determine whether the difference between the observed and predicted error of a certain artifact measurement is consistent with the predicted uncertainty of the error model. Such inconsistencies may be due to errors not included in the model (e.g., finite stiffness effects).

Regarding the optimization of calibrations, we generally prefer minimizing the determinant of $(X^T X)^{-1}$. One of the attractive features of this so-called D-criterion is that designs that are optimal with respect to it are invariably 'good' in many respects (e.g. low variances for the parameters, low correlations among the parameters, low maximum variance in the predicted errors). Essentially the criterion tries to minimize the contents of the p - dimensional confidence region associated with the estimated parameters. Although the comparison of existing calibrations using this or other criteria is quite straightforward, optimization is a very complicated process. The most frequently encountered difficulties are:

- The large number of parameters which must be handled and the associated large size of the matrix $(X^T X)^{-1}$.
- The complex nature of object function $\det(X^T X)$, especially the existence of several local minima.
- The large number of design variables which describe the configuration of the artifact(s)'s measurable points, its location(s) in the machine workspace and the probe extension(s) used to measure it.
- The complex boundaries of the design space and the often discrete character of certain design variables (e.g. available probe extensions and artifacts).

Here attention will be restricted to the optimization of the location(s) of existing artefact(s). In the chosen approach (see e.g. [76, 132, 133, 134]) to the optimization problem, a discrete design space X is defined of r so-called candidates x_1, \dots, x_r . Each candidate represents an artifact at a certain location in the machine workspace. The design problem can now be defined as the choice of n not necessarily distinct observations $x_{(1)}, \dots, x_{(n)}$ from X . The adapted (exchange) algorithm commences with an initial random design of n points (observations) and makes a number of excursions whereby the design is improved until no further progress can be made. Each excursion is a series of additions or subtractions of one or more candidates to the current collection of design points, eventually returning to a possibly new and better n -point design.

4.4 An example

As an example of the proposed estimation procedure and the optimization of the calibration setup, we consider the simplified two-dimensional coordinate measuring machine depicted in Figure 4.2. Its errors are limited to linear scale errors in the position of both axes and a constant squareness error in their respective orientation. The machine is calibrated using length measurements.

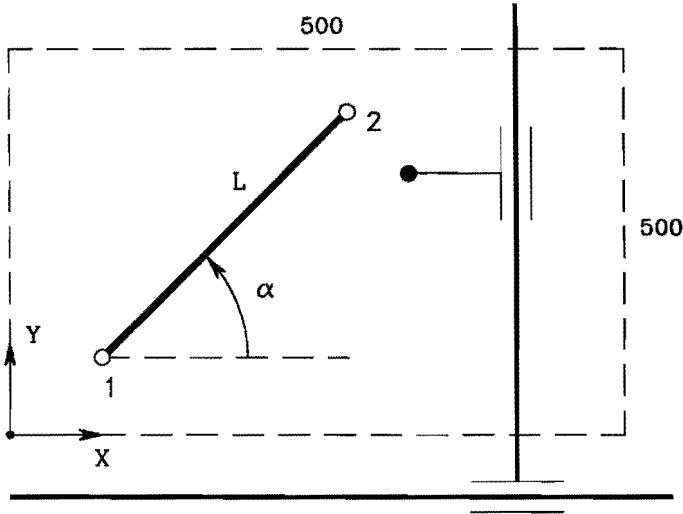


Figure 4.2: 2D CMM.

First, the kinematic model is used to describe how the parametric errors affect the measured position of a point. Disregarding the probe offset, errors \underline{e} in a measured position can be expressed as:

$$\begin{bmatrix} e_x \\ e_y \end{bmatrix} = - \begin{bmatrix} -y & 1 & 0 \\ 0 & 0 & 1 \end{bmatrix} \begin{bmatrix} {}_0e_{1x} \\ {}_0e_{1x} \\ {}_1e_{2y} \end{bmatrix} \quad (4.13)$$

where:

$$\begin{aligned} {}_0e_{1x} &: \text{squareness error} \\ {}_0e_{1x} &: \text{scale error X-axis} \\ {}_1e_{2y} &: \text{scale error Y-axis} \end{aligned} \quad (4.14)$$

Note that the minus sign in Equation 4.13 is introduced because the error in a *measured* position is described.

The second step involves the formulation of a model for each relevant parametric error. In accordance with the introduction of this section, the proposed parametric models are:

$${}_0e_{1x} = \beta_1 \quad (4.15)$$

$${}_0e_{1x} = \beta_2 x \quad (4.16)$$

$${}_1e_{2y} = \beta_3 y \quad (4.17)$$

Here β denotes a parameter that has to be estimated from the calibration measurements. Inserting the parametric error models into the kinematic error model yields:

$$\begin{bmatrix} e_x \\ e_y \end{bmatrix} = - \begin{bmatrix} -y & x & 0 \\ 0 & 0 & y \end{bmatrix} \begin{bmatrix} \beta_1 \\ \beta_2 \\ \beta_3 \end{bmatrix} \quad (4.18)$$

Next, a model is required that relates the error ΔL in a measured length L to the errors \underline{e}_1 and \underline{e}_2 in the measured end-points 1 and 2 of the length. According to Equation 4.5, this relation can be approximated as:

$$\Delta L \approx \begin{bmatrix} \cos \alpha & \sin \alpha \end{bmatrix} \begin{bmatrix} e_{2x} - e_{1x} \\ e_{2y} - e_{1y} \end{bmatrix} + \gamma \quad (4.19)$$

Here α denotes the orientation of the length relative to the X-axis of the machine. By combining Equations 4.18 and 4.19, the error ΔL in a measured length can be approximated as a linear combination of the unknown parameters β :

$$\Delta L \approx \begin{bmatrix} \cos \alpha & \sin \alpha \end{bmatrix} \begin{bmatrix} L \sin \alpha & -L \cos \alpha & 0 \\ 0 & 0 & -L \sin \alpha \end{bmatrix} \begin{bmatrix} \beta_1 \\ \beta_2 \\ \beta_3 \end{bmatrix} + \gamma \quad (4.20)$$

$$= L \begin{bmatrix} \cos \alpha \sin \alpha & -\cos^2 \alpha & -\sin^2 \alpha \end{bmatrix} \underline{\beta} + \gamma \quad (4.21)$$

Note that this error is unrelated to the position of the length in the machine workspace. If n lengths are measured, the regression problem can be expressed as:

$$\begin{bmatrix} \Delta L_1 \\ \vdots \\ \Delta L_n \end{bmatrix} = \begin{bmatrix} L_1 \cos \alpha_1 \sin \alpha_1 & -L_1 \cos^2 \alpha_1 & -L_1 \sin^2 \alpha_1 \\ \vdots & \vdots & \vdots \\ L_n \cos \alpha_n \sin \alpha_n & -L_n \cos^2 \alpha_n & -L_n \sin^2 \alpha_n \end{bmatrix} \begin{bmatrix} \beta_1 \\ \beta_2 \\ \beta_3 \end{bmatrix} + \begin{bmatrix} \gamma_1 \\ \vdots \\ \gamma_n \end{bmatrix} \quad (4.22)$$

$$\Rightarrow \Delta \underline{L} = X \underline{\beta} + \underline{\gamma} \quad (4.23)$$

The least squares estimates of the parameters $\underline{\beta}$ can be calculated according to Equation 4.10.

We now consider the choice for the location of the lengths in the machine workspace to 'optimally' estimate the parameters $\underline{\beta}$. In this analysis, the set of

candidates is confined to ball bars with a length of 400 mm. Their position and orientation are separated by intervals of 50 mm and 15 degrees respectively. As an example, the number of ball bar measurements to calibrate the machine is limited to six. In Table 4.1, the properties of two proposed experimental designs 1 and 2, and the calculated D-optimal design 3 (See Figure 4.3) are shown.

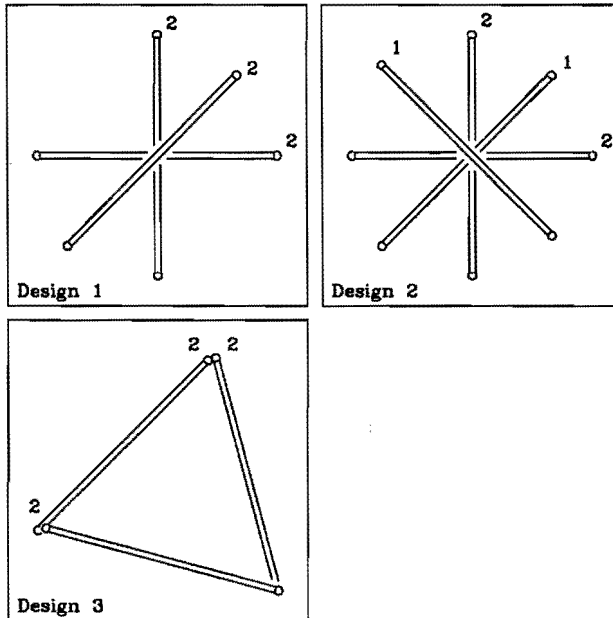


Figure 4.3: Proposed experimental designs 1 and 2, and the calculated D-optimal design 3.

The calculated D-optimal design is superior to the proposed designs with respect to all criteria mentioned. In order to analyse this difference, the variance-covariance matrices $\text{Cov}(\hat{\beta})$ of the designs are calculated:

$$\text{Design1: } \text{Cov}(\hat{\beta}) = \frac{\sigma^2}{2} L^{-2} \begin{bmatrix} 6 & 1 & 1 \\ 1 & 0 & \\ & 1 & \\ & & 1 \end{bmatrix} \quad (4.24)$$

$$\text{Design2: } \text{Cov}(\hat{\beta}) = \frac{\sigma^2}{2} L^{-2} \begin{bmatrix} 4 & 0 & 0 \\ & 0.83 & -0.17 \\ & & 0.83 \end{bmatrix} \quad (4.25)$$

Selected candidates of design 1			
Replications	X	Y	Angle α
2	50	250	0
2	100	100	45
2	250	50	90
Selected candidates of design 2			
Replications	X	Y	Angle α
2	50	250	0
1	100	100	45
1	100	400	315
2	250	50	90
Selected candidates of design 3			
Replications	X	Y	Angle α
2	50	150	45
2	450	50	105
2	450	50	165
Design properties			
Design	$\det^{1/3}$ covariance matrix	Average variance response	Maximum variance response
1	2.98 E-5	4.35	9.00
2	2.60 E-5	3.20	4.00
3	2.50 E-5	3.00	3.00

Table 4.1: Properties of the proposed experimental designs 1, 2, and the calculated D-optimal design 3. The X - and Y -coordinates correspond to the position of the first sphere. All results are scaled for the number of observations and error variance.

$$\text{Design3: Cov}(\hat{\beta}) = \frac{\sigma^2}{2} L^{-2} \begin{bmatrix} 2.67 & 0 & 0 \\ & 1 & -0.33 \\ & & 1 \end{bmatrix} \quad (4.26)$$

Although the first design exhibits no covariance between the scale parameters β_2 and β_3 (matrix element [2,3]), the variance of its squareness parameter β_1 is quite high (matrix element [1,1]) and shows significant covariance with both scale parameters (matrix elements [1,2] and [1,3]). This explains the higher efficiency of the calculated D-optimal design. The D-optimality of this design was proven by evaluating all possible designs based on six ball bar measurements whose orientation is limited to the above mentioned discrete angles. In Figure 4.4 values of the inverted optimality criterion (i.e. $\det(X^T X)$) are shown for a subset of these designs. Here two ball bars are located at a 45° angle with the X-axis of the machine. The remaining four ball bars are divided into two sets of two ball bars with the same orientation. Further analysis showed that, for this problem, any design consisting of a triangular arrangement of the various ball bars is D-optimal.

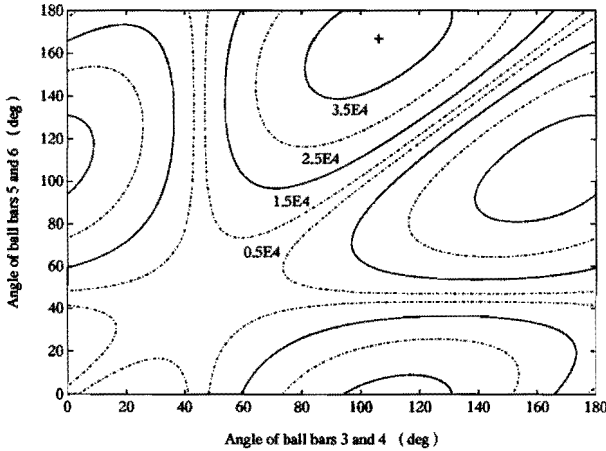


Figure 4.4: Contour lines of constant $\det(X^T X)$ of experimental designs with six ball bars of which ball bars 1 and 2 are located at a 45° angle with the X-axis of the machine. The numerical values for this inverted optimality criterion are scaled for the number of parameters (three) and observations (six). The calculated D-optimal design is denoted by the symbol '+'.

5

Validation

Subject of this chapter is the validation of both the modelling and estimation procedures presented in this thesis. In the first part of this chapter, models for the geometric, finite stiffness, and thermal errors of the five-axis milling machine are estimated and verified. Here the geometric error model is estimated using calibration data for each individual parametric error. Models that describe the change in the parametric errors due to the weight of moving machine components and workpiece are also estimated from calibration data on each parametric error (see Section 3.3). The obtained geometric and finite stiffness error models are validated by comparing the predicted and observed errors in hole plate measurements executed by the machine. A software error compensation algorithm for the geometric errors is implemented in the controller. The accuracy of the compensated machine is tested using hole plate measurements. Regarding the thermal errors, only the heat generated by the main spindle drive is considered. This is by far the major heat source of the machine. The respective models are validated by comparing the predicted and observed zero-point drift of the tool during characteristic duty-cycles of the spindle.

5.1 Error models of a five-axis milling machine

In this section models for the geometric, finite stiffness, and thermal errors of the five-axis milling machine are estimated and verified. The studied machine is depicted in Figure 5.1. The tool chain of the machine contains a prismatic and a revolute joint, both with a horizontal axis. The workpiece chain consists of two prismatic joints, one vertical and one horizontal, and a revolute joint with a vertical axis of rotation. Measurement scales with a resolution of $1 \mu\text{m}$ are used to monitor the position of the prismatic joints. The machine can mill with a vertical and a horizontal spindle. In the latter case, the swiveling head is moved to a vertical position and a tool holder contained in the ram is used. In this horizontal mode, the C-axis is not part of the structural loop.

5.1.1 Geometric errors

In this subsection the estimation and validation of the geometric error model is discussed. Only the parametric errors introduced by the three prismatic joints are analysed.

Measurement procedure

Each geometric parametric error associated with the prismatic joints is individually measured. The scale errors and most angular errors are measured using a laser interferometer. Electronic levels are used to assess the roll errors of the X- and Z-axis. This is not possible for the Y-axis roll error (rotation in a horizontal plane). This error is estimated from the observed difference of two straightness measurements (in Z-direction) executed with a different probe offset in X-direction (after correction for the xrx roll error). These and other straightness errors, and the three squareness errors, are measured using a square reference block and displacement transducers. The various errors (especially scale errors) are generally measured along lines through the center of the workspace. This to reduce the effect of angular error uncertainty on the uncertainty of the estimated model.

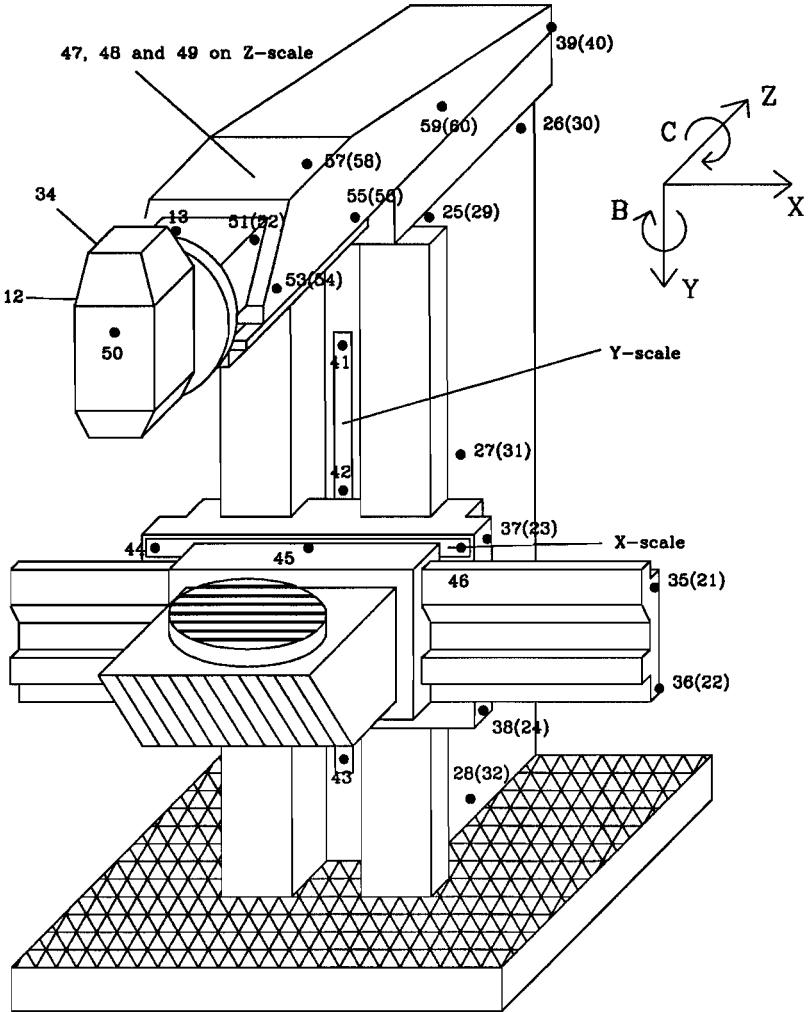


Figure 5.1: The studied five-axis milling machine and the location of the temperature sensors

As described in Chapter 3, all measurements are executed fully automatically [115]. In general a sampling distance of 10 mm is used. At each measurement point the axis movement is halted. After a short delay to eliminate dynamic effects caused by the axis motion, five samples are taken of the error. For most errors, five back-and-forth measurements are executed over the complete axis range. The measurements are executed at an ambient temperature of $23 \pm 0.5 \text{ }^\circ\text{C}$ with the machine fully heated up by its (constant) internal heat sources (see Chapter 3.1). To verify the expansion coefficient of the scales, the respective parametric errors are also measured at an ambient temperature of $18 \text{ }^\circ\text{C}$.

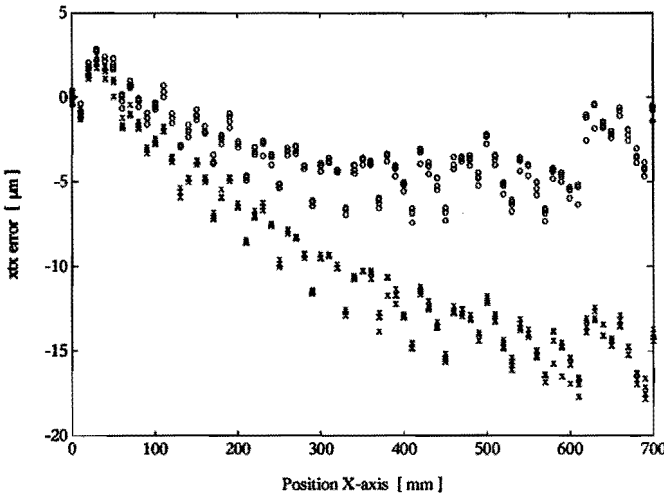


Figure 5.2: Measured xtx error at different ambient temperatures. The symbols \circ and \times correspond to an average scale temperature of respectively 25.3 and $20.4 \text{ }^\circ\text{C}$. The measurements are compensated for the thermal expansion of the scale using the expansion coefficient supplied by the manufacturer. They are executed at the same position in the machine workspace.

For the X-axis, measurement of the scale errors at different ambient temperatures showed strange results. Some results of these experiments are depicted in Figure 5.2. Based on the measured temperatures at the start, middle, and end of the scale, the depicted scale errors have been compensated for the thermal expansion of the scale, and hence should reflect its errors at a temperature of $20 \text{ }^\circ\text{C}$. The respective correction is based on a thermal expansion

coefficient of $9.75 \mu\text{m m}^{-1} \text{K}^{-1}$, supplied by the manufacturer. The depicted results, however, suggest that the real coefficient of expansion is significantly higher, namely $13.5 \mu\text{m m}^{-1} \text{K}^{-1}$. It is unlikely that this is in fact the case. Furthermore, the large scale error of $-15 \mu\text{m}$ at 20°C is suspect (the measurements are compensated for the effect of angular errors and should reflect the scale error). Further experiments showed that both, the scale error at 20°C and its apparent coefficient of expansion, vary when the X-axis scale is subjected to significant temperature variations.

The cause of these effects has been traced to the used scale mounting. The scale is attached to the machine frame by two fixed points. This construction does not allow a free thermal expansion of the scale. Thus the apparent thermal expansion coefficient of the scale is partly determined by that of the surrounding machine structure. The variation in its errors is due to a stick-slip effect in the scale mounting.

Validation of the geometric error model

Based on the measurements described in the preceding section, models are estimated for the various parametric errors using the procedure described in Chapter 3. Combined with the kinematic model of Chapter 2, a model is obtained that describes the accuracy of the machine in its reference state (excluding certain finite stiffness related errors). To assess the predictive power of this model, several validation measurements are executed. A powerful validation method is based on the measurement of a calibrated hole plate by the machine.

A hole plate is a two-dimensional artifact that contains a grid of holes. The relative position of these holes has been measured with a laser interferometer and a high accuracy CMM, and is known with a relative error of less than 10^{-6} . The respective calibration was executed by the PTB [94]. The studied milling machine has the capability to switch its tool for a probe system and thus perform measurements on a part. In this case, the machine is used to measure the relative position of the various holes. The errors of the machine result in deviations in the measured hole positions relative to their calibrated

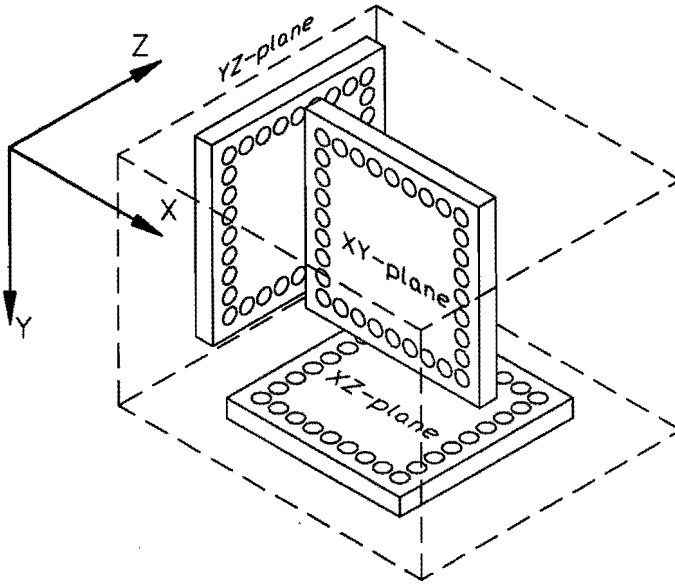


Figure 5.3: Different hole plate locations

values. If the estimated error model is correct, we should be able to predict these errors.

The hole plate is placed on the machine in three different planes: the XY-, XZ- and YZ-plane (see Figure 5.3). Kunzman [62] showed that the measurements of the hole plate in these locations are highly sensitive to all geometric errors of the machine.

To determine whether deviations between the observed and predicted measurement errors of the hole plate are significant, we need to know the repeatability of these measurements. This repeatability is affected by the used probe stylus. Three different probe styli are used to measure the hole plate in the described locations (see Figure 5.4). Table 5.1 presents the results of repeatability tests for these styli when measuring the position of a hole. The largest uncertainty is observed for measurements in the YZ-plane. This is due to the complex stylus configuration required to perform measurements in this plane. Figure 5.5 presents the measurement setup in this plane.

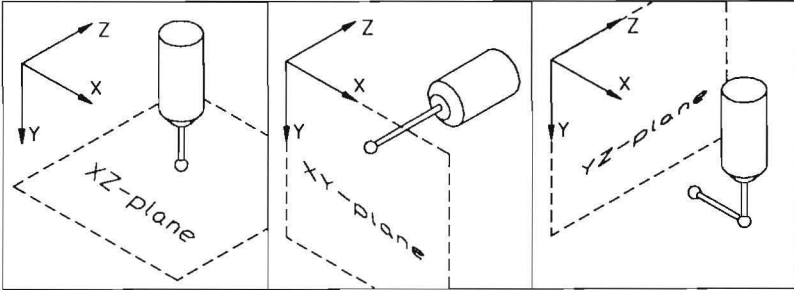


Figure 5.4: Different probe configurations

Plane	Repeatability		
	$2S_x$	$2S_y$	$2S_z$
XZ-plane	$0.6\mu m$		$0.8\mu m$
XY-plane	$1.1\mu m$	$0.8\mu m$	
YZ-plane		$1.3\mu m$	$2.4\mu m$

Table 5.1: Repeatability of the measured hole position in several planes

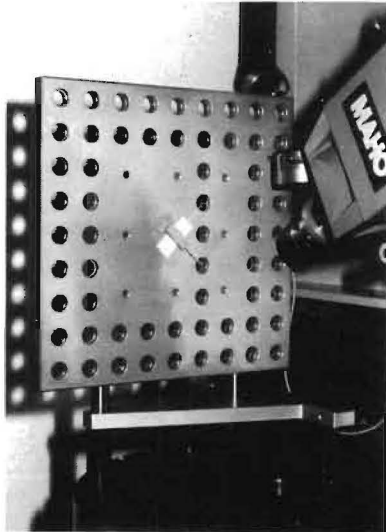


Figure 5.5: Hole plate measurement in the YZ-plane

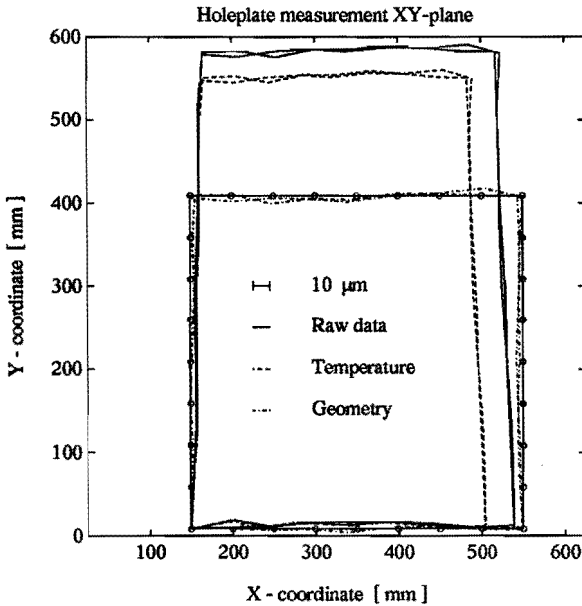


Figure 5.6: Observed and compensated errors in the XY-plane

Software is developed that uses the estimated error model to predict errors in the measurements executed by the machine. These simulated errors are used to compensate the errors in the actual measurements of the hole plate. First, however, the raw measurement data is compensated for errors due to the thermal expansion of both hole plate and machine scales. Also errors due to misalignment of the plate relative to the machine axes are compensated. If the developed models are correct, the compensated errors should be close to the observed repeatability of the hole plate measurements. Figures 5.6, 5.7, and 5.8 present the observed errors for three different coordinate planes (compensated for misalignment) and the residual errors after correction for the modelled thermal and geometric errors.

The maximum residuals between the observed and predicted errors are in the $10\mu\text{m}$ range. These residuals have a systematic pattern that indicates a squareness error. Especially in Figures 5.7 and 5.8 there is a significant error in the modelled squareness error of the machine. However, the uncertainty of the squareness measurements used to estimate the geometric error model is

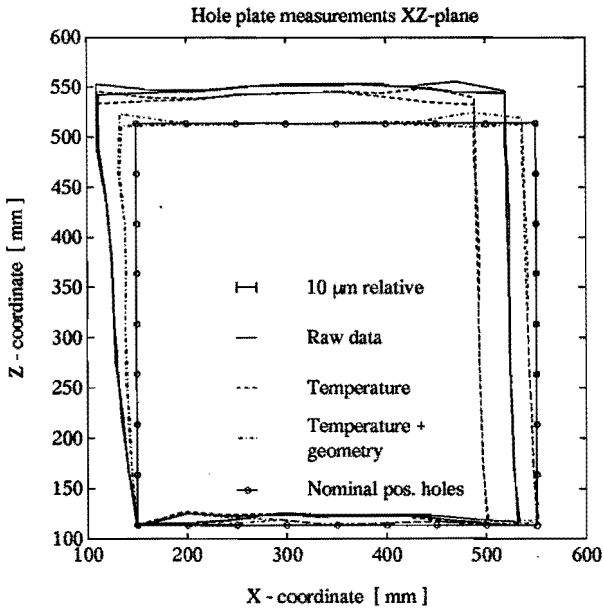


Figure 5.7: Observed and compensated errors in the XZ-plane

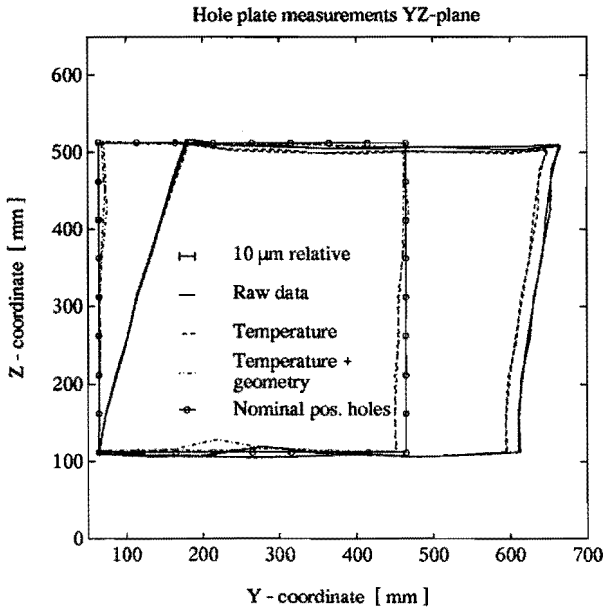


Figure 5.8: Observed and compensated errors in the YZ-plane

too small (approximately $5 \mu\text{rad}$) to explain the residuals. Further analysis showed that the residuals are mainly caused by variations in the geometric errors due to wear.

The error model is based on geometric error measurements executed several months prior to the hole plate measurements. During this period, the geometric errors of the machine have changed. Figures 5.6 and 5.8 indicate the presence of large geometric errors in the investigated five axis milling machine. These errors are due to a large yrx error (rotation around x when moving y) caused by worn bearing surfaces of the milling machine. These surfaces are coated with a special synthetic material to enable smooth movement of the carriage. When this coating is worn, the bearing surfaces will show an increased wear rate resulting in quickly changing geometric errors. Especially the Y -axis suffers from this problem. This also caused the hysteresis error described in Chapter 3.

Real-time geometric error correction

An important application of error models is software error compensation. To this effect, the geometric error model is implemented in the controller of the machine [29, 96, 109]. In cooperation with the respective manufacturer, a reduced, efficient error model was developed. This model can be quickly evaluated, which is essential in the real-time environment of the controller. In order to validate the performance of the adapted model, the hole plate is measured with and without software compensation.

Again the hole plate is measured in all three coordinate planes. In Figure 5.9 the measurement results of the YZ -plane are depicted. As predicted by the simulations, the software compensated machine still has a significant squareness error. The maximum observed error of the software error compensated machine equals $11\mu\text{m}$ versus $109\mu\text{m}$ before compensation. For the hole plate measurements, the model reduction has not deteriorated the predictive power of the error model.

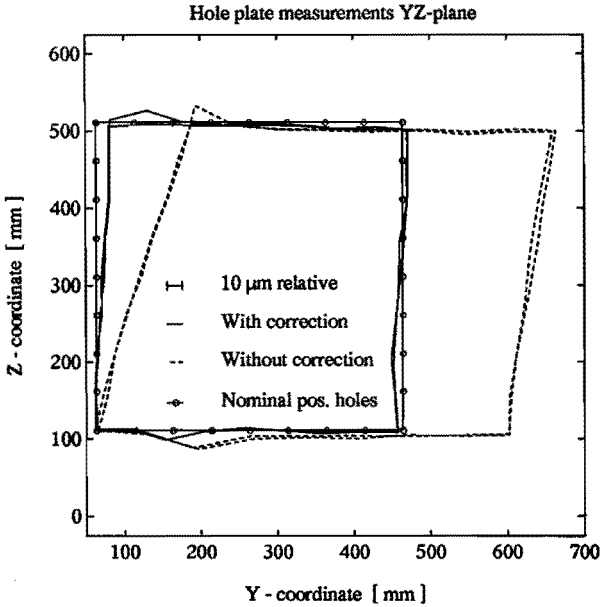


Figure 5.9: Validation of the real-time error compensation in the YZ-plane

5.1.2 Errors due to mechanical loads

Weight of moving machine components

In Chapter 3, measurement results are presented that indicate that the angular error y_{rx} (rotation around X when moving Y) is dependent on both the position of the X- and Y-axis. This so-called cross-coupling is due to the weight of the moving X-axis carriage. Due to this dependency on the X-axis position, the apparent scale error of the Y-axis (i.e. the y_{ty} error) is also related to the position of the X-axis. Furthermore, the apparent roll error of the X-axis will be dependent on the position of the Y-axis. For the more likely candidates for cross-coupling (e.g. dependency y_{rz} error on X, and y_{rx} error on Z) no significant interaction terms were observed.

In order to validate the respective error model, the errors observed in the hole plate measurements are again compensated for the predicted errors (off-line). Two different models have been used for these simulations. A model

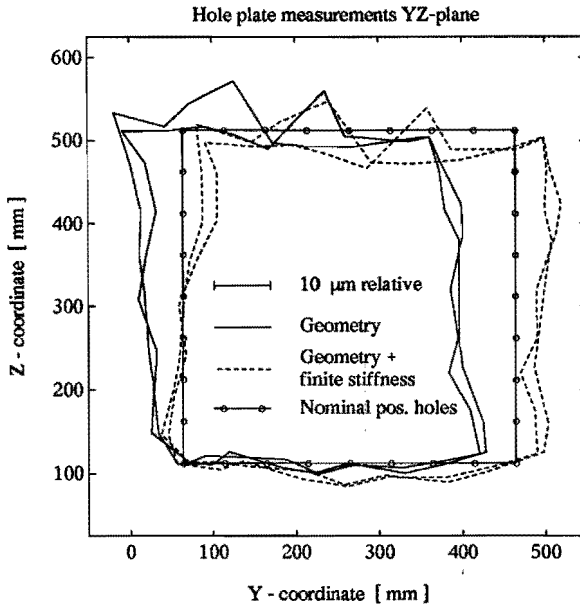


Figure 5.10: Compensation of hole plate measurement errors using a model with and without yrx cross-coupling

that describes the geometric errors of the milling machine without cross-coupling, and one that includes the described cross-coupling. The results of this comparison are presented in Figure 5.10. The residuals are smaller when cross-coupling is included in the model.

Workpiece weight

In Chapter 3, the effect of the workpiece weight on the accuracy of the milling machine is analysed. To validate the estimated error model, hole plate measurements are executed with workpiece weight.

The milling machine is loaded with a workpiece weight of 3500 N located at a Z-position of -189 mm relative to the center of the workpiece table. Hole plate measurements are executed in the XY- and XZ-plane. Figures 5.11 and 5.12 present the compensated measurement errors in both planes. The measure-

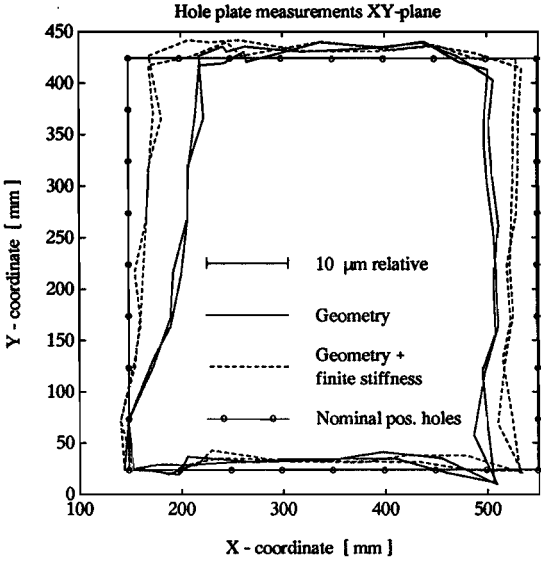


Figure 5.11: Residual errors after compensation for geometry and workpiece weight. (XY-plane, load 3500 N)

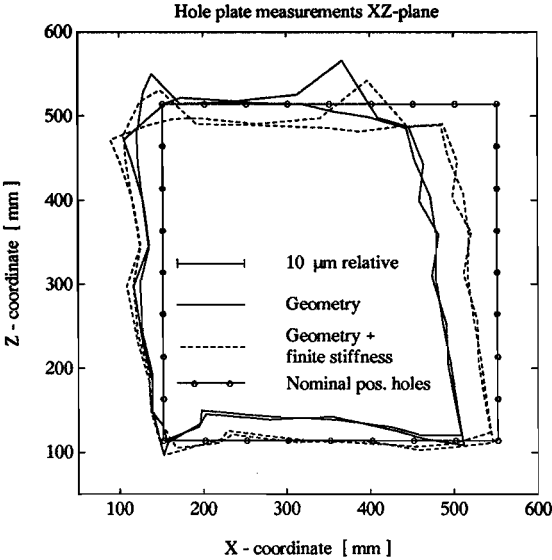


Figure 5.12: Residual errors after compensation for geometry and workpiece weight. (XZ-plane, load 3500 N)

ments are compensated using the geometric error model and the model describing the errors due to workpiece weight.

Both Figures 5.11 and 5.12 indicate a relatively small contribution of the finite stiffness errors to the total errors of the milling machine (see Figure 5.6). In Chapter 3 it is shown that the workpiece weight mainly affects the parallelism error between the B-axis and the Y-axis. This parametric error does not contribute to the observed errors, since the B-axis is not moved during the hole plate measurements.

The residuals after compensation for the workpiece weight are smaller than the residuals observed during the validation of the geometric error model without workpiece weight. This somewhat peculiar result is due to the age difference between both models. The measurements and validation of the finite stiffness errors directly succeeded each other. The geometric error model, on the other hand, is relatively old. The parametric errors due to the workpiece weight are estimated from the difference between the observed parametric errors with workpiece weight and without workpiece weight. The latter data is relatively old. Hence the finite stiffness model contains both the effect of the workpiece weight and geometric error variation due to wear.

5.1.3 Thermal errors

In Chapter 3, two approaches are presented to model the thermal errors of a multi-axis machine. In the first instance, an empirical dynamic model is estimated that relates the temperature distribution of the structural loop to the values of a small number of temperature sensors. The estimated temperature distribution is the input of an analytical model, which results in the various parametric errors. These parametric errors are then inserted in the kinematic model to obtain the errors in the relative location of the end-effector. The second modelling approach is based on the estimation of a dynamic model that directly relates the observed errors in the relative location of the end-effector to the values of a limited number of temperature sensors.

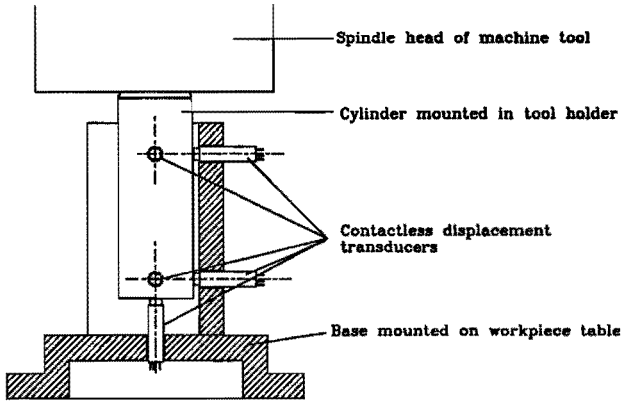


Figure 5.13: Measurement setup to measure zero-point drift

In order to estimate and verify the various models, several experiments are executed. Here only the heat generated by the spindle drive is considered. This is by far the major heat source of the machine. Furthermore, only the horizontal spindle is analysed. The experiments are based on a setup developed by Theuws [115]. This setup enables the simultaneous measurement of temperature elevations and the zero-point drift of the tool holder.

A large number of Pt-100 temperature sensors are attached to the milling machine. The position of each sensor is depicted in Figure 5.1. The choice for these positions is determined by careful consideration of both the location of the internal heat sources and the requirements of analytical model. The model requires that the thermal gradients in all directions are measured. This is achieved by placing the sensors at the corners of each beam segment, so that linear temperature gradients in three orthogonal directions can be estimated. To measure the zero point drift, a cylinder is mounted in the tool holder of the milling machine. The workpiece table contains a base with five eddy current displacement transducers. With these contactless displacement transducers, the position of the tool holder is measured in three orthogonal directions. Also, two relevant rotations can be measured. The measurement setup is depicted in Figure 5.13.

The analytical model

First the analytical model for the thermal errors is validated, using the measured temperatures of the various sensors as input. During the experiment, the machine is loaded with a constant spindle speed of 6000 rpm during six hours (warming up) and spindle stop during eight hours (cooling down). The Z-axis is fully extracted (i.e. $Z = 0$). The position of the X- and Y-axis during all the experiments equal respectively 350 mm and 160 mm. The temperature elevations of five characteristic sensors are depicted in Figure 5.14. The predicted and observed zero-point drift of the tool during this experiment are presented in Figure 5.15.

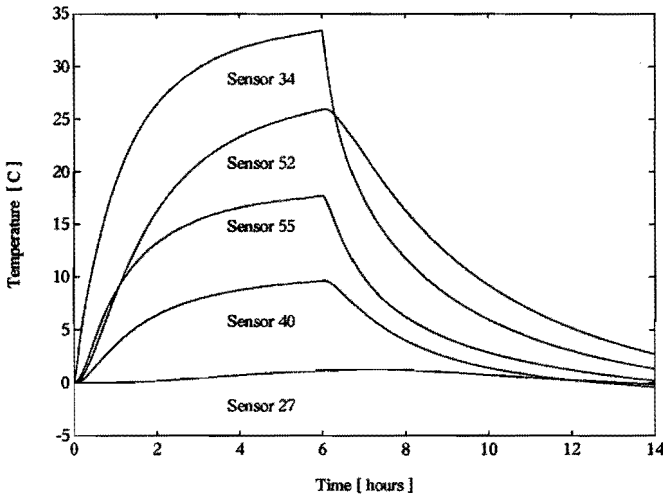


Figure 5.14: Temperature elevation during a load of 6000 rpm for six hours ($Z = 0$)

The agreement between the predicted and observed errors is quite good in X- and Y-direction. Here the maximum difference is in the order of $10 \mu\text{m}$. In Z-direction, however, there are major problems, especially during warming up. This discrepancy is mainly due to the expansion of the tool. The implemented model calculates the tool expansion assuming that the temperature of the tool equals that of the tool holder. In reality, the tool is much colder due to the forced convection that occurs when it is rotating at 6000 rpm. In the first

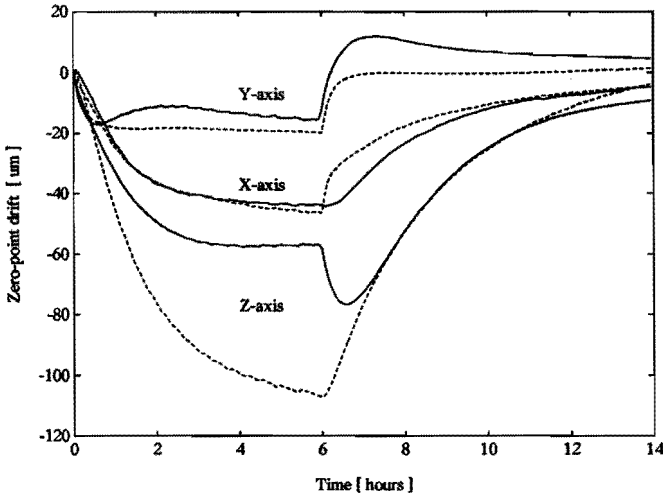


Figure 5.15: Drift of the tool during a load of 6000 rpm for six hours ($Z = 0$). The observed and predicted errors are presented by respectively solid and dashed lines. Analytical model.

half hour after spindle stop, the tool actually increases its temperature due to the absence of this convection, giving rise to an increased zero-point drift. An illustration of this effect is the change in tool diameter during the experiment (see Figure 5.16). This diameter was measured using two opposite sensors.

To assess the validity of the model for more practical situations, the machine is loaded with a spindle spectrum as defined in DIN 8602 (see Figure 5.17). This spectrum contains a sequence of spindle speeds, varying from zero to the maximum spindle speed. The latter equals 6300 rpm for the investigated machine. The results of this test are presented in Figure 5.18. In Figures 5.19 and 5.20 the analytical model is similarly verified when the Z-axis is fully retracted (i.e. $Z = 600$ mm). From these tests we can conclude that the analytical model is capable of describing thermal errors resulting from relatively fast load changes.

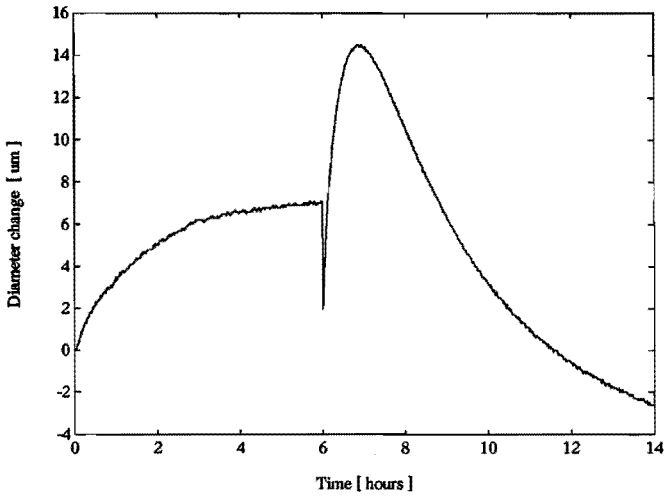


Figure 5.16: Change in tool diameter during a load of 6000 rpm for six hours. Note the sharp increase in diameter after spindle stop (6 hours).

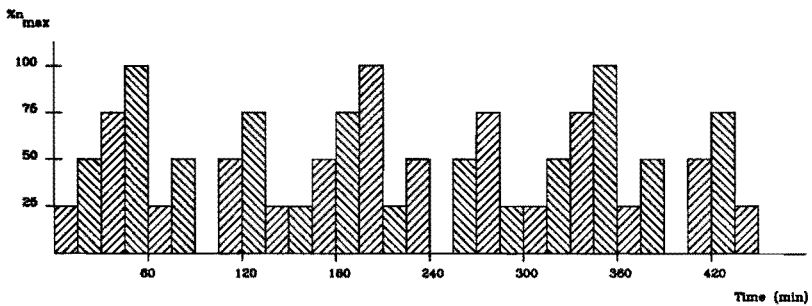


Figure 5.17: Duty cycle according to DIN 8602

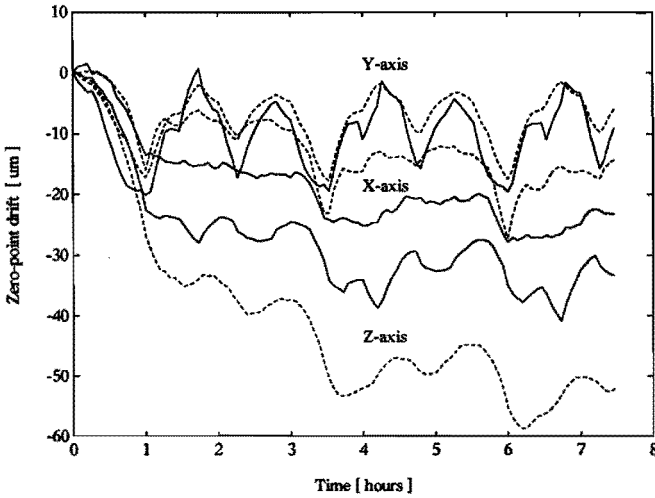


Figure 5.18: Drift of the tool during a load according to DIN 8602 ($Z = 0$). The observed and predicted errors are presented by respectively solid and dashed lines. Analytical model.

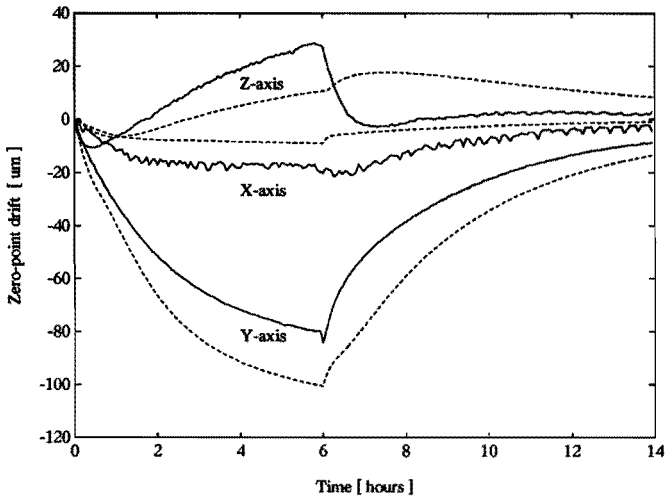


Figure 5.19: Zero-point drift during a load of 6000 rpm for six hours ($Z = 600$). The observed and predicted errors are presented by respectively solid and dashed lines. Analytical model.

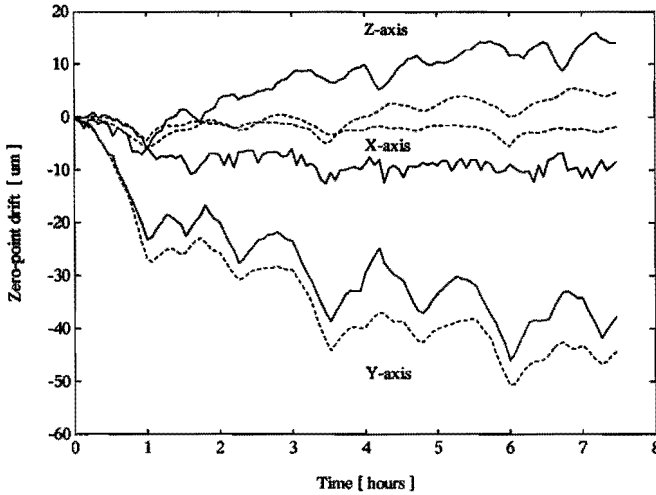


Figure 5.20: Drift of the tool during a load according to DIN 8602 ($Z = 600$). The observed and predicted errors are presented by respectively solid and dashed lines. Analytical model.

The empirical model for the temperature distribution

The empirical model for the thermal distribution uses two temperature sensors to predict the temperature elevation of all other sensors: sensor 34, mounted on the ram, and sensor 52, mounted on the swiveling head. Both sensors are located in close proximity to gear transmissions and bearings in the main spindle drive. The model has three time constants. The parameters in this model are estimated from one experiment. During this experiment, the machine is loaded with a constant spindle speed of 6000 rpm during six hours (warming up) and spindle stop during eight hours (cooling down). The predicted temperature elevations of three characteristic sensors are depicted in Figure 5.21. The predicted temperatures are now used as input for the analytical model. The respective results for a duty cycle according to DIN 8602 are presented in Figure 5.22. Using the predicted instead of the actual temperatures only marginally affects the accuracy of the drift predictions. In X-direction the accuracy is even improved.

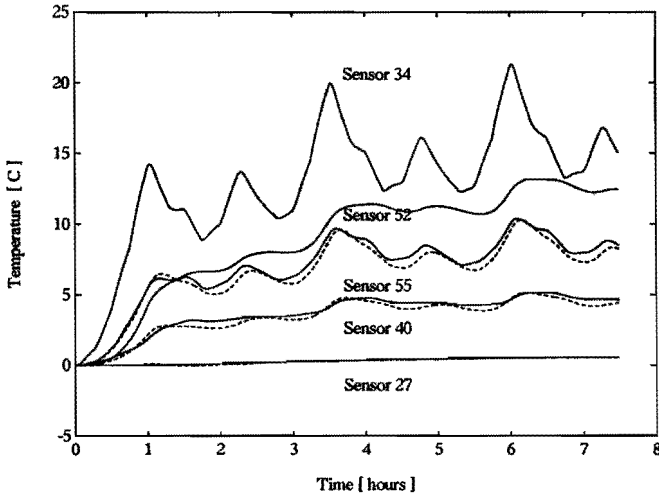


Figure 5.21: Temperature elevations during a load according to DIN 8602 ($Z = 0$). The observed and predicted temperatures are presented by respectively solid and dashed lines.

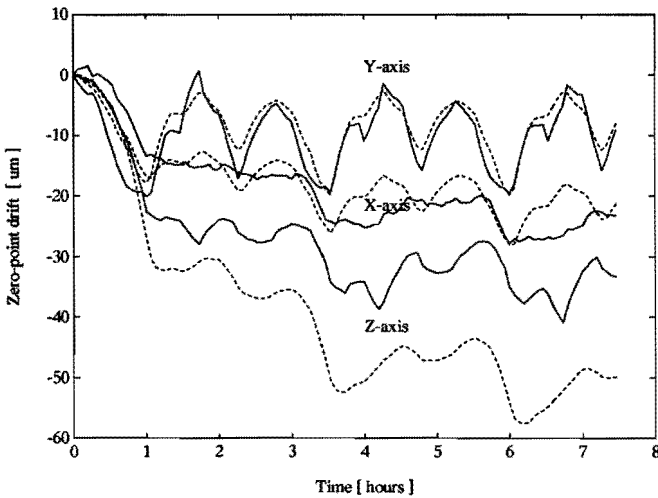


Figure 5.22: Drift of the tool during a load according to DIN 8602 ($Z = 0$). The observed and predicted errors are presented by respectively solid and dashed lines. Analytical model using the empirical model for the temperature distribution.

The empirical model for the zero-point drift

The empirical model for the zero-point drift directly relates the measured temperatures to the displacement of the tool holder. This model uses the same two temperature sensors as the empirical model for the temperature distribution. It is also estimated from one experiment where the machine is loaded with a constant spindle speed of 6000 rpm. Results obtained with the estimated model are presented in Figures 5.23 and 5.24. The use of spindle spectra to estimate the model parameters only slightly improved the predictive power of the model for other spectra. However, in these cases, the respective model showed problems when predicting errors during constant loads.

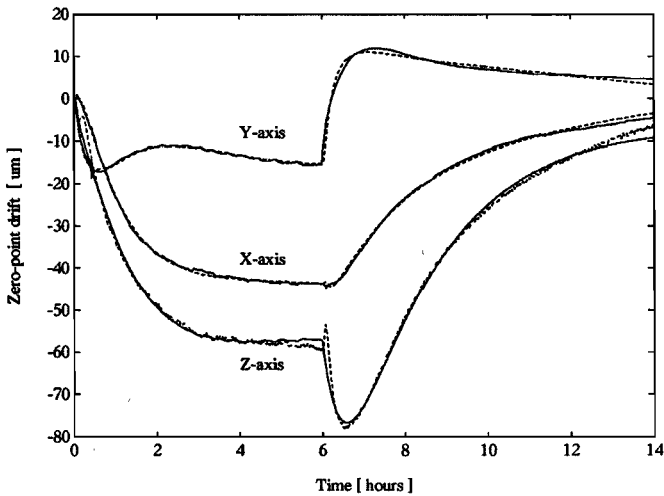


Figure 5.23: Drift of the tool during a load of 6000 rpm for six hours ($Z = 0$). The observed and predicted errors are presented by respectively solid and dashed lines. Empirical model (estimation dataset).

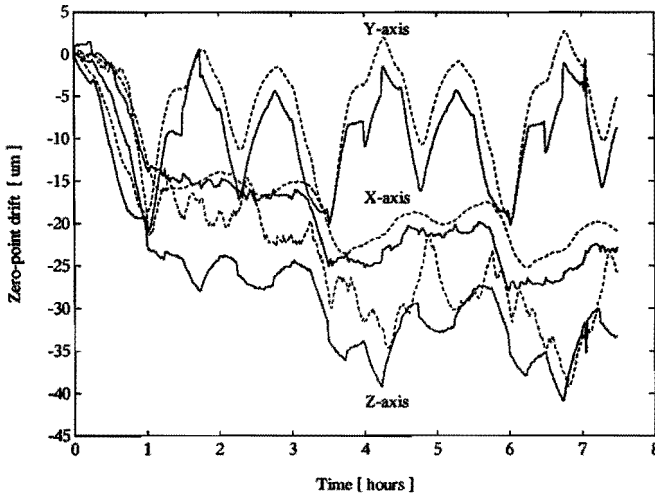


Figure 5.24: Drift of the tool during a load according to DIN 8602 ($Z = 0$). The observed and predicted errors are presented by respectively solid and dashed lines. Empirical model (validation dataset).

5.2 Error estimation of a three-axis CMM using artifacts

The procedure outlined in Chapter 4 is applied to calibrate the bridge-type CMM depicted in Figure 5.25. The CMM has a resolution of $0.5\mu m$, and its accuracy is stated by the manufacturer as [143]:

$$\begin{aligned}
 1D & : U_{95} = 1.6\mu m + 3.3 \cdot 10^{-6} \cdot L \\
 3D & : U_{95} = 2.6\mu m + 5.0 \cdot 10^{-6} \cdot L
 \end{aligned}
 \tag{5.1}$$

Not included in the calibration are the errors introduced by the CMM's (measuring) probe system. Furthermore a constant probe offset is used. Hence, angular errors which affect the measurement accuracy only through the used probe offset (in our case zrz and xrz) are not estimated. When using a constant probe offset, it is not possible to separate the effect of the Z-axis straightness errors ztx and zty from respectively the zry and zrx angular errors. Hence these straightness errors are also not estimated. As with probing errors, dedicated tests, using different probe offsets, are better suited to as-

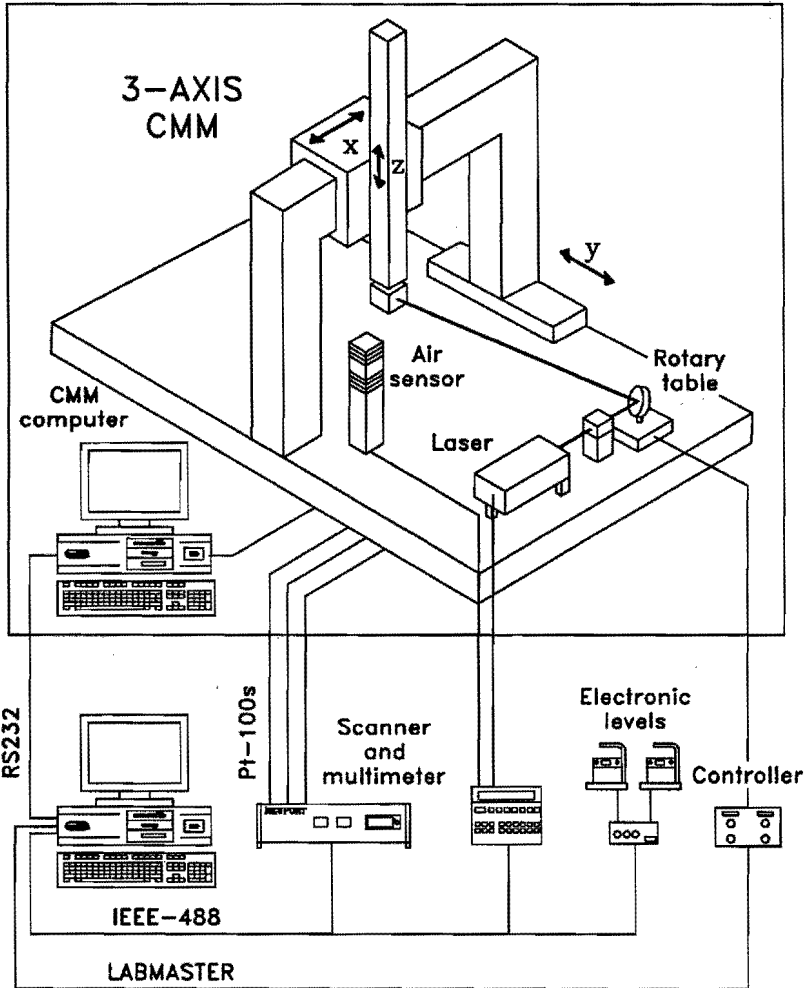


Figure 5.25: Investigated CMM and calibration equipment

sess the angular and straightness errors that are not considered. A correction was implemented for the thermal expansion of the scales, using two to three temperature sensors (Pt-100s) per scale (see Figure 5.25).

In the subsequent sections, three different calibration setups based on length measurements are described. The calibrations use respectively a laserinterferometer in distance mode, a checking gauge, and a relatively small number of length measurements in optimized locations. The results will be compared with a conventional calibration based on the separate measurement of the various parametric errors (using a laserinterferometer and electronic levels).

5.2.1 “Brute Force” calibration

The philosophy of this method is to measure *many* lengths in *many* different locations uniformly distributed throughout the complete workspace of the machine. Thus, parametric errors estimated with this data optimally describe the length measuring capability of the machine, which represents the essence of its accuracy. Since the various lengths are measured throughout the workspace, analysis of the residuals between the observed and modelled deviations yields powerful information with respect to the accuracy of the error model (e.g., the presence of finite stiffness related errors not implemented in the model). The method represents an extreme of the fundamental calibration compromise described in Chapter 4. Since little intelligence is used in selecting the location and choice of the lengths measured, the calibration’s efficiency in the estimation of modelled errors is rather low (i.e., many measurements are required). However this lack of assumptions in the experimental design, results in a maximum ability to detect from the calibration data (unexpected) machine tool errors not implemented in the proposed model.

As a first approach to reduce the significant experimental effort necessary for calibrations of this kind, we used a laserinterferometer to measure the various lengths in combination with a mirror mounted on a motorized rotary table (see Figure 5.26). A large retroreflector is attached to the machine’s ram, and the interferometer is placed between laser source and mirror. The mirror setup is (software) aligned by measuring the location of the reflected

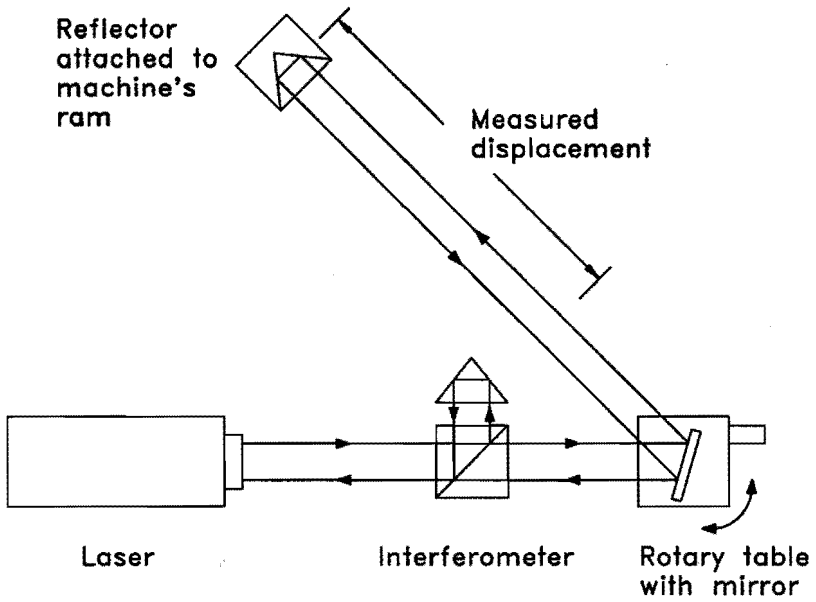


Figure 5.26: Experimental setup "Brute Force" calibration

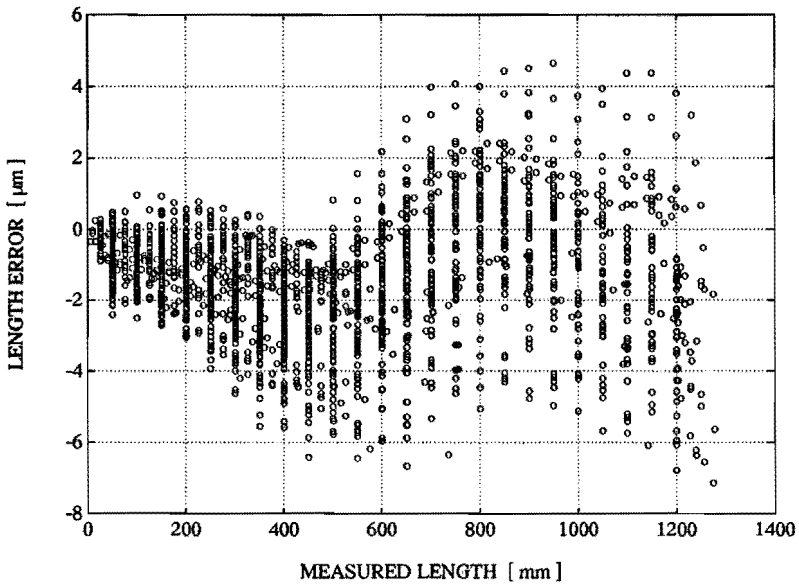


Figure 5.27: Errors in the measured lengths

beam for several angles of the rotary table. Each location is estimated from the machine's scale readings at two different, manually tuned, positions where the laser beam is optimally returned to the laser head. From this information, the host computer is able to calculate the position and direction of the reflected laser beam for any angle of the rotary table. At a certain fixed position of the rotary table, the machine's ram is now automatically moved along the reflected laser beam. At certain positions, the machine is stopped, and its indicated travel is compared with the respective laser reading. After a complete back and forth movement, the mirror is automatically rotated by a certain angle and the process is repeated. Thus, a large number of lengths can be measured fully automatically.

Note that for this application the accuracy requirements of the rotary table are rather low. Since the position of the mirror is fixed during each length measurement, errors in its location only affect the calibration accuracy by cosine errors (in our setup $< 10^{-7} \cdot L$). Similarly, the accuracy requirements of the mirror surface and the retroreflector are rather low. A drawback of the method is the increased distance between the interferometer and the starting point of the length measurements, due to mirror and rotary table. Significant 'deadpath' errors may occur in case of an unstable environment and slow execution of the back and forth measurement.

The total number of approximately 4000 lengths measured throughout the workspace is split into an estimation dataset and a validation dataset. The estimation dataset is used to estimate the unknown parameters $\underline{\beta}$ that describe the machine's error model. The validation dataset is used to study the predictive capabilities of the model. Figure 5.27 presents the observed errors in the measurement of these lengths (average of five samples). In Figures 5.28 and 5.29, the residuals between the predicted and observed length deviations of this dataset are depicted for models estimated with respectively the conventional calibration and the "Brute Force" calibration (73 estimated significant parameters $\underline{\beta}$).

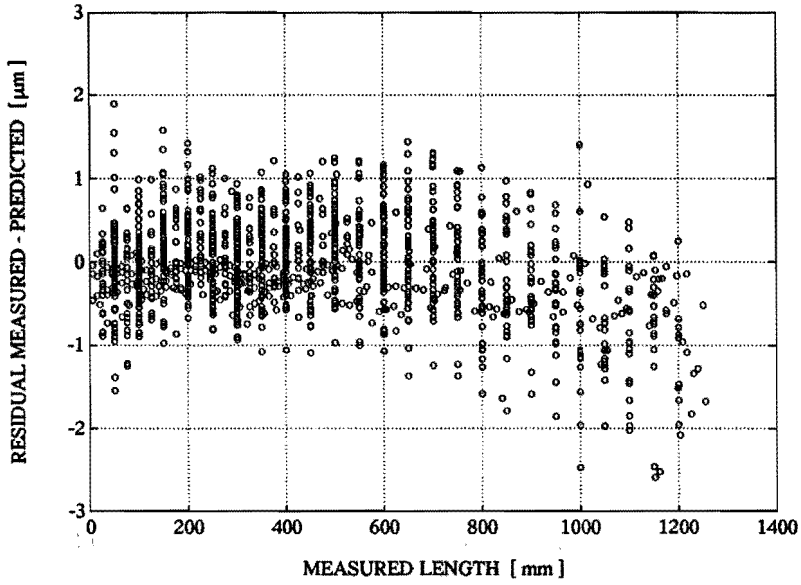


Figure 5.28: Residuals conventional calibration

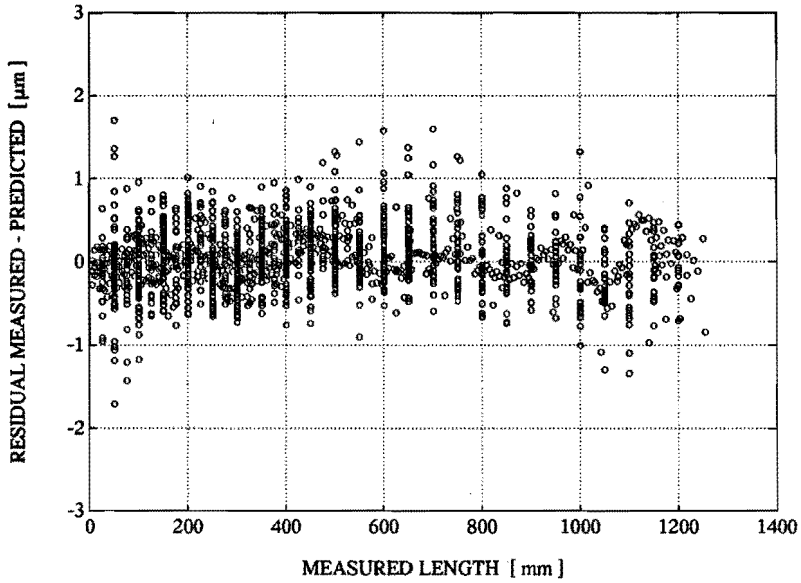


Figure 5.29: Residuals "Brute Force" calibration

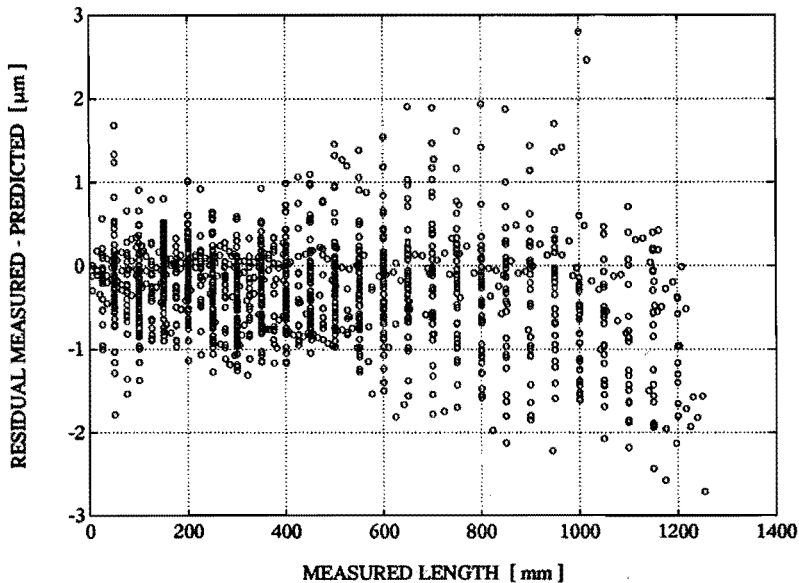


Figure 5.30: Residuals calibration using a Machine Checking Gauge

5.2.2 Calibration using a Machine Checking Gauge

A Machine Checking Gauge consists of a fixed reference length of unknown dimension supported by respectively a pillar with pivot ball and the machine's probe tip. Since three-point contact locations are used at either end, the MCG self-aligns to the probe and reference pivot and thus only one touch is needed to measure its current end position with respect to the pivot. The machine manipulates and measures the reference length in several orientations. This provides a truncated sphere of points centred around the reference pivot. From the many possible combinations of pivot position and reference length, we chose a set of 10 combinations (three different lengths of 226, 380, and 532 mm yielding a total of 932 measurements). The effects of probe lobing and probe sphere roundness were compensated using the errors observed when measuring the pivot sphere in the same approach directions as during the checking gauge measurements (this was not possible for the -45° elevations). Since the reference lengths used are not calibrated, the performance data was augmented with a set of laserinterferometric distance measurements taken

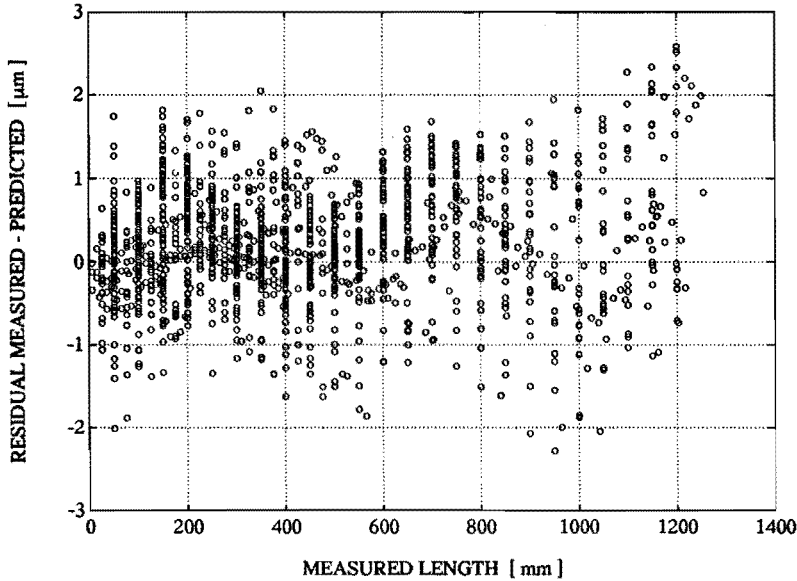


Figure 5.31: Residuals calibration using 50 length measurements

along one line parallel to the machine's Y-axis. From this data, the error model was estimated. The proposed model had the same unknown parameters $\underline{\beta}$ as the model used in the "Brute Force" calibration. Figure 5.30 depicts the residuals between the predicted and observed length deviations of the validation dataset.

5.2.3 Calibration using a small number of measurements

In this section, the optimal design theory presented in chapter 4 is applied to calibrate the CMM using a relatively small number of length measurements. Compared with the "Brute Force" calibration, this setup presents the other extreme of the fundamental calibration compromise. Since the choice and position of the measured lengths is optimized according to the proposed error model of the machine, the efficiency in the estimation of the unknown parameters $\underline{\beta}$ of this model is high (i.e., a small number of measurements is required). However a too rigorous optimization, will significantly reduce the possibilities

to detect from the calibration machine tool errors not implemented in the model.

In order to facilitate the comparison of the calibration methods described, the design space was defined as the total collection of length measurements performed during the “Brute Force” calibration. The number of lengths used in this calibration was chosen as 50 (a number slightly higher than that allowed by the American standard for performance evaluation of CMMs (40 measurements) [5]). In order to determine the trend of the various errors, low order (quadratic or linear) polynomials were used in their proposed model, which yields a total of 32 unknown parameters to be estimated. The residuals between the predicted and observed length deviations of the validation dataset are depicted in Figure 5.31.

6

Conclusions and recommendations

6.1 Conclusions

In this thesis a systematic approach is presented to analyse the accuracy of multi-axis machines. The general goal is a model for the errors in the relative location of end-effector and workpiece reference during an arbitrary task.

The core of the proposed approach is the so-called kinematic model. This model is a mathematical entity that enables the separation of the structural loop into different segments, whose so-called parametric errors can be measured and analysed independently. The presented kinematic model can be applied to multi-axis machines consisting of an arbitrary serial configuration of revolute and prismatic joints. It is completely defined by the nominal geometry of the structural loop. For a five-axis milling machine and a three-axis CMM, the model is successfully applied to describe the propagation of all studied parametric errors. It is further shown that the model is an important tool for the uncertainty analysis of multi-axis machines.

The studied parametric errors in this thesis are those due to the limited accuracy of structural loop components in an unloaded reference state, those due to static and slowly varying forces introduced by the dead weight of machine components and workpiece, and those due to thermally induced strains in the

structural loop. The respective error sources are analysed separately, and their combined effect on the parametric errors is obtained by superposition.

The models for geometric parametric errors are based on least squares fitted, piecewise polynomials defined on the domain of the joint enclosed by the respective coordinate frames. These models are simple to use, yet have a high degree of flexibility to accommodate the often irregular nature of geometric errors. For straightness and periodic errors special versions of these models are presented. Software is developed to automate the estimation of the geometric errors. Various statistical tests are used to validate the accuracy of the estimated models and to remove statistically insignificant parameters.

The modelling procedure for geometric errors is applied to a five-axis milling machine and a three-axis CMM. In the first instance, the model is verified by predicting the errors of hole plate measurements executed by the machine in various coordinate planes. The observed errors of maximum 110 μm can be predicted with a maximum uncertainty of 10 μm . Using a simplified version of this model, an algorithm for software error compensation is implemented in the controller of the machine. Hole plate measurements executed by the compensated machine show a maximum error of 11 μm . For the CMM, the model is verified by predicting the errors of a large number of length measurements executed by the machine in various locations. The observed errors of maximum 8 μm can be predicted with a maximum uncertainty of 2 μm . In both cases, we can conclude that the estimated models for the geometric errors, in combination with the kinematic model of the machine, adequately describe the accuracy of the machines in an unloaded (reference) state.

Parametric errors introduced by the weight of moving machine components and workpiece are again described using piecewise polynomials. In the first instance, parametric error dependencies are introduced on the position of joints other than that enclosed by the respective coordinate frames (cross-coupling). These dependencies are generally of a very regular nature (often linear). In the second instance, also the position and weight of the workpiece are variables in the parametric error models.

The analysed milling machine shows one significant cross-coupling error. By modelling this error, the uncertainty in the predicted hole plate measurement errors is reduced from $10\ \mu\text{m}$ to $4\ \mu\text{m}$ in one coordinate plane. Assuming linear elastic behaviour, models are derived for the errors of the milling machine resulting from different workpiece weights, located at various positions on the machine table. The respective components of the affected parametric errors are estimated from their variation when a certain load is applied. The change in the parametric errors due to an arbitrary workpiece load is obtained by interpolation. With the exception of the parallelism error between rotary table and machine column, the effect of workpiece weight on the parametric errors is relatively small. The respective change in these errors due to an arbitrary workpiece weight can be accurately predicted. The effect of the workpiece weight on the accuracy of hole plate measurements is small compared to the repeatability of the machine.

The thesis presents three models to describe the errors introduced by thermal loads acting on the structural loop. The first two models are empirically estimated. The input of these models is the change in the measured temperatures of a small number of sensors (two for the studied five-axis milling machine) located in close proximity to relevant heat sources. The output is respectively the temperature distribution of the structural loop, or errors in the relative location of the end-effector. In both cases, the respective dynamic multi-input multi-output system is modelled using a state-space approach. The third model reflects an analytical approach to relate the parametric errors to the temperature distribution of the structural loop. The latter is either estimated from temperatures measured by sensors distributed over the complete structural loop or described by output of the first empirical model. The analytical model is based on the approximation of stress-free thermal deformation of the structural loop.

The three models are applied to predict the zero-point drift of a five-axis milling machine during characteristic duty cycles of the main spindle. The following conclusions can be drawn:

- The observed thermal drift of maximum $80\ \mu\text{m}$ can be predicted with a maximum uncertainty of $40\ \mu\text{m}$ (mainly due to the tool expansion), using

the analytical model in combination with approximately 30 temperature sensors. When using the empirical model to predict these sensor readings, based on the readings of two temperature sensors, this accuracy is only marginally affected. The latter two sensors are located in close proximity to the main heat sources. The empirical model that directly predicts the thermal drift using the two sensors has a maximum uncertainty of approximately 10 μm . However, it should be noted that this model is only valid for a certain tool and at a certain position of the machine axes.

- Due to the dynamic nature of the empirical models, they require a significantly lower number of temperature sensors compared to other (static) models used in this field.
- The analytical model results in parametric errors. Hence it can be used in conjunction with the kinematic model to predict the errors in the relative location of the end-effector at any position of the machine axes. Both empirical models are only valid for a certain position of the machine axes. To describe the errors at other positions, models have to be estimated at different axis positions in combination with a suitable interpolation scheme.
- When the various sensors are suitably placed, the analytical model is valid for moving axes, coolant, and various ambient temperatures and ambient temperature gradients. For the empirical models, these effects must be considered in the modelling procedure and included in the various experiments.
- Although the basic principles of the analytical model are relatively simple, its application requires experience and specific knowledge on the construction of the machine. Due to the large number of underlying assumptions, the analytical approach often requires several iterations to derive an acceptable model. Problems are introduced due to the fact that it is usually not possible to position the sensors at their ideal locations. In contrast, the estimation of the empirical models is relatively easy, can be largely automated, and requires little specific knowledge about the analysed machine. A drawback is the danger of overfitting. In this

respect, the estimation data should reflect the typical temperature loads during machine operation.

- The analytical model is probably valid for all machines of a certain factory type. Wear, preload, and tolerances affect the intensity and distribution of the heat sources, not the thermal deformation given a certain temperature field. However, since the temperature field is estimated from a limited number of sensors, a significant change in the intensity and position of the heat sources may affect the predictive power of the model.
- The analytical model provides insight in the thermal deformation of the structural loop. This information can be used to improve the design of the machine and the placement of temperature sensors.

A general method is presented to estimate the quasi-static parametric errors of multi-axis machines using artifact measurements. The use of standard regression techniques in the estimation of the parametric errors yields a uniform approach regarding the nature of the machine being studied (e.g. the presence of revolute joints or finite stiffness effects), and the choice and location of the artifacts measured. The method can be applied to most existing calibration procedures based on artifact measurements. In many cases a more efficient use of the calibration data will be achieved. Using statistical experimental design techniques, it is shown that the efficiency of such procedures can be unambiguously assessed and optimized. Also statistical techniques can be readily used to verify the estimated error model.

The method is applied to calibrate a three-axis CMM by three different methods, all using length measurements. The "Brute Force" calibration uses a large number of length measurements in many different orientations. It yields better results than a conventional calibration based on the individual measurement of each parametric error. The results obtained with respectively a Machine Checking Gauge and a limited number (50) of length measurements in optimized locations are comparable with those obtained by conventional calibration techniques, though require less effort and equipment.

6.2 Recommendations

Regarding the quality of the error models, their estimation, and their application, research on the following topics is recommended.

General

- **Superposition.** The proposed modelling procedure relies heavily on the assumption that the total error of the machine can be obtained by superposition of the effects of various error sources. This assumption needs to be verified with respect to the interaction of mechanical and thermal loads.
- **State-space approach.** The presented empirical models for the temperature distribution and thermal drift are based on a state-space presentation. Application of the state-space approach is obviously not limited to thermal errors. The (combined) analysis of other (dynamic) error sources and their interactions might benefit from the systematics of the state-space approach and the wealth of techniques developed in this field. In this context, it might be possible to develop a state space model where the respective state comprises all information required to describe the combined effect of the various error sources, including their interactions.
- **Task accuracy.** Models are required that relate errors in the relative trajectory of the end-effector to the resulting errors of an executed task. This requires analysis of the end-effector - workpiece interaction, and often the consideration of additional error sources (e.g. the numerical properties of the estimation software used by a CMM). These models can be used to predict the accuracy of parts produced by a machine (e.g. in order to select a suitable machine, to optimize manufacturing parameters, and to eliminate trial runs), to realize traceability of coordinate measurements, and to facilitate quality control in a flexible manufacturing environment (see next item).

- **Quality control.** Traditional quality control techniques are based on trends in the realized accuracy of similar parts in time. These techniques are difficult to apply in a flexible manufacturing environment. Hence, techniques are required where trends in the error sources of a machine are estimated from data on the realized accuracy of different products.
- **Uncertainty.** Methods are required to quickly assess the uncertainty of the predicted errors. This is especially important for the realization of traceability of coordinate measurements.
- **Long time stability of error models.** Due to wear and aging, the accuracy of a machine changes in time. Research is required as to which error sources are sensitive and over which time intervals error models remain valid.
- **Type dependent errors.** Research is required as to which error classes have type dependent characteristics. This in order to reduce the experimental and modelling effort for each individual machine. It is especially required for errors due to mechanical and thermal loads, as the modelling effort for these errors is quite large.
- **Software compensation.** An important application of the derived error models is software error compensation. Realization and implementation of the required compensation routines is relatively straightforward for measuring machines. Here the estimated errors can be used to compensate measured coordinates after the measurement has been executed. However for positioning and handling tasks, the position of the joints needs to be compensated during the execution of the trajectory. This limits the time available to calculate compensation values. Furthermore, implementation of the required compensation in the motion controller is a hazardous problem. Care must be taken to avoid instabilities of the control algorithm, especially when errors change rapidly as a function of axis position (compared to the resolution of the measurement systems). The problem is aggravated whenever a joint coordinate requires compensation for more than one error.
- **Design for software compensation.** Software error compensation can be a reliable, flexible, and cost-effective means to improve the accuracy

of multi-axis machines. Full use of its potential requires an approach where the possibilities and limitations of software compensation are considered in the design, manufacturing, and maintenance of both machine and controller. Especially design and manufacturing rules should be tailored towards increasing the type dependent characteristics of errors. Nowadays, software error compensation is often viewed as an add-on feature rather than an integrated component of the machine.

Kinematic model

- **Standardization.** The kinematic model plays a key-role in the accuracy analysis of multi-axis machines. Successful application of this model by 'ordinary' users is dependent on standardization. This affects not only the notation, but also the place where the various errors are defined.
- **Revolute joints.** Except for industrial robots, errors of machines with revolute joints have received little attention. Standardization of the respective error parameters is required, especially when machines contain more than one revolute joint. Examples are the use of fixed versus moving frames, and the definition of parameters required to describe the position of the joint axis. In the latter case, also measurement procedures need to be defined to assess these parameters.

Mechanical loads

- **Process forces.** The effects of static process forces are not considered in this thesis. Especially during single-pass machining operations, the structural loop deflections due to these forces may become significant. The modelling of these forces is not structurally different from those due to the workpiece weight. Practical problems occur due to the increased number of independent variables in these models and the related increased experimental effort. In contrast to errors due to the workpiece weight, the complete structural loop needs to be considered instead of only the part that supports the workpiece. Furthermore, process forces have a direction and magnitude dependent on process parameters.

Hence, the response of the structural loop to forces acting in different directions needs to be analysed.

- **Estimation mechanical loads.** Application of the error model, especially for software error compensation, requires the estimation of the position and magnitude of the workpiece weight. Since it is usually not practical to let the user supply these characteristics, research is required on sensors to assess these variables (e.g. strain-gauges).

Thermal errors

- **State-space approach.** The presented empirical models for the temperature distribution and thermal drift are based on a state-space presentation. Hence both the model and its estimation might benefit from the extensive amount of techniques developed in this field. Opportunities lie in the fields of model estimation, state reconstruction, and augmented state estimation. In the latter case, the model parameters are considered to be variable in time. During machine operation, these parameters are continuously adjusted such that temperatures measured by an additional number of temperature sensors are optimally described.

The next items address various properties that affect the thermal errors of a multi-axis machine but are not considered in this thesis. Although these effects have been studied in various laboratories, implementation of the respective results to predict the accuracy of arbitrary tasks still requires further research.

- **Coolant.** In this thesis, the effects of coolants on the temperature distribution of the machine and related deformations have not been studied. As coolants are a very effective means of heat transfer, they have a large effect on the temperature distribution of machine and workpiece. When coolants are sprayed on the machine and the workpiece in a well defined constant manner, no changes in the presented empirical methods are required. Problems occur when the coolant flow over the machine during manufacturing varies. In that case, the use of many temperature

sensors may be the only solution to assess the resulting temperature distribution.

- **Tool expansion.** The thermal expansion of the milling tool represents a major uncertainty in thermal error models and merits further analysis. Problems occur due to tool changes (cold tool on a warm machine), and forced convection for rotating tools with increased heat transfer rates. The latter is influenced by the geometry of the tool, spindle speed, and the amount of workpiece surrounding the tool.
- **Workpiece expansion.** Models are required that describe the thermal workpiece expansion. Especially the non-uniform thermal deformation during machining where no coolant is used represents problems. The analysis is complicated by the effect of workpiece fixturing, moving heat sources of tool and machining process, and forced convection with increased heat transfer rates for rotating workpieces (which also limits the possibilities of temperature sensors).
- **Machining process.** The effect of heat generated by the machining process as well as heat transported by the chips has to be studied. Especially for those cases where no coolant is used. Furthermore, the effects of tool wear and built-up-edge need to be considered.
- **Moving axes.** For the empirical models, research is required regarding the effect of moving axes. Movement of an axis results in heat generation, heat transport by the carriage, and a changed structural loop with different thermodynamic properties. A possible approach to this problem is to divide the machine into several bodies, separated by kinematic elements. For each body, a model is estimated that relates its temperature distribution to the temperatures measured by sensors located near its heat sources and sensors near the boundary with other bodies. The latter sensors describe the heat sources or heat sinks embodied by these neighbours. Thus a model might be obtained that is valid for any position of the machine axes as well as moving axes.
- **Multiple heat sources.** The empirical thermal models have only been estimated and verified for a single dominant heat source. Research is

required concerning the experiments and modelling procedures in case more independently variable heat sources are active.

Artifact based calibration methods

- **Sequential update.** A promising concept, that merits further research, is the sequential augmentation of a calibration with extra measurements based on calibration data already obtained. Here suitable software suggests additional artifact measurements at certain locations, when the estimated error model cannot describe the observed errors of measurements already executed. Thus a sequential refinement of the error model can be achieved. The same concept can also be used to find artifact locations where maximum errors are obtained.
- **Subsets of parametric errors.** Research is required regarding the evaluation and optimization of calibrations to estimate subsets of the parametric errors. Especially those parametric errors that are sensitive to wear (typically scale and angular errors).
- **Planning and evaluation of experiments in the face of model uncertainty.** The presented optimization of a calibration assumes that the proposed error model of the machine contains all the parameters required to fully describe its accuracy. Research is required on model robust experimental designs that yield reasonable results for the model proposed even though it is known to be inexact, and model sensitive designs that highlight suspect inadequacies.
- **Errors due to thermal and mechanical loads.** The proposed method to estimate the parametric errors from artifact measurements is only valid when the machine has a constant temperature distribution. Research is required to also assess transient thermal errors using artifact measurements. Furthermore, the application of artifact measurements might reduce the extensive amount of experiments required to analyse the errors introduced by the workpiece weight.

Bibliography

- [1] E. Abbe. "Meßapparate für Physiker". *Zeitschrift für Instrumentenkunde*, 10:446–448, 1890.
- [2] M. H. Attia and L. Kops. "Calculation of thermal deformation of machine tools, in transient state, with the effect of structural joints taken into account". *Annals of the CIRP*, 28(1):247–251, 1979.
- [3] M. H. Attia and L. Kops. "Nonlinear thermoelastic behavior of structural joints —solution to a missing link for prediction of thermal deformation of machine tools". *ASME, Journal of Engineering for Industry*, 101:348–354, 1979.
- [4] M. H. Attia and L. Kops. "A new method for determining the thermal contact resistance at machine tool joints". *Annals of the CIRP*, 30(1):259–264, 1981.
- [5] ANSI/ASME B89.1.12M. "Methods for the performance evaluation of coordinate measuring machines". The American Society of Mechanical Engineers, New York, USA, 1990.
- [6] A. Balsamo, D. Marques, and S. Sartori. "A method for thermal-deformation corrections of cmms". *Annals of the CIRP*, 39(1):557–560, 1990.
- [7] M. Bamback and A. Fürst. "Bestimmung der Antastunsicherheit elektronischer 3-D-Tastsysteme". *VDI-Berichte*, (378):15–20, 1980.
- [8] G. Belforte et al. "Coordinate measuring machines and machine tools selfcalibration and error correction". *Annals of the CIRP*, 36(1):359–364, 1987.

- [9] BIPM, IEC, ISO, and OIML. "International vocabulary of basic and general terms in metrology". Technical report, ISO, 1984.
- [10] B. A. Boley and J. H. Weiner. *"Theory of thermal stresses"*. Robert E. Krieger Publishing Company, Malibar, FL, 1960.
- [11] G. L. Bowen and L. S. Duncan. "Integrated metrology systems". *Precision Engineering*, 7(1):23–30, 1985.
- [12] H. Brauning. *"Ein Numerisches Rechenmodel zur Berechnung der Instationären Temperaturverteilung in Werkzeugmaschinen, Programmiert für Elektronische Datenverarbeitung"*. PhD thesis, TH Aachen, 1972.
- [13] J. B. Bryan. "International status of thermal error research". *Annals of the CIRP*, 16(1):203–215, 1968.
- [14] J. B. Bryan. "Closer tolerances — economic sense". *Annals of the CIRP*, 19(2):115–120, 1971.
- [15] J. B. Bryan. "The Abbé principle revisited: An updated interpretation". *Precision Engineering*, 1(3):129–132, 1979.
- [16] J. B. Bryan. "International status of thermal error research (1990)". *Annals of the CIRP*, 39(2):645–656, 1990.
- [17] J. B. Bryan and J. W. Pearson. "Machine tool metrology". Technical Report UCRL-71164, Lawrence Livermore National Laboratory, P.O. Box 808, Livermore, CA 94550, 1968.
- [18] J. B. Bryan and P. Vanherck. "Unification of terminology concerning the error motion of axes of rotation". *Annals of the CIRP*, 24(2):555–562, 1975.
- [19] K. Busch, H. Kunzmann, and F. Wäldele. "Numerical error correction of a coordinate measuring machine". In *Proceedings International Symposium on Metrology and Quality Control in Production*, pages 278–282, 1984.
- [20] K. Busch, H. Kunzmann, and F. Wäldele. "Calibration of coordinate measuring machines". *Precision Engineering*, 7(3):139–144, 1985.

- [21] C. Butler. "An investigation into the performance of probes on coordinate measuring machines. *Industrial Metrology*, 1(2):59-70, 1991.
- [22] A. Camera, M. Favareto, and F. D'Aprile. "Analysis of the thermal behaviour of a machine tool table using the finite element method". *Annals of the CIRP*, 25(1):297-300, 1976.
- [23] H. S. Carslaw and J. C. Jaeger. "*Conduction of heat in solids*". Clarendon press, Oxford, 1959.
- [24] P. Y. Chao, P. M. Ferreira, and C. R. Liu. "Applications of GMDH-type modeling in manufacturing". *Journal of Manufacturing Systems*, 7(3):241-253, 1990.
- [25] C. Chatfield and A. J. Collins. "*Introduction to multivariate analysis*". Chapman and Hall, London, 1980.
- [26] Comité International des Poids et Mesures. "Recommendation 1 (CI-1981)". *Metrologia*, 18(1):44, 1982.
- [27] ASME B5 TC52 Committee. "Methods for performance evaluation of computer numerically controlled machining centers and work centers (draft standard version 3.0)". The American Society of Mechanical Engineers, New York, USA, 1989.
- [28] P. C. Cresto, M. Di Ciommo, T. Kancheva, D. Marques, V. Mudronja, and S. Sartori. "A method for the identification and correction of thermal deformations in 3-d CMMs". *Measurement*, 9(1):38-43, 1991.
- [29] H. M. de Ruiter, H. A. Spaan, and J. A. Soons. "Real-time parametrische software compensatie". Draft of International Patent Application; Internal Philips Report No. GK 76226, 1993.
- [30] Dea. "Mill retrofit for CMM". *European Machining*, (2):59, 1992.
- [31] D. B. DeBra and J. B. Bryan. "Shower and high pressure oil temperature control". *Annals of the CIRP*, 35(1):359-363, 1986.
- [32] J. Denavit and R. S. Hartenberg. "A kinematic notation for lower pair mechanisms based on matrices". *ASME, Journal of Applied Mechanics*, 77(2):215-221, June 1955.

- [33] M. A. Donmez. "A General methodology for machine tool accuracy: theory, application and implementation". PhD thesis, Purdue university, 1985.
- [34] M. A. Donmez. "Progress report of the quality in automation project for FY90". Technical Report NISTIR 4536, National Institute of Standards and Technology, Gaithersburg, MD 20899, 1991.
- [35] M. A. Donmez, D. S. Blomquist, R. J. Hocken, C. R. Liu, and M. M. Barash. "A general methodology for machine tool accuracy enhancement by error compensation". *Precision Engineering*, 8(4):187-196, 1986.
- [36] M. A. Donmez, C. R. Liu, M. Barash, and F. Mirski. "Statistical analysis of positioning error of a CNC milling machine". *Journal of Manufacturing Systems*, 1(1):33-41, 1986.
- [37] N. A. Duffie and S. J. Malmberg. "Error diagnosis and compensation using kinematic models and position error data". *Annals of the CIRP*, 36(1):355-358, 1987.
- [38] N. A. Duffie and S. M. Yang. "Generation of parametric kinematic error-correction function from volumetric error measurements". *Annals of the CIRP*, 34(1):435-438, 1985.
- [39] P. Dufour and R. Groppetti. "Computer aided accuracy improvement in large NC machine tools". In *MTDR Conference Proceedings*, pages 611-617, 1980.
- [40] K. F. Eman, B. T. Wu, and M. F. DeVries. "A generalized geometric error model for multi-axis machines". *Annals of the CIRP*, 36(1):253-256, 1987.
- [41] C. Ericson. "Machine alignment — The first step towards product accuracy". *ASTME*, Tech. Paper MM66-171, 1966.
- [42] L. J. Everett, M. Driels, and B. W. Mooring. "Kinematic modelling for robot calibration". In *Proceedings of the 1987 IEEE International Conference on Robotics and Automation*, pages 183-189, 1987.

- [43] L. J. Everett and A. H. Suryohadiprojo. "A study of kinematic models for forward calibration of manipulators". In *Proceedings of the 1988 IEEE International Conference on Robotics and Automation*, pages 798–800, 1988.
- [44] P. M. Ferreira and C. R. Liu. "A contribution to the analysis and compensation of the geometric error of a machine center". *Annals of the CIRP*, 35(1):259–262, 1986.
- [45] P. M. Ferreira and C. R. Liu. "An analytical quadratic model for the geometric error of a machine tool". *Journal of Manufacturing Systems*, 5(1):51–63, 1986.
- [46] P. M. Ferreira and C. R. Liu. "A method for estimating and compensating quasistatic errors of machine tools". In *The winter annual meeting of the American Society of Mechanical Engineers, PED-Volume 27*, pages 205–229, 1987.
- [47] D. French and S. H. Humphries. "Compensation for the backlash and alignment errors in a numerically controlled machine tool by a digital computer programme". In *MTDR Conference Proceedings*, pages 707–726, 1967.
- [48] H. Golücke. "*Ein Beitrag zur meßtechnischen Ermittlung und analytischen Beschreibung systematischer Anteile der Arbeitsunsicherheit von Fertigungseinrichtungen*". PhD thesis, RWTH Aachen, 1976.
- [49] G. Hermann. "Process intermittent measurement of tools and work-pieces". *Journal of Manufacturing Systems*, 4(1):41–49, 1985.
- [50] R. J. Hocken, editor. *Machine Tool Accuracy*, volume 5 of *Technology of machine tools: A survey of the state of the art by the Machine Tool Task Force*. Lawrence Livermore National Laboratory, University of California, P.O. Box 808, Livermore, CA 94550, 1980.
- [51] R. J. Hocken et al. "Three dimensional metrology". *Annals of the CIRP*, 26(2):403–408, 1977.

- [52] T. M. Hoffer and W. Fischer. "Abnahme von Werkzeugmaschinen mit einem Laser- Meßsystem, Teil I". *Feinwerktechnik & Messtechnik*, 85(6):229–284, 1977.
- [53] T. M. Hoffer and W. Fischer. "Abnahme von Werkzeugmaschinen mit einem Laser- Meßsystem, Teil II". *Feinwerktechnik & Messtechnik*, 85(7):343–353, 1977.
- [54] T. Jarman and A. Traylor. "Performance characteristics of touch trigger probes". In *Precision metrology with coordinate measurement systems*. SME, 1990.
- [55] J. Jedrzejewski, J. Kaczmarek, Z. Kowal, and Z. Winiarski. "Numerical optimization of thermal behaviour of machine tools". *CIRP Annals*, 39(1):379–382, 1990.
- [56] F. Jouy. "Theoretical modelisation and experimental identification of the geometrical parameters of coordinate measuring machines by measuring a multi-directed bar". *Annals of the CIRP*, 35(1):393–396, 1986.
- [57] C. P. Keferstein et al. "Neue Meß- und Prüfkonzepte mit einem Präzisionsroboter". *VDI Berichte*, 836:139–152, 1990.
- [58] W. Knapp. "Test of the three-dimensional uncertainty of machine tools and measuring machines and its relation to the machine errors". *Annals of the CIRP*, 32(1):459–464, 1983.
- [59] F. Koenigsberger. "Preface to the eighth edition of "Testing machine tools" by G. Schlesinger". Pergamon Press, Oxford, 1977.
- [60] J. P. Kruth, P. Vanherck, and L. De Jonge. "A self-calibration method and a software error correction for three dimensional coordinate measuring machines". In *Proceedings International Symposium on Metrology and Quality Control in Production*, pages 100–115, 1992.
- [61] A. M. Kshirsagar. "A Course in Linear Models". Marcel Dekker Inc, New York, 1981.
- [62] H. Kunzmann, E. Trapet, and F. Wäldele. "A uniform concept for calibration, acceptance test, and periodic inspection of coordinate measuring

- machines using reference objects". *Annals of the CIRP*, 39(1):561–564, 1990.
- [63] A. Kurtoglu. "The accuracy improvement of machine tools". *Annals of the CIRP*, 39(1):417–419, 1990.
- [64] D. L. Leete. "Automatic compensation of alignment errors in machine tools". *International Journal of Machine Tool Design and Research*, 1:293–324, 1961.
- [65] W. J. Love and A. J. Scarr. "The determination of the volumetric accuracy of multi axis machines". In *MTDR Conference Proceedings*, pages 307–315, 1973.
- [66] K. V. Mardia, J. T. Kent, and J. M. Bibby. "*Multivariate analysis*". Academic Press, London, 1979.
- [67] T. Masuda and M. Kajitani. "An automatic calibration system for angular encoders". *Precision Engineering*, 11(2):95–100, 1989.
- [68] "386 Matlab, version 3.5f", 1990.
- [69] M. Matsuo, T. Yasui, T. Inamura, and M. Matsumura. "High-speed test of thermal effects for a machine-tool structure based on modal analysis". *Precision Engineering*, 8(2):72–78, 1986.
- [70] E. R. McClure. "Significance of thermal effects in manufacturing and metrology". *Annals of the CIRP*, 15(1):61–66, 1967.
- [71] E. R. McClure. "*Manufacturing accuracy through the control of thermal effects*". PhD thesis, Lawrence Livermore National Laboratory, 1969.
- [72] P. A. McKeown. "Why precision?". *Precision Engineering*, 1(2):59–59, 1979.
- [73] P. A. McKeown. "High precision manufacturing and the British economy". *Proceedings Institute of Mechanical Engineers*, 200(B3):147–165, 1986.
- [74] P. A. McKeown. "The role of precision engineering in manufacturing of the future". *Annals of the CIRP*, 36(2):495–501, 1987.

- [75] CIRP STC Me working party on 3DU. "A proposal for defining and specifying the dimensional uncertainty of multi-axis measuring machines". *Annals of the CIRP*, 27(2):623-630, 1978.
- [76] T. J. Mitchell. "an algorithm for the construction of "D-optimal" experimental designs". *Technometrics*, 16(2):203-210, 1974.
- [77] D. C. Montgomery and E. A. Peck. "*Introduction to linear Regression Analysis*". John Wiley & Sons, New York, 1982.
- [78] G. E. Myers. "*Analytical methods in conduction heat transfer*". Genium publishing, 1987.
- [79] H. J. Neumann. "Genauigkeitskenngrößen für Drehtische auf Koordinatenmeßgeräten". *Qualitätstechnik*, 33(10):523-528, 1988.
- [80] K. Okushima, Y. Kakino, and A. Higashimoto. "Compensation of thermal displacement by coordinate system correction". *Annals of the CIRP*, 24(1):327-331, 1975.
- [81] R. P. Paul. "*Robot Manipulators: Mathematics, Programming and Control*". MIT Press, Cambridge, MA, 1981.
- [82] Perdue University, School of Industrial Engineering. "The science of and advanced technology for cost-effective manufacture of high precision products", 1983. ONR contract No. 83-K-0385.
- [83] J. Peters. "Metrology in design and manufacturing — facts and trends". *Annals of the CIRP*, 26(2):415-421, 1977.
- [84] T. Pfeifer, M. Bamback, and A. Fürst. "Ermittlung der Meßunsicherheit von 3-D-Tastsystemen". *Technisches Messen*, (2):47-52, 1979.
- [85] T. Pfeifer, M. Bamback, and A. Fürst. "Ermittlung der Meßunsicherheit von 3-D-Tastsystemen". *Technisches Messen*, (4):161-169, 1979.
- [86] V. T. Portman. "Error summation in the analytical calculation of lathe accuracy". *Machines & Tooling*, 51(1):7-10, 1977.
- [87] E. Rabiniwicz. "Friction fluctuations". In *Proceedings of the NATO advanced study institute on fundamentals of friction*, pages 25-34. Kluwer academic publishers, The Netherlands, 1992.

- [88] S. Sartori. "A method for the identification and correction of thermal deformations in a three coordinate measuring machine". *VDI Berichte*, (761):185–192, 1989.
- [89] S. Sartori, P.C. Cresto, M. Di Ciommo, and T.K. Kancheva. "A way to improve the accuracy of a co-ordinate measuring machine". *Measurement*, 6(2):50–54, 1988.
- [90] "SAS STAT, Release 6.03", 1988.
- [91] T. Sata et al. "Development of machine tool structural analysis program (MASAP)". *Annals of the CIRP*, 25(1):287–290, 1976.
- [92] T. Sata, Y. Takeuchi, and N. Okubo. "Improvement of working accuracy of a machining center by computer control compensation". In *MTDR Conference Proceedings*, volume 17, pages 93–99, 1976.
- [93] T. Sata, Y. Takeuchi, N. Sato, and N. Okubo. "Analysis of thermal deformation of machine tool structure and its application". In *MTDR Conference Proceedings*, pages 275–280, 1973.
- [94] P. H. Schellekens et al. "Geometric error modelling of machine tools". In *Development of Methods for the Numerical Error Correction of Machine Tools*. Bureau Communautaire de Référence, 3320/1/0/160/89/8-BCR-NL, Brussels, 1991.
- [95] P. H. Schellekens et al. "Modelling the thermal behaviour of machine tools". In *Development of Methods for the Numerical Error Correction of Machine Tools*. Bureau Communautaire de Référence, 3320/1/0/160/89/8-BCR- NL, Brussels, 1992.
- [96] P. H. Schellekens et al. "Final project report". In *Development of Methods for the Numerical Error Correction of Machine Tools*. Bureau Communautaire de Référence, 3320/1/0/160/89/8-BCR- NL, Brussels, 1993.
- [97] G. Schlesinger. *Inspection Tests on Machine Tools*. Machinery Publishing Co., Ltd., London, 1932.
- [98] R. Schultschik. "Geometrische Fehler in Werkzeugmaschinenstrukturen". *Annals of the CIRP*, 24(1):361–366, 1975.

- [99] R. Schultschik. "The components of the volumetric accuracy". *Annals of the CIRP*, 26(1):223–228, 1977.
- [100] R. Schultschik. "Das volumetrische Fehlerverhalten von Mehrkoordinaten-Werkzeugmaschinen, Grundlagen und Fehlergrößen". *Werkstatt und Betrieb*, 112(2):117–121, 1979.
- [101] R. Schultschik. "The accuracy of machine tools under load conditions". *Annals of the CIRP*, 28(1):339–344, 1979.
- [102] G. A. Seber. "*Linear Regression Analysis*". John Wiley & Sons, New York, 1977.
- [103] Y. C. Shin and Y. Wei. "A statistical analysis of positional errors of a multiaxis machine tool". *Precision Engineering*, 14(3):139–146, 1992.
- [104] P. L. Smith. "Splines as a useful and convenient statistical tool". *The American Statistician*, 33(2):57–62, 1979.
- [105] J. A. Soons. "Letter to the editor". *Precision Engineering*, 15(1):44–45, 1993.
- [106] J. A. Soons and P. H. Schellekens. "The efficiency of artifact based procedures to calibrate coordinate measuring machines". *ASPE Annual Conference*, 4:37–42, 1991.
- [107] J. A. Soons and P. H. Schellekens. "On the calibration of multi-axis machines using distance measurements". In *Proceedings International Symposium on Metrology and Quality Control in Production*, pages 321–340, 1992.
- [108] J. A. Soons, F. C. Theuws, and P. H. Schellekens. "Modelling the errors of multi-axis machines: A general methodology". *Precision Engineering*, 14(1):5–19, 1992.
- [109] H. A. Spaan. "*Software error compensation of machine tools*". PhD thesis, Eindhoven University of Technology, 1994. In preparation.
- [110] R. C. St. John and N. R. Draper. "D-optimality for regression designs: A review". *Technometrics*, 17(1):15–23, 1975.

- [111] D. M. Stein and W. G. Hunter. "Experimental design: Review and comment". *Technometrics*, 26(2):71–97, 1984.
- [112] H. W. Stone and A. C. Sanderson. "A prototype arm signature identification system". In *Proceedings of the 1987 IEEE International Conference on Robotics and Automation*, pages 175–182, 1987.
- [113] N. Taniguchi. "Current status in, and future trends of, ultraprecision machining and ultrafine materials processing". *Annals of the CIRP*, 32(2):1–10, 1983.
- [114] J. M. Teeuwsen, J. A. Soons, and P. H. Schellekens. "A general method for error description of emms using polynomial fitting procedures". *Annals of the CIRP*, 38(1):505–510, 1989.
- [115] F. C. Theuws. "*Enhancement of Machine Tool Accuracy: Theory and Implementation*". PhD thesis, Eindhoven University of Technology, 1991.
- [116] S. P. Timoshenko and J. N. Goodier. "*Theory of Elasticity*". McGraw-Hill Book Company, New York, NY, 1970.
- [117] J. Tlustý. "Systems and methods for testing machine tools". *Microtecnic*, 13(4):162–178, 1959.
- [118] J. Tlustý, editor. *Machine tool mechanics*, volume 3 of *Technology of machine tools: A survey of the state of the art by the Machine Tool Task Force*. Lawrence Livermore National Laboratory, University of California, P.O. Box 808, Livermore, CA 94550, 1980.
- [119] J. Tlustý. "*Testing of accuracy of NC machine tools*", volume 5 of *Technology of machine tools: A survey of the state of the art by the Machine Tool Task Force*. Lawrence Livermore National Laboratory, University of California, P.O. Box 808, Livermore, CA 94550, 1980.
- [120] J. Tlustý. "Comments on the article by A. Kurtoglu". *Annals of the CIRP*, 39(2):772, 1990.
- [121] J. Tlustý and F. Koenigsberger. "Specifications and tests of metal cutting machine tools". Technical report, UMIST, Manchester, 1970.

- [122] J. Tlustý and F. Koenigsberger. "New concepts of machine tool accuracy". *Annals of the CIRP*, 19(1):261–273, 1971.
- [123] E. Trapet and F. Wäldele. "Koordinatenmeßgeräte in der Fertigung — Temperatureinflüsse und erreichbare Meßunsicherheit". *VDI Berichte*, (751):209–227, 1989.
- [124] VDI/VDE 2617. "*Characteristic Parameters and their Checking, Components of Measurement Deviation of the Machine*", volume 3 of *Accuracy of Co-ordinate Measuring Machines*. VDI-Verlag, Düsseldorf, Germany, 1991.
- [125] VDI/VDE 2617. "*Characteristic Parameters and their Checking, Rotary Tables on Coordinate Measuring Machines*", volume 4 of *Accuracy of Co-ordinate Measuring Machines*. VDI-Verlag, Düsseldorf, Germany, 1991.
- [126] W. K. Veitschegger and C. Wu. "Robot accuracy based on kinematics". *IEEE Journal of Robotics and Automation*, RA-2(3):171–179, 1986.
- [127] R. Venugopal. "*Thermal effects of the accuracy of numerically controlled machine tools*". PhD thesis, Purdue university, 1985.
- [128] M. Weck and R. Eckstein. "Meßtechniken zur Beurteilung von Werkzeugmaschinen". *Industrie-Anzeiger*, 107(72):154–157, 1985.
- [129] M. Weck and G. Petuelli. "*Static and dynamic behavior of metal-cutting machine tools*, volume 5 of *Technology of machine tools: A survey of the state of the art by the Machine Tool Task Force*. Lawrence Livermore National Laboratory, University of California, P.O. Box 808, Livermore, CA 94550, 1980.
- [130] M. Weck and L. Zangs. "Computing the thermal behaviour of machine tools using the finite element method — possibilities and limitations". pages 261–273, 1975.
- [131] R. Weill and B. Shani. "Assessment of accuracy of robots in relation with geometric tolerances in robot links". *Annals of the CIRP*, 40(1):395–399, 1991.

- [132] W. J. Welch. "Branch-and-bound search for experimental designs based on D optimality and other criteria". *Technometrics*, 24(1):41–48, 1982.
- [133] W. J. Welch. "A mean squared error criterion for the design of experiments". *Biometrika*, 70(1):205–213, 1983.
- [134] W. J. Welch. "Computer-aided design of experiments for response estimation". *Technometrics*, 26(3):217–224, 1984.
- [135] West European Calibration Cooperation. "Guidelines for the expression of the uncertainty of measurement in calibrations". Technical report, WECC Document 19-1990, 1990.
- [136] West European Calibration Cooperation. "The certification of components using co-ordinate measuring machines; Requirements for CMMs in accredited laboratories within the WECC". Technical report, WECC CMM expert group, version 2.0, 1992.
- [137] S. Wold. "Spline functions in data analysis". *Technometrics*, 16(1):1–11, 1974.
- [138] G. S. Wong and F. Koenigsberger. "Automatic correction of alignment errors in machine tools". *International Journal of Machine Tool Design and Research*, 6(4):171–197, 1966.
- [139] Y. Yoshida and F. Honda. "Thermal deformation of a vertical milling machine', Part ii'. In *MTDR Conference Proceedings*, pages 83–96, 1967.
- [140] Y. Yoshida and F. Honda. "Thermal deformations of machine tool structure — the bed of a lathe". *Annals of the CIRP*, 15(1):337–344, 1967.
- [141] Y. Yoshida, F. Honda, and M. Kubota. "Thermal deformation of a knee-type vertical milling machine". In *MTDR Conference Proceedings*, pages 117–134, 1964.
- [142] L. Zangs. "*Berechnung des thermischen Verhaltens von Werkzeugmaschinen*". PhD thesis, TH Aachen, 1975.
- [143] Zeiss. *Calibration and Inspection Report, UMC550 70971*, 1990.
- [144] G. Zhang et al. "Error compensation of coordinate measuring machines". *Annals of the CIRP*, 34(1):445–448, 1985.

- [145] G. Zhang et al. "A displacement method for machine geometry calibration". *Annals of the CIRP*, 37(1):515–518, 1988.
- [146] J. Ziegert and P. Datsseris. "Basic considerations for robot calibration". In *Proceedings of the 1988 IEEE International Conference on Robotics and Automation*, pages 932–938, 1988.

A

Uncertainty analysis

In this Appendix, the kinematic model is used to evaluate the uncertainty of a measured or realized end-effector location, given the uncertainty of the parametric errors. Note that since the kinematic model is a known mathematical entity, the propagation of the parametric errors to the errors in the relative location of the end-effector is fully defined by this model. As an example, only the errors in a realized or measured position are considered. Extension of the results to problems involving orientation is relatively straightforward.

A.1 Introduction

In the international vocabulary of basic and general terms in metrology [9], uncertainty is defined as an estimate characterizing the range of values within which the true value of a measurand (quantity to be measured) lies. This is after corrections have been made for all known systematic errors [135]. In accordance with this definition, the uncertainty of handling and machining operations will be defined as the range within which the realized task lies. In this Appendix we will consider uncertainty as a random variable, even if it is known to have (unknown) systematic components. This treatment is consistent with the approach recommended by the Comité International des Poids et Mesures [26] as described in the WECC-guideline on the expression of the uncertainty of measurement in calibrations [135].

Some applications, for which an uncertainty analysis is either useful or required, are:

- **Measurement.** The result of a measurement has to be accompanied by a statement of its uncertainty. For CMMs the accuracy of a measurement is usually derived from the length measurement uncertainty of the machine. The latter measure describes the uncertainty of a length measured in an arbitrary location in the machine workspace. As stated in Chapter 1, the use of coordinate measuring machines to certify components requires a more refined error analysis. Here the propagation of the parametric errors to the errors of a measurement task has to be evaluated. The respective uncertainty of the parametric errors is due to the uncertainty in their measurement during calibration (e.g. due to the limited accuracy of the equipment used), the limited sampling density during calibration, and changes in the machine structure after calibration (e.g. due to environmental effects and wear). Another typical uncertainty is caused by the uncertainty in the coefficient of thermal expansion of both machine components and workpiece.
- **Model validation.** The validation of models that describe the accuracy of a multi-axis machine require an uncertainty analysis to determine whether the difference between observed and modeled errors can be explained from the uncertainty of the parametric errors. A statistically significant difference may be due to errors not included in the model (e.g. certain finite stiffness effects). A related application is statistical process control, where it is necessary to determine whether a certain trend in the quality of realized products can be explained by the uncertainty of the machine (or that of its error model) or is due to a significant change in the errors of the machine.
- **Design.** The tolerance of machine components can be determined such that the errors in a family of tasks do not exceed a certain error bound with certain probability.
- **Compact error models.** Especially geometric errors often show an irregular dependency on the position of the respective joint. This leads to complicated parametric error models that limit the practical use of

the machine error model. A more simple error model can be obtained by expressing a parametric error as the sum of a systematic trend (e.g. as determined by a best fit line) and a random variable that describes the irregular remainder (even though it is known to be largely systematic in nature). Thus a simplified error model is obtained that contains fewer error parameters. This is obviously a compromise between ease of use and increased model uncertainty. These models can be used to quickly estimate the accuracy of a machine task, or to select the location where a task can be performed with the highest accuracy.

- **'Random' errors.** As stated in the introduction of this thesis, certain systematic errors are perceived as random due to limited information about the status of machine and workpiece. Dynamic errors, backlash, cutting force variations, and errors due to relatively fast thermal fluctuations are difficult to assess, and therefore usually have to be treated as random variables. This is again a compromise between the costs of sensors and modelling versus uncertainty about the accuracy of the machine.

A.2 Uncertainty of a measured or realized position

The first step in the uncertainty analysis of a task is the uncertainty analysis of end-effector locations that comprise the task. In this section, the known kinematic model is used to calculate the uncertainty of a relative end-effector position from the uncertainty of the parametric errors. With respect to the errors \underline{e}_S in a realized or measured end-effector position S , the kinematic model derived in Section 2.3 can be summarized as:

$$\underline{e}_S = F \underline{E} \quad (\text{A.1})$$

Here the $p \times 1$ vector \underline{E} contains the p parametric errors at the analysed position. Its 6×1 subvectors contain the parametric errors ${}_{k-1}\underline{E}_k$ in the relative location of successive frames. The effect of the parametric errors on the position error of the end-effector is described by the known $3 \times p$ matrix

F . Its 3×6 submatrices contain the lower three rows of the matrices ${}_{k-1}F_k$ described in Section 2.3 (i.e. the components that determine the position errors of the end-effector). Since the above model is linear in the parametric errors, the expected value $E\{\underline{e}_S\}$ and the 3×3 covariance matrix $\text{Cov}\{\underline{e}_S\}$ of \underline{e}_S are:

$$E\{\underline{e}_S\} = F E\{\underline{E}\} \quad (\text{A.2})$$

$$\text{Cov}\{\underline{e}_S\} = E\{(\underline{e}_S - E\{\underline{e}_S\})(\underline{e}_S - E\{\underline{e}_S\})^T\} \quad (\text{A.3})$$

$$= F \text{Cov}\{\underline{E}\} F^T \quad (\text{A.4})$$

In equation A.4, $\text{Cov}\{\underline{E}\}$ represents the $p \times p$ covariance matrix of the parametric errors at location S . The formulation of this covariance matrix, or alternatively that of the position error, is a major problem that requires much skill and insight in the errors of a machine. Numerous examples can be cited where this matrix has been incorrectly specified due to faulty assumptions on the joint distribution of the parametric errors. One of the most notorious assumptions is that the various parametric errors are mutually independent. Although in case of many parametric errors, results obtained under this assumption are practically useful (e.g. regarding the position uncertainty of the end-effector), it must be noted that there are several mechanisms that cause correlated parametric errors. For example, if an instrument is used to measure several parametric errors, the (unknown) systematic error of the instrument causes the uncertainty of these measurements to be correlated. Changes in the parametric errors due to a change in the thermal environment of the machine are generally correlated. Also dynamic and backlash errors usually affect several parametric errors in a correlated manner. Finally, the straightness and angular errors of a joint are often correlated.

In case the position errors in the various coordinate directions are strongly correlated, e.g. due to the presence of large angular errors [105], it may be useful to apply a principle components analysis. Here the original correlated coordinates are transformed to a new set of uncorrelated coordinates called principle components [25]. The new coordinates are derived in decreasing order of importance so that, for example, the first coordinate direction describes the direction of the largest uncertainty. Thus the new coordinate axes can be interpreted as the main axes of the uncertainty zone.

Since the covariance matrix $\text{Cov}\{\underline{e}_S\}$ is symmetric, it can be expressed as:

$$\text{Cov}\{\underline{e}_S\} = \Gamma \Lambda \Gamma^T \tag{A.5}$$

Here Λ is a diagonal matrix with the (real) eigenvalues $\lambda_1 \geq \lambda_2 \geq \lambda_3 \geq 0$ of $\text{Cov}\{\underline{e}_S\}$ in decreasing order on its diagonal. The columns of the orthogonal matrix Γ contain the corresponding eigenvectors. Combining Equations A.5 and A.4 yields:

$$E \{ (\underline{e}_S - E\{\underline{e}_S\}) (\underline{e}_S - E\{\underline{e}_S\})^T \} = \Gamma \Lambda \Gamma^T \Rightarrow \tag{A.6}$$

$$E \{ \Gamma^T (\underline{e}_S - E\{\underline{e}_S\}) (\underline{e}_S - E\{\underline{e}_S\})^T \Gamma \} = \Lambda \Rightarrow \tag{A.7}$$

$$E \{ {}_{pr}\underline{e}_S {}_{pr}\underline{e}_S^T \} = \Lambda \tag{A.8}$$

Where:

$${}_{pr}\underline{e}_S = \Gamma^T (\underline{e}_S - E\{\underline{e}_S\}) \tag{A.9}$$

Thus the principle coordinates in ${}_{pr}\underline{e}_S$ have zero mean, are uncorrelated, and their variance equals the respective eigenvalues of the covariance matrix $\text{Cov}\{\underline{e}_S\}$. According to Equation A.9, they can be obtained from the original position error by a translation followed by an (orthogonal) rotation Γ^T . Hence, the rows of matrix Γ^T (i.e. the eigenvectors of $\text{Cov}\{\underline{e}_S\}$) describe the main axes of the uncertainty zone. The eigenvector corresponding to the largest eigenvalue points in the direction of the largest uncertainty.

Hitherto, the presented results are valid for any distribution of the parametric errors. To further the analysis, it will be assumed that the errors in the position of the end-effector have a multivariate normal distribution, i.e. that any linear compound of \underline{e}_S has an univariate normal distribution [66]. Since \underline{e}_S itself is a known linear combination of the parametric errors, a sufficient condition for the above statement is that each nontrivial parametric error is normally distributed.

Although this may sound very restrictive, the derived results are quite robust, and thus useful, even when the underlying assumptions are not strictly satisfied. Note that the position error of the end-effector is a linear combination of many parametric errors, so one can appeal to the central limit-theorems to support the above statement. However there are cases where normality cannot be assumed. Donmez [36], for example, reports a significant deviation

from normality in the positioning errors of a NC machine tool due to backlash. Also, if only upper and lower limits can be estimated of an influence quantity (e.g. limits of errors of a measuring instrument used to estimate an error, temperature range), the WECC guideline on the determination of uncertainty [135] recommends to treat the quantity as being uniformly distributed within these limits.

Assuming that the position errors have a multivariate normal distribution, the probability density function of \underline{e}_S is given by [66]:

$$f(\underline{e}_S) = \frac{1}{\sqrt{|2\pi \text{Cov}\{\underline{e}_S\}|}} \exp\left(-\frac{1}{2} (\underline{e}_S - E\{\underline{e}_S\})^T \text{Cov}\{\underline{e}_S\}^{-1} (\underline{e}_S - E\{\underline{e}_S\})\right) \tag{A.10}$$

By setting the exponent of Equation A.10 equal to some constant, it can be seen that the probability of \underline{e}_S has constant density on ellipsoids of the form:

$$(\underline{e}_S - E\{\underline{e}_S\})^T \text{Cov}\{\underline{e}_S\}^{-1} (\underline{e}_S - E\{\underline{e}_S\}) = c^2 \tag{A.11}$$

These ellipsoids are centred at the expected value $E\{\underline{e}_S\} = FE\{\underline{E}\}$ of the position errors \underline{e}_S . In terms of the principle components contained in ${}_{pr}\underline{e}_S$ Equation A.11 becomes:

$${}_{pr}\underline{e}_S^T \Lambda {}_{pr}\underline{e}_S = c^2 \Rightarrow \tag{A.12}$$

$$\frac{{}_{pr}e_{S_x}^2}{\lambda_1} + \frac{{}_{pr}e_{S_y}^2}{\lambda_2} + \frac{{}_{pr}e_{S_z}^2}{\lambda_3} = c^2 \tag{A.13}$$

Thus the coordinates of ${}_{pr}\underline{e}_S$ describe the axes of the ellipsoid (See Figure A.1). Note that Equation A.13 contains the sum of uncorrelated normally distributed squared variables normalized for their respective variance. Thus it follows a Chi-squared distribution whose degrees of freedom equals the number of nonzero eigenvalues ν of $\text{Cov}\{\underline{e}_S\}$ [66]. Hence the confidence region of \underline{e}_S with probability α is described by:

$$\frac{{}_{pr}e_{S_x}^2}{\lambda_1} + \frac{{}_{pr}e_{S_y}^2}{\lambda_2} + \frac{{}_{pr}e_{S_z}^2}{\lambda_3} \leq 1 - \chi_{\alpha,\nu}^2 \Rightarrow \tag{A.14}$$

$$(\underline{e}_S - E\{\underline{e}_S\})^T \text{Cov}\{\underline{e}_S\}^{-1} (\underline{e}_S - E\{\underline{e}_S\}) \leq 1 - \chi_{\alpha,\nu}^2 \tag{A.15}$$

Where $\chi_{\alpha,\nu}^2$ is the upper 100α percentage point of the Chi-squared distribution with ν degrees of freedom.

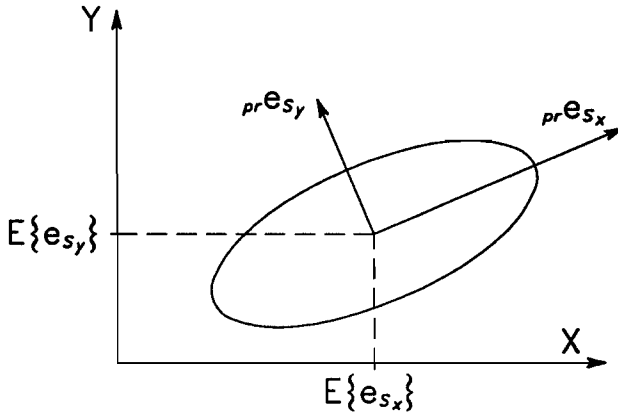


Figure A.1: Confidence region of normally distributed position errors

Analysis of the error propagation from the end-effector trajectory to the machine task is highly task dependent and complicated. Only for relatively simple tasks (e.g. length measurements) it is possible to derive explicit analytical expressions (see Chapter 4). Often, additional error sources need to be considered. Furthermore, the 'random' errors in different locations of the trajectory may be correlated (e.g. due to the uncertainty in the expansion coefficient of a scale), which complicates the analysis. As stated in Chapter 1, analysis of the accuracy of executed tasks is beyond the scope of this thesis.

B

Properties of parametric errors

Due to the relative nature of tasks executed by multi-axis machines, it is not required to completely describe each parametric error identified in Chapter 2. As stated in the introduction, most parametric errors affect the accuracy of a task only through their variations not through their absolute values. In this appendix, the nature of these simplifications is discussed. Throughout this discussion it is important to realize that the various parametric errors are mathematical entities whose sole purpose is to describe the errors in the relative trajectory of the end-effector. If certain aspects of different parametric errors can be lumped together without affecting the completeness of the model, this process yields a simpler model and may even be required to ensure their identification from observed errors in the end-effector trajectory.

For a machine consisting of $m + n$ joints, the kinematic error model described in Chapter 2 contains $m + n + 1$ coordinate frames. Between each two successive coordinate frames there is one kinematic element. The total number of parametric errors describing the relative location of these coordinate frames equals $6 \times (m + n)$. The geometry of the end-effector is described using an extra coordinate frame, yielding 6 additional parametric errors. 12 parametric errors are further required to describe the relative location of the workpiece reference frame and the workpiece deformation.

First, we consider the case where all parametric errors have a constant value. When all joints are at home position, these errors result in certain errors in

the location of the tool frame relative to the reference frame. Even though the parametric errors are constant, the errors in the relative location of the end-effector change due to movement of the joints. The respective variation due to movement of a prismatic joint is determined by the *combined* values of parametric errors that affect the orientation of the joint axis relative to the reference frame (excluding those that only result in angular errors around the joint axis). All other errors are already included in the initial location. Similarly, the error variation due to movement of a revolute joint is determined by the *combined* values of parametric errors that affect the position and orientation of the joint axis relative to the reference (again excluding those that only affect angular errors around the joint axis or translation errors in the direction of the joint axis). Note that the effective arm of the revolute joint is determined by the actual relative position of tool frame and joint axis. This arm is known if both the errors in the location of the joint axis and those in the initial location of the tool frame are known.

An important concept in the analysis of multi-axis machines is, that from measured errors in the location of the end-effector relative to the reference it is not possible nor required to estimate the individual value of each (constant) parametric error. Hence their combined contribution can be assigned to an arbitrary assembly of parametric errors, provided the above errors in the relative location of the end-effector are properly described. For a machine consisting of $n + m$ joints, a possible choice is defined by the following rules:

- There are 6 (constant) parametric errors in the location of the reference frame wr relative to frame bm attached to the machine table. These errors describe the location of the end-effector frame relative to the reference frame when all other parametric errors described below equal zero, for all positions of the joints. Hence they describe the location of the reference relative to the coordinate frame spanned by the machine axes, i.e. the location of the reference relative to the machine.
- For each joint a maximum of two angular parametric errors have a constant value. These errors describe the orientation of the joint axis relative to two different preceding joints in the kinematic chain from frame bm . If the preceding joint axis is nominally parallel, both parametric

errors are defined relative to this joint axis. These errors are usually referred to as squareness and parallelism errors.

- For each revolute joint a maximum of two additional translation parametric errors have a constant value. These errors describe the radial position of its joint axis relative to the position of a preceding revolute joint in the kinematic chain from frame bm .
- There are 6 (constant) parametric errors in the location of the tool frame tl relative to frame an . These errors describe the location of the tool frame tl relative to the reference frame wr when all joints are at home position. Note that errors in the effective arm of all revolute joints are included in these parametric errors.
- There are 6 (constant) parametric errors in the location of the workpiece frame wf relative to frame wr . These errors describe the workpiece deformation during the executed task.
- All other parametric errors equal zero.

For a machine consisting of three prismatic joints, the above rules require $3 + 6 + 6 + 6$ nonzero parametric errors. Three parametric errors are used to describe the relative orientation of the machine axes. Six errors describe the location of the reference. Six errors describe the geometry of the end-effector, and a further six errors are required to describe the deformation of the workpiece. If this machine is augmented with a revolute joint, e.g. a rotary table, two additional parametric errors are required to describe the orientation of its axis relative to two other joint axes. Since there is only one revolute joint, errors in the position of the joint can be described by errors in the dimensions of the end-effector or errors in the position of the reference. Note that the error in the initial angle of the joint (e.g. due to an encoder offset) is described by either an error in the relative location of the reference frame, or an error in the relative orientation of prismatic joints enclosing the revolute joint, or an error in the geometry of the end-effector.

Now we consider parametric errors between two successive coordinate frames whose values are dependent on the position of the enclosed kinematic element.

If the kinematic element is moved, the relative error in the location of the end-effector changes correspondingly. Hence it is both possible and required to determine the respective variation of all 6 parametric errors. However, also in this case some simplifications are possible.

The errors in the end-effector trajectory due to a constant error in the orientation of a prismatic joint cannot be distinguished from those due to a linear trend in a parametric error describing the translation orthogonal to the joint axis (see figure B.1). Hence the latter, so-called straightness errors, are measured and defined relative to the average axis of motion, usually specified in a least squares sense. Similarly, constant errors in the radial axis position of a revolute joint cannot be distinguished from trends in a parametric error describing the translation orthogonal to the joint axis having a sinusoidal component with a wavelength of 360° . The term which is used to refer to such once-per-revolution error motion is fundamental error motion. Since a test ball on a rotating member is perfectly centred when this component vanishes, it follows that fundamental radial motion of a revolute joint does not exist [18] (i.e. is described by the position of the joint axis). Similar trends in parametric errors describing the variation in the orientation of the joint axis yield the same effect on the end-effector trajectory as a constant error in the orientation of this axis. This can be understood by visualizing a perfect cylinder mounted on an axis of rotation. If the orientation of this cylinder is adjusted so that the cylinder has no centring error at either end, then there is no once-per-revolution angular motion [18]. Hence, fundamental angular motion can be described by constant parametric errors in the orientation of the joint. Therefore, parametric errors describing angular and translation errors about/along axes orthogonal to a revolute joint are defined relative to respectively the average orientation and average position of the joint axis, again specified in a least squares sense. Thus they have no once-per-revolution sinusoidal component.

Due to the finite stiffness of structural loop segments, a parametric error can be related to the position of more than one joint. For example, in horizontal arm CMMs, parametric errors describing errors due to bending of the column are both dependent on the position along the column and the extension of the ram. From measured errors in the relative trajectory of the end-effector, it is both not possible nor required to separate the effect of two similar parametric

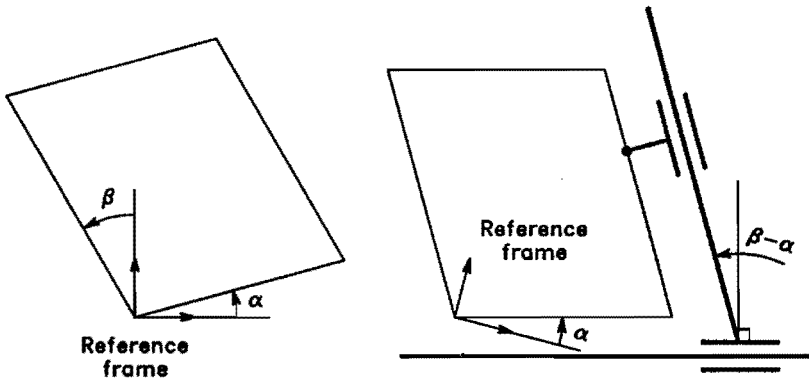


Figure B.1: Observed translation errors in the trajectory of the end-effector due to a linear trend in the 'straightness' errors, and the respective error model of the machine.

errors whose values are related to the same joint position. Thus, a parametric error whose value is dependent on the position of one joint can be lumped together with a similar parametric error dependent on the position of this and other joints. Since for angular parametric errors their Abbe offset is likely to be different, this grouping will affect the value of parametric errors describing translation errors.

Dependent on the nature of the executed task, the number of parametric errors can be further reduced. This reduction is affected by:

- the dimensionality of the task.
- the sensitive direction(s) of the task.
- the method used to generate the workpiece reference frame (i.e. the alignment procedure).
- the method used to determine the dimensions and geometry of the end-effector(s).

The first item addresses the number of axes which are moved during a task. If a certain axis remains at a fixed position during the entire task, the effect of this position on either the value or propagation of certain parametric errors

is constant. This implies that these parametric errors can be combined with other parametric errors. A similar reduction is possible when the same end-effector is used during the entire task. A typical example is the elimination of angular parametric errors associated with the ram of a machine by defining the respective translation parametric errors in the tip of the end-effector. The second item addresses the elimination of those parametric errors whose effect does not affect the relative location of the end-effector in its sensitive direction. Here, a further reduction can usually be achieved by a suitable lumping of various angular and displacement parametric errors.

The location of the workpiece is usually determined by an alignment procedure using the machine. In that case, the parametric errors describing the location of the workpiece reference frame are determined by the other parametric errors of the structural loop. In other cases, the respective parametric errors in the location of the workpiece reference frame must be separately modelled. Part of these errors may be due to errors in the location (especially orientation) of the machine table relative to frame bm , errors of the table itself (e.g. its flatness), and errors in the peripherals that support the workpiece. Note that the errors in the location of the workpiece reference relative to frame bm may change during the task, e.g. due to thermal deformation of the peripherals that support the workpiece. This variation must always be considered.

A further simplification occurs, if the end-effector used to align the workpiece is also used to execute the manufacturing task. During alignment, the location of the reference frame relative to frame bm is adjusted such that at a certain position of the machine axes, tool frame and reference frame partly coincide (usually only their respective position). Thus the effect of certain parametric errors associated with the end-effector is reduced to zero at this position. If both effect and value of these parametric errors do not change during the executed task, they do not cause errors in the relative location of tool frame and reference, and hence need not to be considered. Note that the effect of these parametric errors changes if the machine contains revolute joints. Since errors in the arm of revolute joints are lumped in the end-effector geometry, it is not sufficient to estimate the end-effector errors using measurements of the end-effector geometry. Relevant revolute joints should be active during cali-

bration of the end-effector geometry. Note that this process is only required for a single (reference) end-effector. The errors of other end-effectors are defined by their difference relative to this end-effector. In Chapter 1 it is noted that the nominal location of the tool frame can change during a manufacturing task. This changes the structural loop through the end-effector and hence its parametric errors. A typical example is the effect of probe sphere roundness and diameter when probing in different directions during coordinate measurements. Obviously, changes in the dimensions of the end-effector during a task (e.g. due to thermal deformation) should always be considered.

Curriculum Vitae

Hans Soons was born on June 27th, 1964 in Oss, The Netherlands. He attended the Titus Brandsma Lyceum in Oss, where he obtained his Atheneum-B diploma in 1982. During the same year, he commenced his study of Mechanical Engineering at the Eindhoven University of Technology. He received his Master's degree in April 1988. Immediately afterwards he was engaged by the Faculty of Mechanical Engineering at the Eindhoven University of Technology, where he started his doctoral studies in the field of precision engineering.

During September 1988 - April 1989 and July 1990 - August 1990 he worked as a research engineer at Fanamation Inc., a manufacturer of coordinate measuring machines in Compton CA. Besides his work at the Eindhoven University of Technology, he teaches graduate and post-graduate courses on metrology at the night school of the Hogeschool Eindhoven since September 1989.

Acknowledgments

The research described in this thesis was performed at the precision engineering group of the Eindhoven University of Technology. I would like to thank this group and the Faculty of Mechanical Engineering for the opportunity of realizing this project.

Special thanks go to both the promotors prof. dr. ir. P.H.J. Schellekens and prof. dr. ir. A.C.H. van der Wolf for their patience, insights, and support during this study. In particular I would like to thank my coach, prof. dr. ir. P.H.J. Schellekens, who introduced me to the field of precision engineering and whose influence is strongly reflected in this work. Furthermore I am much obliged to the members of the main promotion committee, prof. dr. ir. J.J. Kok and prof. dr. ir. J.P. Kruth, for the time they spent reviewing this document. Their many helpful comments are much appreciated.

I would like to express my thanks to the staff members and students of the precision engineering group for their cooperation and the pleasant work climate. In particular I would like to thank Henny Spaan and Frank Theuws, whose many-sided talents and insights greatly contributed to this study. Furthermore I would like to state my appreciation to the permanent staff members, Frits Theuws, Adriaan de Gilde, Nick Rosielle, Harry Sonnemans and, last but not least, Klaas Struik for their support and interest in this study.

A special word of thanks goes to Huub Eijsermans, who executed many of the often exotic experiments on the milling machine with high precision. Furthermore I would like to thank Elmar van den Elzen, Henny Spaan, Marcel Renkens, and Wim Weekers who, through their master's theses, made important contributions to this project. I also would like to thank both Wim van Vliet and Wim Weekers for their help during the finishing of this project.

Finally I would like to thank Mark Twaalfhoven and the employees of Fanamtion Inc. for making my stay at their company to a wonderful experience.

Stellingen

behorende bij het proefschrift van

Hans Soons

1. Zoals elk experiment is ook een kalibratie een compromis tussen een efficiënte schatting van bekende verschijnselen en de mogelijkheid tot detectie van onbekende verschijnselen.

Dit proefschrift

2. Doeltreffend gebruik van softwarematige afwijkingencompensatie vereist een aanpak waarbij deze techniek een integraal onderdeel is van het ontwerp, de fabricage en het onderhoud van de machine.

Dit proefschrift

3. Methoden om de nauwkeurigheid van een machine te bepalen dienen het gebruik van de machine zo dicht mogelijk te benaderen. Volumetrische meetmethoden verdienen derhalve de voorkeur boven parametrische meetmethoden.

Dit proefschrift

4. "There is a tendency to confuse the ability to correlate temperature measurements and deflections under steady-state conditions with an ability to predict deflections under dynamic or transient conditions."

E.R. McClure. "Manufacturing Accuracy Through the Control of Thermal Effects", PhD thesis, Lawrence Livermore National Laboratory, 1969.

5. Bij de huidige stand van zaken omtrent de schatting en modellering van afwijkingen kunnen enkel *specifieke* meettaken verricht met een coördinatenmeetmachine gecertificeerd worden.
6. De koppeling van frequentiemeting aan lengtemeting, zoals dat bij continue gaslasers mogelijk is, kan leiden tot een fundamentele verbetering van het meten van verplaatsingen in het nanometergebied.
7. Research en optimalisatie hebben met elkaar gemeen dat het bewandelen van enkel veelbelovende paden veelal leidt tot een lokaal optimum van het resultaat.

8. Het is maatschappelijk gezien de vraag of een verdere verwetenschappelijking van technische universiteiten wenselijk is.
9. In het huidige universitaire technische onderwijs worden studenten te weinig met de praktische realisatie van de door hun ontwikkelde modellen en ontwerpen geconfronteerd. Het vaak iteratieve proces van modelleren, ontwerpen en testen krijgt hierdoor te weinig aandacht.

Adviesraad voor het Wetenschaps- en Technologiebeleid, "Technici en onderzoekers: kwaliteit en kwantiteit", pagina 13, december 1992

10. Experimenteel onderzoek met een praktische doelstelling is essentieel voor wetenschappelijke vooruitgang.
11. De controlerende functie van de Eerste Kamer is ernstig in het ongerede geraakt door het veelvuldig gebruik van het "machtswoord" door het kabinet. Mede gezien het volgzame karakter van de Tweede Kamer, is een vergelijking met het besturen per decreet soms dan ook meer van toepassing dan het besturen met meerderheid van stemmen.
12. Gescheiden afval wordt nog te vaak gecombineerd verwerkt.
13. De laatste fase van een promotie doet het geloof in reïncarnatie versterken.

Eigen ervaring 1993

14. De fiscale afhandeling van parkeerboetes bevestigt het intuïtieve gevoel dat veel burgers hebben ten aanzien van belastingen in Nederland.